Non-Intrusive Gait Recognition Employing Ultra Wideband Signal Detection

by

Soumya Prakash Rana

A thesis presented in partial fulfilment of the requirements for the degree of

Doctor of Philosophy

School of Engineering
Division of Electrical & Electronics Engineering
London South Bank University
London, United Kingdom

October 2019

This thesis is dedicated to

my parents for their love, endless support, and encouragement.

Non-Intrusive Gait Recognition Employing Ultra Wideband Signal Detection

Abstract

A self-regulating and non-contact impulse radio ultra wideband (IR-UWB) based 3D human gait analysis prototype has been modeled and developed with the help of supervised machine learning (SML) for this application for the first time. The work intends to provide a rewarding assistive biomedical application which would help doctors and clinicians monitor human gait trait and abnormalities with less human intervention in the fields of physiological examinations, physiotherapy, home assistance, rehabilitation success determination and health diagnostics, etc.

The research comprises IR-UWB data gathered from a number of male and female participants in both anechoic chamber and multi-path environments. In total twenty four individuals have been recruited, where twenty individuals were said to have normal gait and four persons complained of knee pain that resulted in compensated spastic walking patterns. A 3D postural model of human movements has been created from the backscattering property of the radar pulses employing understanding of spherical trigonometry and vector fields. This subjective data (height of the body areas from the ground) of an individual have been recorded and implemented to extract the gait trait from associated biomechanical activity and differentiates the lower limb movement patterns from other body areas.

Initially, a 2D postural model of human gait is presented from IR-UWB sensing phenomena employing spherical co-ordinate and trigonometry where only two dimensions such as, distance from radar and height of reflection have been determined. There are five pivotal gait parameters; step frequency, cadence, step length, walking speed, total covered distance, and body orientation which have all been measured employing radar principles and short term Fourier transformation (STFT). Subsequently, the proposed gait identification and parameter characterization has been analysed, tested and validated against popularly accepted smartphone applications with resulting variations of less than 5%. Subsequently, the spherical trigonometric model has been elevated to a 3D postural model where the prototype can determine width of motion, distance from

radar, and height of reflection. Vector algebra has been incorporated with this 3D model to measure knee angles and hip angles from the extension and flexion of lower limbs to understand the gait behavior throughout the entire range of bipedal locomotion. Simultaneously, the Microsoft Kinect Xbox One has been employed during the experiment to assist in the validation process. The same vector mathematics have been implemented to the skeleton data obtained from Kinect to determine both the hip and knee angles. The outcomes have been compared by statistical graphical approach Bland and Altman (B&A) analysis.

Further, the changes of knee angles obtained from the normal gaits have been used to train popular SMLs such as, k-nearest neighbour (kNN) and support vector machines (SVM). The trained model has subsequently been tested with the new data (knee angles extracted from both normal and abnormal gait) to assess the prediction ability of gait abnormality recognition. The outcomes have been validated through standard and well-known statistical performance metrics with promising results found. The outcomes prove the acceptability of the proposed non-contact IR-UWB gait recognition to detect gait.

Declaration

The work in this thesis is based on research carried out at the Biomedical Engineering and Communications (BiMEC) Research Centre, School of Engineering, London South Bank University, London, United Kingdom. No part of this thesis has been submitted elsewhere for any other degree or qualification and it is all my own work unless referenced to the contrary in the text.

Acknowledgements

I would like to convey my thanks and gratitude to the following personalities who have unstintedly and untiringly helped and supported me to complete my PhD journey.

At the very outset, I would like to extend my heartfelt gratitude and obedience to my first supervisor Professor Sandra Dudley, Director of Research and Enterprise, London South Bank University for her painstaking, diligent guidance, uninterrupted encouragement, and advice provided throughout the course of this research work. I feel extremely blessed to have such a caring and responsible supervisor. Its also a real privilege to learn the basic qualities for grooming as a good researcher and successful academic near future.

I would also like to thank my second supervisor Professor Mohammad Ghavami, Head of Centre for Biomedical Engineering and Communications (BiMEC), London South Bank University for his constant advice and discussions to carry on this research work in an effective and fruitful way. I would like to commend special thanks to the BiMEC research centre, London South Bank University for providing highest-level facilities, resources, and simulation environment to perform the research experiments.

Besides, the above special thanks are also due to my friend Maitreyee Dey for her unconditional support in every respect and friendship during the tough time of these years. I would also thank to my fellow labmates for their companionship and providing friendly working atmosphere. I would be failing in expressing my gratitude without mentioning the name of Dr. Colin Fu, Lecturer in Business and Management, University of West London, who stood beside me during my hard days.

Lastly, I would like to extend my biggest and grateful thanks and also express my indebtedness to my parents Mrs. Gouri Rana, Dr. Ganesh Chandra Rana, and younger brother Subhra Prakash Rana for all of their unconditional support, encouragement,

and love without which, I would not have been able to come to this level. I am grateful to them for teaching me the moral values that have helped me to gradually uplift my thinking level and showing me the way of developing to the expected level of humanity.

Publications Arising from the Research

☐ **Chapter 3**

1. **S. P. Rana**, M. Dey, R. Brown, H. Siddiqui, S. Dudley. "Remote Vital Sign Recognition Through Machine Learning Augmented UWB", The 12th IEEE International Conference on European Conference on Antennas and Propagation (EuCAP), London, UK, 2018.
2. **S. P. Rana**, M. Dey, H. Siddiqui, G. Tiberi, M. Ghavami, S Dudley. "UWB Localization Employing Supervised Learning Method", The 17th IEEE International Conference on Ubiquitous Wireless Broadband (ICUWB), Salamanca, Spain, 2017.

☐ **Chapter 4**

1. **S. P. Rana**, M. Dey, and S. Dudley. "Signature Inspired Home Environments Monitoring System Using IR-UWB Technology", Sensors, MDPI, 19(2): 385, 2019. ***(Impact factor-3.031)***
2. **S. P. Rana**, M. Dey, M. Ghavami and S. Dudley. "Non-Contact Human Gait Identification through IR-UWB Edge Based Monitoring Sensor", IEEE Sensors Journal, IEEE, 2019. ***(Impact factor-3.076)***

☐ **Chapter 5**

1. **S. P. Rana**, M. Dey, M. Ghavami, S. Dudley. "ITERATOR: A 3D Gait Identification from IR-UWB Technology", The 41st IEEE International Engineering in Medicine and Biology Conference, Berlin, Germany, 2019.
2. **S. P. Rana**, M. Dey, M. Ghavami, S. Dudley. "ITERATOR: A Non-Intrusive 3D Human Gait Analysis from IR-UWB & Spastic Gait Case Study", IEEE Transactions on Biomedical Engineering. ***(Submitted)***

☐ **Chapter 6**

1. **S. P. Rana**, M. Dey, M. Ghavami, S. Dudley. "Intelligent three-dimensional gait analysis using IR-UWB sensing", The 41st PhotonIcs & Electromagnetics Research Symposium (PIERS), Rome, Italy, 2019.
2. **S. P. Rana**, M. Dey, M. Ghavami, S. Dudley. "Intelligent ITERATOR: 3D Gait Recognition Employing IR-UWB", IEEE Sensors Journal. ***(In Preparation)***

Contents

List of Figures

List of Tables

Nomenclature

μD	micro-Doppler
3D	Three-dimensional
AOA	Angle of arrival
AVPS	Augmented video based portable system
B&A	Bland and Altman
BAN	Body area network
BER	Bit error rate
CW	Continuous wave
DFT	Discrete Fourier transform
EIRP	Equivalent isotropically radiated power
EMG	Electromyography
ERP	Effective radiated power
FCC	Federal communications commission
FMCW	Frequency modulated continuous wave
FN	False negative
FP	False positive
FPS	Frames per second
FS	Floor sensors

FVM Free vertical moment

GRF Ground reaction force

IC Initial contact

IP Image processing

IR-UWB Impulse radio ultra wideband

ITERATOR gait disorder identification from impulse radio ultra wideband

kNN k-nearest neighbour

LOS Line of sight

LR Linear regression

LR Logistic regression

LRS Laser range scanners

MAF Moving average filtering

MCC Matthews correlation coefficient

MGAS Modular gait analysis system

MMC Markerless motion capture

NN Neural network

NWS Non-wearable sensor

P410 MRM P410 monostatic radar module

P410 RCM PulsON 410 ranging and communications module

PII Pulse integration index

PRF Pulse repetition frequency

PRI Pulse repetition interval

PRR Pulse repetition rate

PS Pressure sensors

RAPI Radar application program interface

RF Random forest

RFs Radio frequencies

ROI region of interest

RPM Revolutions per minute

SML Supervised machine learning

SNR Signal to noise ratio

SSM State space method

STFT Short term fourier transformation

STP Scan training period

SVM Support vector machine

TC Terminal contact

TN True negative

TOA Time of arrival

TOF Time of flight

TP True positive

TW-TOF Two way time of flight

UEP University ethics panel

UWB Ultra wideband

WS Wearable sensor

WT Wavelet transformation

+

Chapter 1

Introduction

Human motion is an association of several voluntary movements resulting from complex processes where the brain, spinal chord, muscles, nervous system, bones, and joints are involved [1]. The human walk is one of these complex physiological process, which is the bipedal, sinusoidal, forward propulsive movement of the human body. Both the upper and lower limbs coordinate together simultaneously in this translatory process [2]. Physically each and every bone participates in the process, but empirically the bones of the pelvis and lower limbs are usually considered to realise this repetitive locomotion. The rudiments of three different disciplines such as, anatomy, physiology, and biomechanics are obligatory to appreciate movement. Thus, this chapter provides a background understanding of human walk or gait in terms of anatomical reference planes, associated physiological processes and their biomechanical interpretation, followed by different phases and cycle of walk, types and causes of abnormalities, and outlined the thesis at the end.

1.1 Normal Walk & Gait

The words walking and gait are used interchangeably in the gait analysis literature. Thus, these two words have been used synonymously throughout the thesis. However, the word 'walking' explains the method of supporting and propulsing of the human body by two legs alternatively, whereas the manner or style of walking is 'gait' (where characterisation and types are involved) [3]. So, it is important to appreciate and explore

the normal walking process before discussing the characterisation of gait or clinical gait analysis, which provides a reference to analyse unusual gaits. It is a familiar and complex physiological movement and difficult to narrowly define. Normal walk has evolved to move the body forward, and comprises different phases, and cycles, using the minimum energy, pressure on foot, shock for dispersing the force of the body on the ground [4][5]. This is repeated with at least one leg in contact with the ground at all the times. A normal walk includes the following steps [6]:

1. One leg is lifted off of the ground.
2. With the leg in contact with the ground, the body is pushed forward.
3. The lifted leg is swung forward until it is in front of the body.
4. The walker falls forward to allow the lifted leg to contact the ground.
5. Steps 1–4 are repeated for the other leg.
6. Steps 1–5 are repeated to walk continuously.

These six steps are further classified into phases and cycles, and discussed in Section 1.3. Though, the objective of walking is always same, but they are distinguished based on the conditions of leg muscles used during a gait.

1.2 Anatomy, Physiology, and Biomechanics of Gait

Different disciplines have their own way and terminologies to define gait. However, the rudiments from all these disciplines are essential to analyse or characterise gait. Anatomy of gait explains the relationships between different body parts involved in walking based on their anatomical positions. There are three reference planes in the anatomy; sagittal, frontal, and transverse all used to describe human motion [2]. These planes are shown in Figure 1.1, where (a) sagittal plane divides a human body into its left and right halves, (b) frontal plane divides the body into back and front, (c) transverse plane divides the body in upper and lower parts. The joints and their muscles of human skeleton can only move to one or two directions in the reference planes and they are classified further based on the direction of movements from the body. The movements related to gait

in reference planes are flexion, extension, abduction, adduction, internal and external rotation [7]. Flexion describes a bending movement that decreases the angle between the lower limb and center of the body. Extension is the opposite of flexion, which describes a straightening movement that increases the angles. Flexion and extension take place in the sagittal plane. Abduction is the motion of the lower limb away from the midline while adduction refers to motion towards the center of the body. Abduction and adduction take place in the frontal plane. Internal rotation (or medial rotation) indicates rotation of lower limb towards the axis of the body. External rotation (or lateral rotation) states rotation of leg away from the center of the body. Internal and external rotation take place in the transverse plane [8].

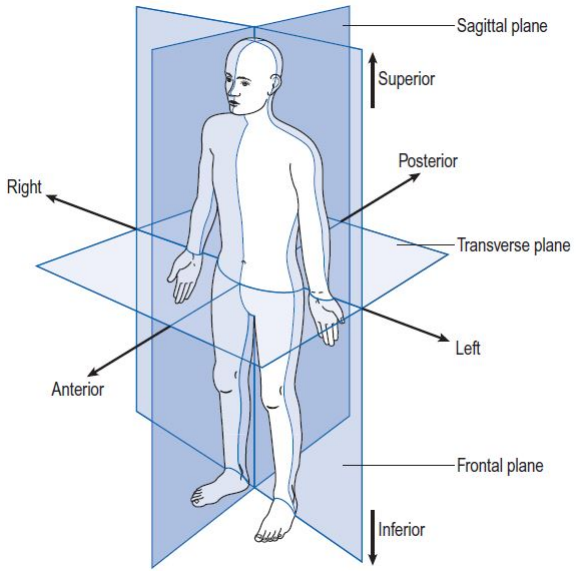

Figure 1.1: The anatomical positions of human body parts with respect to three reference planes [2].

Gait physiology involves different nervous systems and signals transmitted or received from the relevant motor system, where this communication transforms into a motion. The motor neurons receive nerve impulses from both the brain and other neurosystems through the spinal chord. Later, a complex and coordinated pattern of nerve signals are sent to muscles which moves joints, limbs, and the remainder of the body [2]. There are three types of muscle; smooth, skeletal, and cardiac in the human body where skeletal muscles are primarily responsible for walking or gait.

Biomechanics studies these biological movements of human walk with the help of mechanical engineering. Descriptors such as, time, angle, mass, force, center of gravity,

moments of force, linear and angular motion [9] from the domain are employed for human gait description, identification, analysis, and recognition. These descriptors are known as gait parameters and used for different clinical or pathological gait analysis. Gait parameters are predominantly used to measure lower limb movement practically, where the quality of movements are analysed by anatomy and physiology. The gait parameters have been discussed in detail on Chapter 2.

1.3 Cycle & Phases of Gait

Human locomotion is typically studied through its cycle information. A single gait cycle is the period between two consecutive events i.e., the period from when one foot contacts the ground to when that same foot makes contact again. This results in the propulsion of the human body to the direction of motion. The distance covered by one cycle is known as the stride length and distance covered by two successive and alternative legs is known as the step length. The cycle is further divided into more events and phases. Figure 1.2 shows the phases and events related to one cycle, which begins with the movement of the right foot meeting contact with the ground and the left foot also goes through exactly same event and phases as the right, but displaced in time by half of a cycle [10]. Predominantly, a cycle is divided into two phases; stance and swing phases. Stance phase is the interval when the foot is in contact with the ground and stance phase is the interval when a foot is in the air during propulsion on the body. Also, if the body is supported by two legs at the beginning or end of a cycle this is considered as double support.

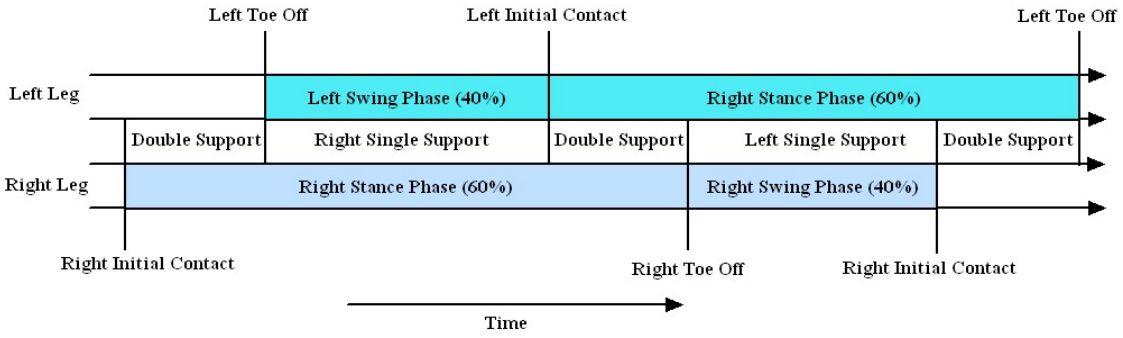

Figure 1.2: Timing of single and double support during a little more than one gait cycle, starting with right initial contact [11].

These two phases are further subdivided into seven major events such as, initial contact, opposite toe off, heel rise, opposite initial contact, toe off, feet adjacent, and tibia vertical, which help to realise a cycle in detail. Thus, there are two periods of double support and single support in each gait cycle. The stance, swing, and each period of double support lasts approximately 60%, 40%, 10% respectively in each gait cycle. However, these spans vary with the speed of walking, where the swing phase becomes proportionately longer, the stance phase and double support phases become shorter with increasing speed [11].

1.4 Pathological Gait

Pathological or abnormal gait is the walking pattern when a person is unable to walk in the 'usual' way. This manifests because of a defect of any interactive system, which causes additional pains or aches associated to the walk. There are four goals to be accomplished during normal gait [12]; (a) support the body weight without collapsing, (b) the body must be balanced in single stance leg condition, (c) swing leg must be in an advance position to take over the body support, and (d) sufficient power must be in the body to move limbs and the trunk. If any one of those goals is not achieved the result is an abnormal gait pattern.

1.5 Causes & Types of Gait Abnormalities

Medically, the common causes of unusual gait are, injuries to the legs or feet, arthritis, infections in the soft tissue of the legs, broken bones in feet and legs, birth defects, infections in the inner ear, cerebral palsy, stroke, tendonitis, conversion disorder or other psychological disorders, shin splints, etc. where people need to put extra effort to walk and experience complicacy during walk. Abnormalities are categorised into five types based on the symptoms such as, spastic gait, scissors gait, steppage gait, waddling gait, and propulsive gait [13]. The types abnormal gaits have been shown in Figure 1.3.

For example, when a person drags his/her feet while walking is known as spastic gait. A person whose legs bend inward suffers from a scissors gait, legs cross and may hit each other while walking in this case. Propulsive gait is when a person walks with

(a) Spastic (b) Scissor (c) Propulsive (d) Steppage (e) Waddling

Figure 1.3: Types of abnormal gaits and reflections on individual's walk [14].

his/her head and neck pushed forward. The propulsive abnormality is often seen among older people. Steppage gait occurs when a person's toes point towards the ground while walking. Generally, the toes scrape against the ground when the person steps forward. A person with a waddling gait moves from side to side when walking that involves taking steps as well as swinging the body. This type of abnormality is often seen among children.

1.6 Diagnosis of Gait in the Modern Era

There are two types of evaluation to characterise a person's lower limb movement; subjective evaluation which is carried out by observing the gait pattern in a clinical environment, and objective evaluation which is carried out by modern techniques and devices. Objective evaluation is more accurate and reduces the error in gait parameter measurements which can occur with subjective observation. The most commonly used technologies for human gait analysis are ultrasound, infrared video, video, floor sensors, wearable sensors, etc. [15]. These technologies involve the measurement, description, and assessment of kinetic and kinematic parameters that define human gait [16]. Gait events and musculoskeletal functions are quantitatively determined and applied in sports, physiotherapy, home assistance, rehabilitation, health diagnostics, and biometric recognition fields [17, 18]. Additionally, in some areas, human gait analysis is employed to improve athlete performance [19], monitor patient healing progress [20], assist in cases of Parkinson's disease [21, 22], and recognize individuals through their unique walking pattern [23]. The types of technologies are explored further in Chapter 2.

1.7 Scope of Gait Quantification Employing IR-UWB

Remote sensing of gait is particularly useful in case of gait patients where direct contact with the subject and use of camera are either impossible or unwanted and can be applied in local environment such as home. Avoidance of problems such as skin irritation, antenna, and sensor contacts is desirable in a number of health-care applications, including gait monitoring of patients with compromised skin [24]. Development of reliable noninvasive physiological monitoring is an important goal in modern health-care research. Knowledge of routinely monitored gait patterns are clinically useful in many situations where patients often suffer skin damage from adhesive tape, electrode markers with some lesions leaving scars [25]. A non-contact gait monitoring system could fill the needs for the patients in this case. The Doppler radar has been demonstrated potential for human gait monitoring [26]. A Doppler radar based approach for gait monitoring and fall detection was proposed, with good accuracy in distinguishing common fall events from normal movements [27]. Such a system could be potentially linked to medical monitoring personnel to provide better human gait monitoring facility. Thus, the study intends to establish a new gait identification and analysis technique through non-contact and non-invasive methods. The healthcare research has interest to measure and develop non-ionising RF based communication or measurements. Impulse radio ultra wideband (IR-UWB) technology is a wide electromagnetic spectrum band which allows health care research under federal communications commission (FCC) report and order, where radio frequencies (RFs) must be operated within the range of 3.1 GHz to 10.1 GHz. with very low equivalent isotropically radiated power (EIRP). RF transmission within this specification doesn't harm biological cell or human skin i.e., non-ionizing radiation. IR is a type of RF communication of UWB technology where radio sources typically use pulse modulation technique to transmit short RF pulse, which doesn't penetrate human body and back-scatter to device receiver end. The received pulses convey the information regarding the presence and movement of any biological section of human body.

1.8 Thesis Objectives

The associated physiological processes and body areas associated with movement need to be investigated to characterise gait mechanics, causes and types of abnormalities, advanced diagnosis, and field of application have been discussed. Unnatural settings, intrusiveness, compulsory lab requirements, discomfort, and privacy issue have been found as major prohibitions in todays gait diagnosis methods. Thus, the state of the art for gait assessment and characterisation methods are studied to appreciate strong alternative methods to address those issues with high precision outcomes. The study has found impulse radio ultra wideband (IR-UWB) technology is the one which can address all of these issues. Thus, IR-UWB has been employed in this research work to identify and analyse human gait. A new IR-UWB based mathematical method has been developed to identify and analyse human gait. The prototype has been tested in anechoic chamber and normal environment to check the robustness, efficiency, and cost effectiveness of the model. The multipath reflections are relevant part of the experiment in normal environment and have been tried to handle and mirror results like anechoic chamber environment. The work is supported by mathematical modeling and rigorous simulation results. The promising results indicates the potentiality of prototype for human gait identification in future.

1.9 Thesis Outline

The thesis began with an overview of human gait, interpretation of walking from different scientific fields, phases of walking, causes and types of gait abnormalities, gait diagnosis in Chapter 1. The parameters to characterise gait and the existing methodologies are reviewed in Chapter 2 and areas for improvement have been depicted with the problem definition. The data collection protocol has been explained with detailed subject profiles in Chapter 3. Additionally the employed measurement systems with configuration has been demonstrated here. A 2D model of gait identification has been developed with the help of radar principles and trigonometric ratios to characterise gait in Chapter 4. The study has been supported by rigorous simulation results and validation process. The 2D model has been improved into a 3D model to capture the human locomotion and measure more gait parameters in Chapter 5. The obtained results have

been compared with the results of Kinect sensor system to establish the correctness of the findings. In Chapter 6 demonstrates an intelligent IR-UWB protocol where proposed 3D model has been aided with supervised machine learning (SML) system to identify gait abnormalities automatically. Statistical measurements have been implemented to validate the performance of the developed gait analysis model. Finally, a conclusion of the thesis has been drawn in Chapter 7 with future research directions.

References

[1] Andrew B Schwartz. "Movement: how the brain communicates with the world". In: *Cell* 164.6 (2016), pp. 1122–1135.

[2] Michael W Whittle. *Gait analysis: an introduction*. Butterworth-Heinemann, Elsevier, 2014.

[3] Jeffrey M Hausdorff. "Gait variability: methods, modeling and meaning". In: *Journal of neuroengineering and rehabilitation* 2.1 (2005), p. 19.

[4] Alberto E Minetti. "The biomechanics of skipping gaits: a third locomotion paradigm?" In: *Proceedings of the Royal Society of London. Series B: Biological Sciences* 265.1402 (1998), pp. 1227–1233.

[5] Justin Greisberg. *Biomechanics of Walking*. https://footeducation.com/biomechanics-of-walking-gait/. Online; accessed 10th April, 2019. 2019.

[6] Kai J Chi and Daniel Schmitt. "Mechanical energy and effective foot mass during impact loading of walking and running". In: *Journal of biomechanics* 38.7 (2005), pp. 1387–1395.

[7] Frank H Netter et al. *Atlas of human anatomy*. Ciba-Geigy Corporation, 1989.

[8] Elaine N Marieb and Katja Hoehn. *Human anatomy & physiology*. Pearson Education, 2007.

[9] Barbara A Gowitzke and Morris Milner. *Scientific bases of human movement*. Williams & Wilkins, 1988.

[10] Leon Chaitow and Judith DeLany. "Chapter 3 - Gait analysis". In: *Clinical Application of Neuromuscular Techniques, Volume 2 (Second Edition)*. Ed. by Leon Chaitow and Judith DeLany. Second Edition. Oxford: Churchill Livingstone, 2011, pp. 61 –84.

[11] Melissa P Murray. "Gait as a total pattern of movement: Including a bibliography on gait". In: *American Journal of Physical Medicine & Rehabilitation* 46.1 (1967), pp. 290–333.

[12] Jacquelin Perry et al. "Gait analysis: normal and pathological function". In: *Journal of Pediatric Orthopaedics* 12.6 (1992), p. 815.

[13] Jenna Fletcher. *What is abnormal gait?* https://www.medicalnewstoday.com/articles/320481.php. [Online; accessed 10th March, 2019]. Sun 31 December 2017.

[14] Dictio. *What are the symptoms of abnormal walking or gait abnormalities?* https://www.dictio.id/t/apa-saja-gejala-dari-cara-berjalan-yang-tidak-normal-atau-walking-gait-abnormalities/6367. [Online; accessed 10th March, 2019]. Thursday 10 November 2017.

[15] Alvaro Muro-De-La-Herran, Begonya Garcia-Zapirain, and Amaia Mendez-Zorrilla. "Gait analysis methods: An overview of wearable and non-wearable systems, highlighting clinical applications". In: *Sensors* 14.2 (2014), pp. 3362–3394.

[16] Salim Ghoussayni et al. "Assessment and validation of a simple automated method for the detection of gait events and intervals". In: *Gait & Posture* 20.3 (2004), pp. 266–272.

[17] Liang Wang, Weiming Hu, and Tieniu Tan. "Recent developments in human motion analysis". In: *Pattern recognition* 36.3 (2003), pp. 585–601.

[18] Weilin Zang and Ye Li. "Gait-Cycle-Driven Transmission Power Control Scheme for a Wireless Body Area Network". In: *IEEE journal of biomedical and health informatics* 22.3 (2018), pp. 697–706.

[19] Kajiro Watanabe and Masaki Hokari. "Kinematical analysis and measurement of sports form". In: *IEEE Transactions on Systems, Man, and Cybernetics-Part A: Systems and Humans* 36.3 (2006), pp. 549–557.

[20] Stefan Kimmeskamp and Ewald M Hennig. "Heel to toe motion characteristics in Parkinson patients during free walking". In: *Clinical biomechanics* 16.9 (2001), pp. 806–812.

[21] Arash Salarian et al. "Ambulatory monitoring of physical activities in patients with Parkinson's disease". In: *IEEE Transactions on Biomedical Engineering* 54.12 (2007), pp. 2296–2299.

[22] Kostas M Tsiouris et al. "A decision support system based on rapid progression rules to enhance baseline evaluation of Parkinson's disease patients". In: *Biomedical & Health Informatics (BHI), 2018 IEEE EMBS International Conference on.* IEEE. 2018, pp. 329–332.

[23] Jian Li et al. "Segmentation-based image copy-move forgery detection scheme". In: *IEEE Transactions on Information Forensics and Security* 10.3 (2015), pp. 507–518.

[24] Olga Boric-Lubecke et al. *Doppler radar physiological sensing.* Wiley Online Library, 2016.

[25] Paul B Colditz et al. "Anetoderma of prematurity in association with electrocardiographic electrodes". In: *Journal of the American Academy of Dermatology* 41.3 (1999), pp. 479–481.

[26] Yazhou Wang and Aly E Fathy. "Micro-Doppler signatures for intelligent human gait recognition using a UWB impulse radar". In: *2011 IEEE International Symposium on Antennas and Propagation (APSURSI).* IEEE. 2011, pp. 2103–2106.

[27] Marco Mercuri et al. "Analysis of an indoor biomedical radar-based system for health monitoring". In: *IEEE Transactions on Microwave Theory and Techniques* 61.5 (2013), pp. 2061–2068.

Chapter 2

Literature Review

Traditionally, an individual's gait is measured by subjective or objective methods. The physiological expert or medical personnel observes a person's gait followed by a question and answer session in order to pursue the subjective evaluation of gait patterns. This is known as qualitative analysis of gait. The objective evaluation of gait includes the measurement of biomechanical parameters (or gait parameters) through advanced technical instruments, known as quantitative analysis of gait, with qualitative measurements parameters are implied by their visual appearance to the clinicians [28]. Quantitative gait analysis methods are more reliable for clinicians and medical practitioners, because the instruments provide a number of high precision gait parameters, which can not be achieved through subjective evaluation. However, these approaches have pros and cons, thus alternative gait analysis methods can offer advantages to these limitations. The chapter presents advanced instruments employed for gait analysis and it's classification, most commonly used gait parameters by the field experts, thorough review of existing works performed by the researchers, which leads to find out the issues in existing techniques and construct the problem definition, and make a prototype towards creating a novel gait analysis method for resolving the issues.

2.1 Gait Parameters of Interest

Clinical experts rely more on quantitative measurements than qualitative measurements because of the accuracy and precision of instruments. Thus, quantitative methods gain

more attention. This study comprises several biomechanical gait parameters are used to characterise gait behaviour and it depends upon the field of research. For instance, in the security field where gait is considered one of the significant physiological trait is always focused on the silhouette of lower limbs during locomotion [29] whereas, sports and rehabilitation fields are concerned about the force exerted by lower limb muscles during movement [30]. The most significant and frequently used gait parameters are used in real life gait analysis are summarised in Table 2.1. Table 2.1 includes the name of gait parameters, their definitions, and the associated research processes employed to characterise gait. It provides an overview of different gait parameters and state-of-the-art schemes used in the gait analysis field. Parameters measured by different gait identification and recognition methods are discussed in the following sections.

2.2 Retrospective Research

Figure 2.1 presents a taxonomy of advanced instruments which are used for quantitative gait analysis. Technological devices employed to study human gait can be classified into two different groups: non-wearable sensor (NWS) and wearable sensor (WS) based technologies. NWS systems require the access of controlled research facilities where the sensors are located and capture gait data while individuals walk on clearly marked walkway (testbed). In contrast, WS systems make it possible to analyse human motion data outside the laboratory and capture information about the human gait during the person's everyday activities. There is also a third group of hybrid systems that uses the combination of both methods.

NWS systems are further classified into three subgroups: (a) those based on image processing (IP), (b) those based on floor sensors (FS), and (c) ultra wideband (UWB) radar technology. IP systems capture data on the subject's gait through one or more optic sensors and take objective measurements of the different parameters through digital image processing. Analog or digital cameras are the most commonly used devices in this context. Other types of optic sensors such as, laser range scanners (LRS), infrared sensors and time of flight (TOF) cameras are also popular for human gait analysis. There are two systems within this category, with and without markers. The FS systems are based on sensors located along the floor on the force platforms, where the gait information

Table 2.1: Overview of gait parameters and descriptions

Gait parameters	**Description**	**Related Works**
Velocity	Speed of walk in a given direction	[31, 32]
Short step length	Linear distance between two successive placements of the same foot	[33, 34]
Long step or stride length	Linear distance between the placements of both feet	[33, 34]
Cadence	Number of steps completed per time unit	[35, 36]
Step width	Linear distance between two equivalent points of both feet	[35, 36]
Step angle	Direction of the foot during the step	[37, 38]
Short step time	Time between heel strike of one foot to subsequent heel strike of contralateral foot	[37, 38]
Swing time for each foot	Time from the moment the foot lifts from the floor until it touches it again, for each foot	[39, 40]
Support time	Time from the moment the heel touches the floor until the toes are lifted, for each foot	[39, 40]
Distances traveled	Distance covered within a given observation time	[41, 42]
Gait autonomy	Maximum time a person can walk, taking into account the number and duration of the stops	[43, 44]
Duration of the stop	Time takes by patients while stopping in between walk due to pain and aches	[45, 46]
Existence of tremors	Rhythmic, muscle contraction, and relaxation involving oscillations or twitching movements of legs	[47, 48]
Record of falls	Number of times the patient move from higher level to lower level, typically rapidly, and without control during observation	[49, 50]
Uneven terrain covered	Difference of height between drops and rises	[51, 52]
Routes taken	Sketch of path contributed in floor due to gait, abrupt changes are found in case gait disorders	[53, 54]
Gait phases	Deviation caused by gait disorders in stance and swing phase, where primarily stance is affected by a prolonged stance phase	[55, 56]
Direction of leg segments	The legs are bent in some disorders, where feet, hips, and knees are internally or externally rotated during walk	[57, 58]
Ground Reaction Forces	Measurement which is equal in magnitude and opposite in direction to the force that body exerts on supporting surface through foot	[55, 56]
Angles of the different joints	Specifically in ankle, knee, and hip	[59, 60, 61]
Electrical activity	Electromyography (EMG) is used to describe muscle's electric activity through simultaneous signal analysis to identify phases of gait cycle	[62, 63, 64]
Momentum and forces	Moments of force are produced across joints during walking cycle	[59, 60, 61]
Body posture	Provides information about body posture and capability of musculoskeletal system to adjust physical stressors	[62, 63, 64]

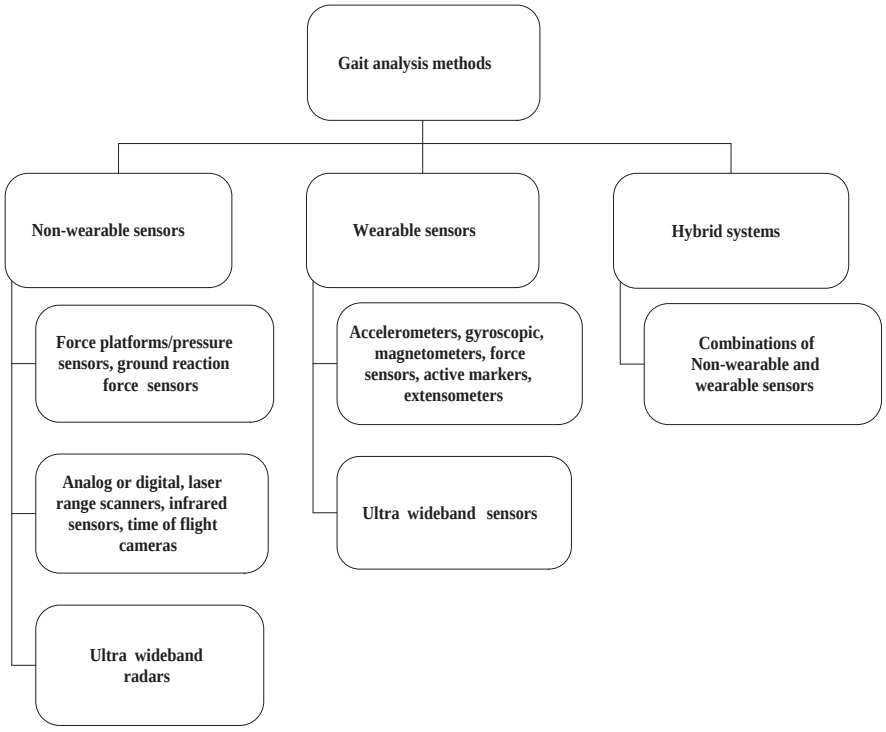

Figure 2.1: Taxonomy of existing gait analysis methods.

are measured through pressure sensors (PS) and ground reaction force (GRF) sensors, which measure the force exerted by the subject's feet on floor at the time of walking.

The WS systems use sensors located on several parts of the body such as, feet, knees, thighs and waist to capture the various signals that further characterise the human gait. The popular sensors of this group include accelerometers, gyroscopic sensors, magnetometers, force sensors, extensometers, goniometers, active markers, electromyography, etc.

2.2.1 Non-Wearable Sensor (NWS) Gait Analysis Methods

NWS systems include image processing employing fixed sensors placed on the ground surrounded by cameras for data collection. Subsequently, the gait parameters are extracted from image or video frames using filtering or segmentation methods. Ugbolue et. al., proposed an augmented video based portable system (AVPS) for clinical gait analysis. The data are collected using light indicator and video cameras to extract the kinematic event and tibia inclination angle of gait. The experiment was supported with gold standard 3D motion analysis data and validated by statistical evaluation [65]. Pfister et. al., captured 3D gait characteristics in sagittal plane through Microsoft Kinect

sensor. The authors analysed hip and knee angular displacement during flexion and extension of muscles. The Vicon Nexus model is used in parallel to compare the obtained results and estimated the performance of the prototype. The authors pointed out and anlysed the error needs to be addressed for employing Kinect in clinical gait analysis [66]. Other forms of NWS gait analysis are conducted with motion capture sensors. Corazza et. al., developed a markerless motion capture (MMC) system where ten joint centers and body shape are learned through linear regression (LR) to recognise gait kinematic and human body morphology. Performance of the study is evaluated by comparing the outcomes of laser scan and visual hull. The work indicates that performance can be improved using more training data and handling skin artefact problem [67]. Postalache et. al., presented a practical gait assessment approach through microwave Doppler radar for rehabilitation. Radar responses are further transformed employing short term fourier transformation (STFT), wavelet transformation, and moving average filtering (MAF) to obtain gait velocity and stride length of individuals. Though, STFT is effective to extract gait parameters by local convolution it needs to manually set the length of the convolution window which is highly disadvantageous [68]. Force platforms are also well known for gait assessment in controlled laboratory and observation settings. Lim et. al., prototyped a model to measure step phases through GRFs acquired from sensors employed to inspect lower limb exoskeleton [55]. These systems are effective to determine foot pressure, but unable to measure the horizontal and vertical vector components of that pressure [69], which require a large amount of pressure to be applied for activation. Thus it may be unsuitable for elderly or weaker patients. Also, another measurement alike GRF is free vertical moment (FVM) that does not receive much attention for gait analysis hitherto. Begue et. al., considered FVM as a gait behaviour indicator which provides information about torsional stress and lower limb movements. It measures internal foot rotation, adduction, gait speed from stance phase and their correlation during the movement of foot and pelvis [56]. Some of the researchers used continuous wave (CW) Doppler radars to characterise human gait. Ahtiainen et. al., employed CW radars to identify human gait from Doppler spectogram which is limited to detection of human movement while walking and does not provide enough parameters to realise the gait [70]. Seo et. al., proposed a model employing pulsed Doppler radar to detect human walking and associated physiological movements. But, the work only provides range information, which implies the location of occurrence but not the nature of movement [71]. Seifert et. al., modeled gait recognition prototype from frequency

modulated continuous wave (FMCW) Doppler radar to classify different types of gait such as, normal, assisted, and abnormal for rehabilitation and assisted living. The radar responses are interpreted into time-frequency representation by wavelet transformation (WT) to analyse micro-Doppler (μD) signatures of human walk which are classified further using machine learning techniques. The work only identifies the type of gait from μD signature. The work can not locate abnormalities in the lower limb making it difficult to use for rehabilitation [72]. Mokhtari et. al. prototyped a UWB model to identify signatures generated by different person's gait augmenting region of interest (ROI) method. Further, the back-scattered energy reflected from human body is used as features to categorise different human subjects employing support vector machine (SVM), random forest (RF), logistic regression (LR), k-nearest neighbour (kNN) and neural network (NN) models [73]. Wang et. al., modelled a WiFi based gait identification framework for human authentication from Channel State Information (CSI). The short term fourier transformation (STFT) is performed to generate spectrograms from CSI measurements to obtain unique human walking signatures which are denoised employing principal component analysis (PCA). The features are extracted from the signatures such as, gait cycle time, torso speed, footstep size, leg speed which are then fed into a radial basis function (RBF) based support vector machine (RBF-SVM) algorithm for human classification [74]. Zeng et. al. and Zhang et. al. both proposed device free WiFi based human classification from CSI based on walking signature. These methods are able to identify a person from small indoor group of people with the accuracy of 92%-93% [75, 76]. Fathy et. al., employed UWB radar for human motion monitoring from μD signatures where the location of movement is identifiable but no detailed study is provided to understand the participant's gait [77]. Ren et. al., developed a gait assessment model from IR-UWB Doppler radar based on STFT and state space method (SSM). The work developed a new short term SSM model to analyse back scattered pulses from human body to identify right foot, left foot, and torso trajectories even in a low signal to noise ratio (SNR) environment. But, the UWB device employed here had low pulse repetition frequency (PRF) of 75 Hz, hence the work suffers from weak back scattering and restricted to obtain the expected result [78].

2.2.2 Wearable Sensor (WS) Gait Analysis Methods

Widely used WSs are FSs, accelerometers, gyroscope, extensometers, goniometers, electromyography, and active markers etc. placed at the hips, feet, etc. to assess gait characteristics [79]. Recently, few works have been published where wearable UWB sensor networks are employed. Bruening and Ridge reviewed the existing algorithms which deal with gait event, velocity, and acceleration of foot/heel strike, toe off. The data are collected through foot and sacrum marker initially to form the ground truth information and perform the simulation for obtaining gait parameters. The work claims that the existing study carried out by Ghoussayni et. al. [80] to measure sagittal velocity is reliable for clinical gait application while a single algorithm is not useful to measure all gait events. The authors proposed an event detection algorithm which is useful for different gait event detection purposes [81]. Greene et. al., developed an adaptive algorithm to measure gait parameters via gyroscopes. The work is focused on measurement of initial contact (IC) and terminal contact (TC) timing of foot. Additionally, it calculates angular velocity, stride length, swing time, stance time, step times from human gait. The study includes force measurement plates and optical motion capture system to compare obtained results with the proposed algorithm. The algorithm contains high errors in case of stride, swing, stance, and step time calculation [82]. Bugane et. al., investigated state of art methods and prototyped an accelerometer based gait characterisation model. It measures single and double support interval from gait events. Also, it determines spatial and temporal parameters, such as stride length and duration, cadence, and speed. Popular gait analysis methods, stereophotogrametry and dynamometry are employed for validation. Significant errors are found to use the algorithm for gait cycle, single and double support measurement [83]. Some studies rely on wearable and BAN based UWB technologies. Renzo et. al., proposed an UWB based body area network (BAN) for human motion and gait analysis. The work contributed towards the reduction of complexity where TOF is employed for measurements. The study focused on improvement of channel impulse response and existing TOF based ranging algorithms. It considered gait parameters obtained from male and female participants; parallel arm, perpendicular arm, inline leg, perpendicular leg, thigh, torso motion at different angles i.e., 45°, parallel, perpendicular to evaluate and validate the performance of the study [84]. Shaban et. al., investigated the impulse radio ultra wideband (IR-UWB) technology in wireless wearable body area network (WWBAN) for gait assessment applications. The work

ensures the accuracy of IR-UWB is 1 mm at 18 dB signal to noise ratio (SNR) in dense multipath environment, which is ten times better than any existing system. The experiment further studied bit error rate (BER) and time of arrival (TOA) and concluded, that an ignorable performance degradation is found the required power consumption of the UWB device. Also, the power consumption could be further optimised by two orders of magnitude [85]. Shaban et. al., presented further work with an extended experiment by adding white noise in realistic channel scenario. The work proves 1.1 mm accuracy can be practically achieved at SNR 20 dB. This work would help the measurement of gait patients affected by unstable mobility disease [86]. El-Nasr et. al., improved Shaban et. al.'s [85] work for low power gait analysis by wearable UWB solution. The study proved measurement accuracy of angular displacement of knee flexion angle is 1°. Additionally, the model is integrated with FS for accurate measurement of tele-rehabilitation [87]. Cao et. al., assembled wireless BAN with UWB sensor, gyroscope, and acceleration sensor based on TOA technology to assess the human gait in 3D space. It defines local and global coordinates to explore lower limb kinematics of human gait [88]. Ashhar et. al., employed UWB technology to make wearable wireless sensor network to determine 3D foot trajectories. The system employs high resolution and pulse repetition frequency (PRF), low power spectral density (PSD) which increases the appropriate detection of trajectory. Also, a camera sensor is used to benchmark the data. The work achieved superior performance for spatial and temporal gait parameter measurement from foot movement which might be a good candidate for clinical gait analysis [89].

2.2.3 Hybrid Gait Analysis Methods

Industry is also working in parallel with academics towards creating robust and efficient gait analysis tools. CONTEMPLAS^{TM} produced a professional motion analysis software platform TEMPLO® for clinical gait analysis [90]. This is a hybrid approach for gait measurement comprises both NWS and WS systems in the diagnosis framework. It provides a complete overview of patient's gait through high quality image and video recording. Additionally, it uses force and pressure sensor platforms, Electromyography (EMG) and force vector to generate synchronous information for comprehensive analysis. EMG sensors record the activity of the muscles under consideration. With the help of force plates, horizontal and vertical forces in three dimensions (F_x, F_y and F_z) are measured synchronously to TEMPLO video analysis. The measurements provide

doctors, therapists and scientists meaningful information about the forces acting on the body during movement. For one-dimensional measurements (F_z) CONTEMPLAS offers a force plate developed for use in professional sports and rehabilitation, which provides high accuracy, robustness and portability. Tekscan is a company who makes pressure mapping, force measurement, and tactile sensors for clinical gait assessment [91]. They primarily focus on force platforms but use additional instruments such as, video scan and EMG analysis to construct a hybrid tools for gait characterisation. Tekscan's computerised gait analysis systems are used by clinicians and researchers to detect and correct pathomechanical dysfunctions of the foot, assess to improve athletic performance, and measure the changes after treatment. Modular gait analysis system (MGAS) is used to scan and capture accurate force, pressure and spatial-temporal parameters, compare left and right sides with symmetry tables, gait cycle tables provide insights into stride length, time, velocity and more. There are other companies such as, Zebris [92], Sensor Medica [93], Mediologic [94] who fabricate devices to analyse gait. Predominantly, they focus on force platforms, and are integrated with computerised software to visualise walking patterns.

2.3 Problem Definition

The potential to monitor physiological events remotely is more useful in situations where direct contact with the subject is either impossible or unwanted. The WS systems (especially the marker based systems) are considered as gold standard in gait analysis hitherto. However, marker based systems can cause skin irritation, scaring, restriction of breathing during spirometry and reversibility testing, and all current gold standard systems are considered 'invasive gait analysis methods'. To avoid these problems, development of reliable non-invasive, non-contact physiological monitoring is an important goal in modern healthcare research where, patients could be assessed remotely e.g. at home by NWSs preferably without any image or video recording. Also, clothing affects gait parameters extracted from NWS and WS systems, restricting their success. Image processing based works are limited by participants clothing, which can affects gait parameters detection, and force researchers to work on image segmentation method rather than significant gait parameters. It adds to the overhead complexity and reduces real-time reading opportunities.

Physiological measurements performed by researchers using continuous wave (CW) radar are limited by functional restrictions. Conventional CW radar operates electromagnetic radiation all the time at a constant interval thus there is no intermediate basis to calculate propagation time delay as well the range of an object. Measurement of Doppler frequency shift and the derivation of rate-of-change of range are viable. Therefore, CW radar is only used to estimate the frequency of a moving body section and limited to be utilised for further physiological information extraction. On the contrary, IR-UWB radar has been successfully implemented for human gait and vital sign identification but, the potentiality of IR-UWB radar has been overlooked by the state-of-art research. A number of works have been accomplished for gait and other physiological parameters but furthermore physiological factors could have been explored have not been done yet. Mostly, the researchers have used back-scattered energy received by the radar to identify the gait related parameters such as, step frequency, range, and speed only. However, more quantitative gait parameters are required for gait analysis which are also used (through observation) by doctors to diagnose the group of people who run the risk of walking disorder. The gait parameters such as, length of each steps, change of these lengths during stance and swing phase, knee angle (for each leg) i.e., the angle between thigh and shank, change of knee angle during stance and swing phase, angle between thighs and variation during stance and swing phase etc.

2.4 Contribution

IR-UWB technology has several advantages over typical narrowband communication systems such as large bandwidth, short pulse width, RF levels that are safe to use, and enables high resolution, making it suitable for biomechanical applications [73]. IR-UWB is a technology which operates for communication and measurements systems over the frequency band of 3.1 GHz to 10.1 GHz with -10 dB bandwidth according to FCC [95]. IR-UWB measurements employ RF with very low effective radiated power (ERP) typically in the sub-milliwat range. The ERP used in IR-UWB is a non-ionizing measurement method. Communication is based on a transmitter and receiver frequency band and power levels that do not penetrate because of permeability and dielectric constant of living cell material restricts the spread of pulse's electromagnetic field inside biological

matter with low ERP (allocated for UWB application). Radio frequencies (RFs) of IR-UWB back-scatter from living body and provide location information based on Doppler frequency change with high data transmission rate. Thus, IR-UWB pulsed radar has been chosen for the study. Short duration IR-UWB pulsed radar is time modulated and can be individualized. These short duration pulses are less sensitive to multiple reflections making the system robust and resistive within multipath environments [96, 97]. The superior penetration properties of UWB signals limit the effect of clothing and other obstacles e.g. walls. It has the capacity to work with low SNR enabling it to detect moving objects in hostile environments. The work describes the first time use of pulsed UWB to identify and filter gait patterns from other simultaneous biomechanical activities such as, heartrate, breathing, and arm movements.

The contributions of thesis are as follows: the first reported three-dimensional (3D) spherical trigonometric based theory has been developed and implemented to identify parameters which can define a person's gait trait. The resulting gait parameters (walking speed, leg orientation, and traversed distance) have been corroborated via popular smartphone applications to prove the correctness of the outcomes. The prototype has been further improved to capture human motion in three-dimensional plane modeled by spherical trigonometry. Here, motion is interpreted through anatomical planes frontal, sagittal, and transverse plane. Further, the height has been used heuristically to distinguish the movements of upper limbs from lower limbs. The mathematical model has been formulated by employing vector algebra based on IR-UWB sensing phenomena to calculate step frequency, walking speed, step length, angle between thighs, knee angle. Simultaneously, the model has been corroborated with Kinect Xbox One sensor. Kinect system is a well-known, camera based, and popular sensor for body posture measurement and had been employed for gait analysis by several researchers as discussed previously. Bland and Altman (B&A) statistics has been measured between proposed IR-UWB prototype and Kinect sensor results to verify the agreement of results by proposed work and Kinect sensor. Proposed models have been further experimented and realized in both ideal (anechoic chamber) and normal/multi-path environment to demonstrate its efficiency and robustness.

References

[28] Jessica Rose et al. “The energy expenditure index: a method to quantitate and compare walking energy expenditure for children and adolescents.” In: *Journal of pediatric orthopedics* 11.5 (1991), pp. 571–578.

[29] Arun N M Gomatam and Sreela Sasi. “Multimodal Gait Recognition Based on Stereo Vision and 3D Template Matching.” In: *CISST*. 2004, pp. 405–410.

[30] Scott C White and David A Winter. “Predicting muscle forces in gait from EMG signals and musculotendon kinematics”. In: *Journal of Electromyography and Kinesiology* 2.4 (1992), pp. 217–231.

[31] Stuart Hagler et al. “Unobtrusive and ubiquitous in-home monitoring: A methodology for continuous assessment of gait velocity in elders”. In: *IEEE transactions on bio-medical engineering* 57.4 (2010), p. 813.

[32] Kara K Patterson et al. “Gait symmetry and velocity differ in their relationship to age”. In: *Gait & posture* 35.4 (2012), pp. 590–594.

[33] John G Nutt et al. “Freezing of gait: moving forward on a mysterious clinical phenomenon”. In: *The Lancet Neurology* 10.8 (2011), pp. 734–744.

[34] Alfonso Fasano et al. “Modulation of gait coordination by subthalamic stimulation improves freezing of gait”. In: *Movement Disorders* 26.5 (2011), pp. 844–851.

[35] Takeshi Yamaguchi and Kei Masani. “Effects of age-related changes in step length and step width on the required coefficient of friction during straight walking”. In: *Gait & posture* 69 (2019), pp. 195–201.

[36] Kedar S Mate et al. “Putting the best foot forward: Relationships between indicators of step quality and cadence in three gait vulnerable population”. In: *NeuroRehabilitation* Preprint (2019), pp. 1–7.

[37] Stijn A A N Bolink et al. “Validity of an inertial measurement unit to assess pelvic orientation angles during gait, sit–stand transfers and step-up transfers: Comparison with an optoelectronic motion capture system”. In: *Medical engineering & physics* 38.3 (2016), pp. 225–231.

[38] Daniel K Y Chen, Markus Haller, and Thor F Besier. "Wearable lower limb haptic feedback device for retraining Foot Progression Angle and Step Width". In: *Gait & posture* 55 (2017), pp. 177–183.

[39] Rachael C Birch et al. "Selective subcortical contributions to gait impairments in males with the FMR1 premutation". In: *J Neurol Neurosurg Psychiatry* 88.2 (2017), pp. 188–190.

[40] Johan Larsson, Michael Miller, and Eva Ekvall Hansson. "Vestibular asymmetry increases double support time variability in a counter-balanced study on elderly fallers". In: *Gait & posture* 45 (2016), pp. 31–34.

[41] Alexandra König et al. "Objective measurement of gait parameters in healthy and cognitively impaired elderly using the dual-task paradigm". In: *Aging clinical and experimental research* 29.6 (2017), pp. 1181–1189.

[42] David F Wozniak et al. "Conditional knockout of UBC13 produces disturbances in gait and spontaneous locomotion and exploration in mice". In: *Scientific reports* 9.1 (2019), p. 4379.

[43] Dan Hristea et al. "Combining intra-dialytic exercise and nutritional supplementation in malnourished older haemodialysis patients: Towards better quality of life and autonomy". In: *Nephrology* 21.9 (2016), pp. 785–790.

[44] Thibaud Sader et al. "Gait disorders in subacute stroke: Meta-analysis and case series". In: *Annals of Physical and Rehabilitation Medicine* 61 (2018), e200.

[45] Enrique Hortal et al. "EEG-based detection of starting and stopping during gait cycle". In: *International journal of neural systems* 26.07 (2016), p. 1650029.

[46] Abdul H A Razak et al. "Wireless Integrated Gait Analysis System for Heel-Strike and Toe-Off Measurement". In: *Journal of Telecommunication, Electronic and Computer Engineering (JTEC)* 9.2-8 (2017), pp. 127–132.

[47] Qiannan Li et al. "Classification of gait anomalies from kinect". In: *The Visual Computer* 34.2 (2018), pp. 229–241.

[48] Jaimie A Roper et al. "Spatiotemporal gait parameters and tremor distribution in essential tremor". In: *Gait & posture* 71 (2019), pp. 32–37.

[49] Pamela Newland et al. "Exploring the feasibility and acceptability of sensor monitoring of gait and falls in the homes of persons with multiple sclerosis". In: *Gait & posture* 49 (2016), pp. 277–282.

[50] Nise R Marques et al. “The ability of gait kinematic parameters to predict falls in older adults with cognitive impairments living in long term institutions”. In: *Clinical biomechanics* 65 (2019), pp. 123–127.

[51] Timothy D Coleman, Haley J Lawrence, and W Lee Childers. “Standardizing methodology for research with uneven terrains focused on dynamic balance during gait”. In: *Journal of applied biomechanics* 32.6 (2016), pp. 599–602.

[52] Yilin Xu et al. “Hexapod adaptive gait inspired by human behavior for six-legged robot without force sensor”. In: *Journal of Intelligent & Robotic Systems* 88.1 (2017), pp. 19–35.

[53] Pei H Chen et al. “Walking Turns in Parkinson’s Disease Patients with Freezing of Gait: The Short-term Effects of Different Cueing Strategies”. In: *International Journal of Gerontology* 10.2 (2016), pp. 71–75.

[54] Erica Twardzik et al. “What features of the built environment matter most for mobility? Using wearable sensors to capture real-time outdoor environment demand on gait performance”. In: *Gait & posture* 68 (2019), pp. 437–442.

[55] Dong H Lim et al. “Development of real-time gait phase detection system for a lower extremity exoskeleton robot”. In: *International Journal of Precision Engineering and Manufacturing* 18.5 (2017), pp. 681–687.

[56] Jérémie Begue et al. “Influence of gait speed on free vertical moment during walking”. In: *Journal of biomechanics* 75 (2018), pp. 186–190.

[57] Jos Meuleman et al. “LOPES II—design and evaluation of an admittance controlled gait training robot with shadow-leg approach”. In: *IEEE transactions on neural systems and rehabilitation engineering* 24.3 (2015), pp. 352–363.

[58] Wouter Hoogkamer, Zrinka Potocanac, and Jacques Duysens. “Quick foot placement adjustments during gait: direction matters”. In: *Experimental brain research* 233.12 (2015), pp. 3349–3357.

[59] Anne D Koelewijn and Antonie J Bogert. “Joint contact forces can be reduced by improving joint moment symmetry in below-knee amputee gait simulations”. In: *Gait & Posture* 49 (2016), pp. 219–225.

[60] Richard R Neptune and Craig P McGowan. “Muscle contributions to frontal plane angular momentum during walking”. In: *Journal of biomechanics* 49.13 (2016), pp. 2975–2981.

[61] Ryan F Pinto et al. "Reliability and validity of knee joint angles and moments in patients with knee osteoarthritis using a treadmill-based movement analysis system". In: *Osteoarthritis and Cartilage* 26 (2018), S375–S376.

[62] Thomas Schauer et al. "Realtime EMG analysis for transcutaneous electrical stimulation assisted gait training in stroke patients". In: *IFAC-PapersOnLine* 49.32 (2016), pp. 183–187.

[63] Katherine Plewa, Ali Samadani, and Tom Chau. "Comparing electro-and mechano-myographic muscle activation patterns in self-paced pediatric gait". In: *Journal of Electromyography and Kinesiology* 36 (2017), pp. 73–80.

[64] Annachiara Strazza et al. "Surface-EMG analysis for the quantification of thigh muscle dynamic co-contractions during normal gait". In: *Gait & posture* 51 (2017), pp. 228–233.

[65] Ukadike C Ugbolue et al. "The evaluation of an inexpensive, 2D, video based gait assessment system for clinical use". In: *Gait & posture* 38.3 (2013), pp. 483–489.

[66] Alexandra Pfister et al. "Comparative abilities of Microsoft Kinect and Vicon 3D motion capture for gait analysis". In: *Journal of medical engineering & technology* 38.5 (2014), pp. 274–280.

[67] Stefano Corazza et al. "Automatic Generation of a Subject-Specific Model for Accurate Markerless Motion Capture and Biomechanical Applications". In: *IEEE Transactions on Biomedical Engineering* 57.4 (2010), pp. 806–812. ISSN: 0018-9294.

[68] Octavian Postolache et al. "Gait rehabilitation assessment based on microwave Doppler radars embedded in walkers". In: *2015 IEEE International Symposium on Medical Measurements and Applications (MeMeA) Proceedings*. 2015, pp. 208–213.

[69] Carl J Payton and Adrian Burden. *Biomechanical evaluation of movement in sport and exercise: the British Association of Sport and Exercise Sciences guide*. Routledge, 2017.

[70] Juhana Ahtiainen, Sami Terho, and Sampsa Koponen. "Radar based detection and tracking of a walking human". In: *IFAC Proceedings Volumes* 43.16 (2010), pp. 437–442.

[71] Yun Seo Koo et al. "UWB MicroDoppler radar for human gait analysis, tracking more than one person, and vital sign detection of moving persons". In: *2013 IEEE MTT-S International Microwave Symposium Digest (MTT)*. IEEE. 2013, pp. 1–4.

[72] Ann K Seifert, Moeness G Amin, and Abdelhak M Zoubir. "New analysis of radar micro-Doppler gait signatures for rehabilitation and assisted living". In: *2017 IEEE International Conference on Acoustics, Speech and Signal Processing (ICASSP)*. IEEE. 2017, pp. 4004–4008.

[73] Ghassem Mokhtari et al. "Non-wearable UWB sensor for human identification in smart home". In: *IEEE Sensors Journal* 17.11 (2017), pp. 3332–3340.

[74] Wei Wang, Alex X Liu, and Muhammad Shahzad. "Gait recognition using wifi signals". In: *Proceedings of the 2016 ACM International Joint Conference on Pervasive and Ubiquitous Computing*. 2016, pp. 363–373.

[75] Yunze Zeng, Parth H Pathak, and Prasant Mohapatra. "WiWho: WiFi-Based Person Identification in Smart Spaces". In: *2016 15th ACM/IEEE International Conference on Information Processing in Sensor Networks (IPSN)*. 2016, pp. 1–12.

[76] Jin Zhang et al. "WiFi-ID: Human Identification Using WiFi Signal". In: *2016 International Conference on Distributed Computing in Sensor Systems (DCOSS)*. 2016, pp. 75–82.

[77] Aly E Fathy et al. "Continuous Long Term Patient Motion Monitoring Using Ultra Wide Band Radar". In: *2018 IEEE International Symposium on Antennas and Propagation & USNC/URSI National Radio Science Meeting*. IEEE. 2018, pp. 15–16.

[78] Lingyun Ren et al. "Short-time state-space method for micro-Doppler identification of walking subject using UWB impulse Doppler radar". In: *IEEE Transactions on Microwave Theory and Techniques* 66.7 (2018), pp. 3521–3534.

[79] Bijan Najafi et al. "Ambulatory system for human motion analysis using a kinematic sensor: monitoring of daily physical activity in the elderly". In: *IEEE Transactions on biomedical Engineering* 50.6 (2003), pp. 711–723.

[80] Salim Ghoussayni et al. "Assessment and validation of a simple automated method for the detection of gait events and intervals". In: *Gait & Posture* 20.3 (2004), pp. 266–272.

[81] Dustin A Bruening and Sarah Trager Ridge. "Automated event detection algorithms in pathological gait". In: *Gait & posture* 39.1 (2014), pp. 472–477.

[82] Barry R. Greene et al. "An adaptive gyroscope-based algorithm for temporal gait analysis". In: *Medical & Biological Engineering & Computing* 48.12 (2010), pp. 1251–1260. ISSN: 1741-0444.

[83] Francesca Bugané et al. "Estimation of spatial-temporal gait parameters in level walking based on a single accelerometer: Validation on normal subjects by standard gait analysis". In: *Computer Methods and Programs in Biomedicine* 108.1 (2012), pp. 129 –137. ISSN: 0169-2607.

[84] Marco Di Renzo, R Michael Buehrer, and Jaime Torres. "Pulse shape distortion and ranging accuracy in UWB-based body area networks for full-body motion capture and gait analysis". In: *IEEE GLOBECOM 2007-IEEE Global Telecommunications Conference*. IEEE. 2007, pp. 3775–3780.

[85] Heba Shaban, M Abou El-Nasr, and R Michael Buehrer. "Performance of ultralow-power IR-UWB correlator receivers for highly accurate wearable human locomotion tracking and gait analysis systems". In: *GLOBECOM 2009-2009 IEEE Global Telecommunications Conference*. IEEE. 2009, pp. 1–6.

[86] Heba A Shaban, Mohamad Abou El-Nasr, and R Michael Buehrer. "Toward a highly accurate ambulatory system for clinical gait analysis via UWB radios". In: *IEEE Transactions on Information Technology in Biomedicine* 14.2 (2009), pp. 284–291.

[87] Mohamad A El-Nasr, Heba A Shaban, and Michael Buehrer. "Key design parameters and sensor-fusion for low-power wearable UWB-based motion tracking and gait analysis systems". In: *Progress In Electromagnetics Research* 29 (2012), pp. 115–126.

[88] Fucheng Cao, Xin Li, and Xilu Zhao. "3D Gait Analysis Based on UWB Wireless Body Area Networks". In: *2014 International Conference on Mechatronics, Control and Electronic Engineering (MCE-14)*. Atlantis Press. 2014.

[89] Karalikkadan Ashhar, Cheong B Soh, and Keng H Kong. "Wireless Ultrawideband Sensor Network for Gait Analysis in Rehabilitation Clinics". In: *2018 IEEE International Conference on Systems, Man, and Cybernetics (SMC)*. IEEE. 2018, pp. 1524–1529.

[90] CONTEMPLAS. *TEMPLO Clinical Gait Analysis*. https://www.contemplas.com/clinical-gait-analysis.aspx. Online accessed: December, 2017.

[91] Tekscan. *Pressure Mapping, Force Measurement & Tactile Sensors*. https://www.tekscan.com/gait-analysis-systems. Online accessed: January, 2018.

[92] Zebris Medical GmbH. *Dynamic gait analysis on the treadmill*. https://www.zebris.de/en/medical/products-solutions/gait-analysis-fdm-t/. ISO 13485:2016, Online accessed: January, 2018. 2016.

[93] Technology in Motion Sensor Medica. *Run Time Treadmill*. https://www.sensormedica.com/site/en/products/baropodometric-treadmill. Online accessed: January, 2018.

[94] T&T medilogic Medizintechnik GmbH. *Mediologic*. https://medilogic.com/en/home/. Online accessed: December, 2017.

[95] Federal Communications Commission. "In the matter of revision of part 15 of the commission's rules regarding ultra-wideband transmission systems". In: *First Report And Order, ET Docket 98-153* (2002).

[96] Jeongwoo Han and Cam Nguyen. "Development of a Tunable Multiband UWB Radar Sensor and Its Applications to Subsurface Sensing". In: *IEEE Sensors Journal* 7.1 (2007), pp. 51–58. ISSN: 1530-437X. DOI: 10.1109/JSEN.2006.888585.

[97] Qilian Liang. "Radar Sensor Wireless Channel Modeling in Foliage Environment: UWB Versus Narrowband". In: *IEEE Sensors Journal* 11.6 (2011), pp. 1448–1457. ISSN: 1530-437X. DOI: 10.1109/JSEN.2010.2097586.

Chapter 3

Experimental Framework

Gait analysis methods have been presented and the research problem explained in Chapter 2. The aptness of impulse radio ultra wideband (IR-UWB) technology to develop a human gait characterisation method and details of the experimental setup are outlined in this chapter. As mentioned, the human walk is a complex physiological process, where human participants must be involved during the research and data collection is a first salient step of the work. An existing UWB radar module has been employed to collect the RF responses of human motion, which have been transformed through the development of a novel mathematical model to capture the movements of the upper and lower limbs. The proposed model captures motion in three dimensions by considering three anatomical planes i.e., the sagittal, frontal, and transverse. The model has been tested in an anechoic chamber at LSBU and a multipath environment (normal environment) to investigate the robustness of the proposed prototype. This chapter describes the framework of the experiment performed for model testing and evaluation. Additionally, the obtained results have been corroborated via smart phone sensor and Microsoft Kinect sensor to inspect error margins of gait parameter measurement. The chapter presents the architecture of experimental setup, details of instruments used, and profiles of participants recruited. A schematic of the proposed study is included in this chapter, where the components of the experiment of both ideal (anechoic chamber) and real (multi-path) environments have been presented. Initially, the radar is configured and the raw radar scan data acquired through a radar application program interface (RAPI). The radar module is also configured to retrieve detection information from the different environmental conditions.

3.1 IR-UWB and Human Gait Measurement

The work intended to model a non-invassive, non-contact, smart human gait monitoring system that can identify and record important musculoskeletal-related parameters. Also, the system needs to be flexible to mobility and infrustructure, easily installable, and low cost. Such requirements would have attained employing IR-UWB radar technology. The IR-UWB antennas don't need to wear for movement measurement. This employs two way time of flight (TW-TOF) measurements and multilateration technique with RF electromagnetic spectrum of 3.1 GHz to 10.6 GHz (shown in Figure 3.1) and now 21 GHz to 140 GHz [98].

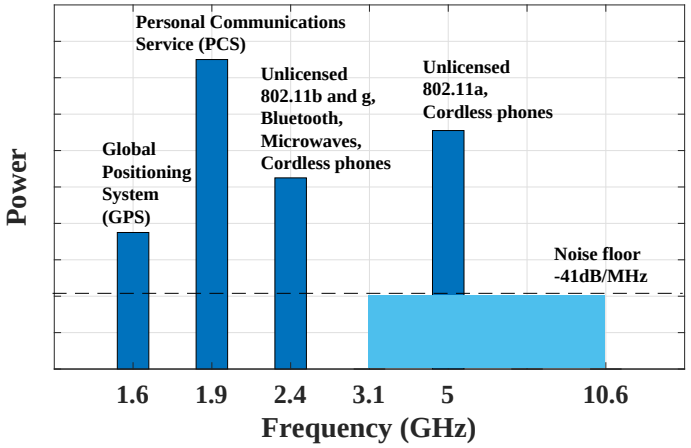

Figure 3.1: UWB spectrum

The employed IR-UWB (with frequency range of 3.1 GHz to 5.3 GHz) provides the resolution of approximately 10 mm and less which allows to measure very small changes in musculoskeletal movement. Thus, IR-UWB has been chosen for gait analysis to make a viable gait monitoring system can be developed by combining miniaturized, durable, low-cost and compact sensors with the advanced communication technologies and data processing techniques. Also, the pulses provide UWB system better immuneing to multipath making it suitable for gait analysis in normal environments without expensive laboratory support. Subsequently, it operates with high speed and data rate that allow the systems to be efficient and accurate for real time gait detection with high spatial resolution (10 mm). Also, IR-UWB system has the ability to effectively reduce fading and interference in different wireless propagation channel environments because of the limited transmitted power of UWB systems with high signal to noise ratio (SNR).

3.2 Participant Recruitment & Data Acquisition Protocol

Human gait identification and analysis from electromagnetic UWB responses presented in this thesis is three fold; 2D gait identification from IR-UWB, where the concept of frontal and transverse reference planes are incorporated involved (discussed in Chapter 4), 3D gait identification where all three reference planes (sagittal, frontal, and transverse planes) have been involved (discussed in Chapter 5), classification of gaits based on the characteristics obtained from proposed model (discussed in Chapter 6). Twenty four participants have been recruited hitherto, where twenty persons have normal or healthy gait and four persons with spasticity in this research. The first fifteen participants have been involved in the 2D gait experiment, then as the number of participants increased, all were involved in the 3D gait experiment and classification work. Full ethical approval (Reference Number: Eng_01Dec2017) was gained from London South Bank University, where the research code of practice and ethical guidelines are governed by the university ethics panel (UEP).

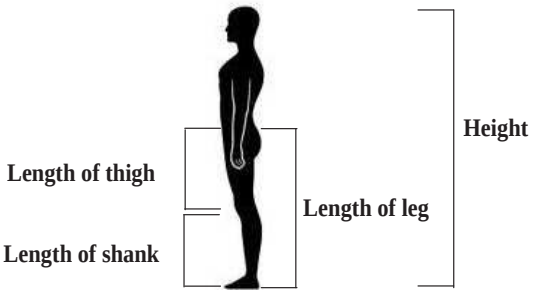

Figure 3.2: The measured body parts for subjective knowledge collection.

All procedures performed in this study were done so in accordance with the ethical standards of the institutional and/or national research committee and with the 1964 Helsinki declaration and it's later amendments or comparable ethical standards [99]. Initially, gender and anatomical information (height, length of the limbs) were recorded for each individual as shown in Figure 3.2. The measured body proportions have been listed in Table 3.1. Measurements, such as, leg lengths have been heuristically employed later to identify the movements that normally occur in lower limb of the human body and includes the essence of walking. Shank movements have been distinguished from thigh movement using these measurements and the detailed procedure has been discussed in

Chapter 4 and 5. So far ideal (in anechoic chamber) and multi-path/normal (in laboratory) environments have been used for the data collection. These two environments are shown in Figure 3.4b and 3.4c.

Table 3.1: Subjective data related to fifteen individuals.

No	Gender	Height (Meters)	Length of Leg (Meters)	Length of Thigh (Meters)	Length of Shank including heel height (Meters)
1	Female	1.58	0.85	0.43	0.42
2	Female	1.54	0.83	0.42	0.41
3	Female	1.64	0.88	0.45	0.43
4	Female	1.73	0.93	0.47	0.46
5	Female	1.62	0.87	0.44	0.43
6	Female	1.71	0.91	0.46	0.45
7	Female	1.69	0.91	0.46	0.44
8	Male	1.67	0.88	0.45	0.43
9	Male	1.76	0.91	0.46	0.45
10	Male	1.71	0.88	0.45	0.43
11	Male	1.72	0.88	0.45	0.43
12	Male	1.64	0.84	0.42	0.42
13	Male	1.78	0.92	0.47	0.45
14	Male	1.79	0.92	0.46	0.46
15	Male	1.78	0.92	0.47	0.45
16	Male	1.78	1.00	0.52	0.48
17	Male	1.75	1.02	0.52	0.50
18	Male	1.72	1.00	0.51	0.49
19	Female	1.55	0.95	0.50	0.45
20	Female	1.53	0.94	0.50	0.44
21	Male	1.76	1.03	0.54	0.49
22	Male	1.78	1.01	0.53	0.48
23	Female	1.65	0.97	0.50	0.47
24	Female	1.58	0.95	0.49	0.46

3.3 Setup & Data Post Processing

A schematic of the experimental architecture is shown in Figure 3.3. The first step of the experimental work is to configure the radar Time Domain PulsON 410 ranging and communications module (P410 RCM) and P410 monostatic radar module (P410 MRM) which are used to collect all the physiological sensing phenomenon reported here, shown in Figure 3.4a. The module has been used in all publications [100, 101, 102, 103] from this thesis work. The anechoic chamber and multipath environment both have been considered here to gather the gait data using following settings of Table 3.2. Photos of

the experimental environments of anechoic chamber and lab environment are shown in Figures 3.4b and 3.4c respectively.

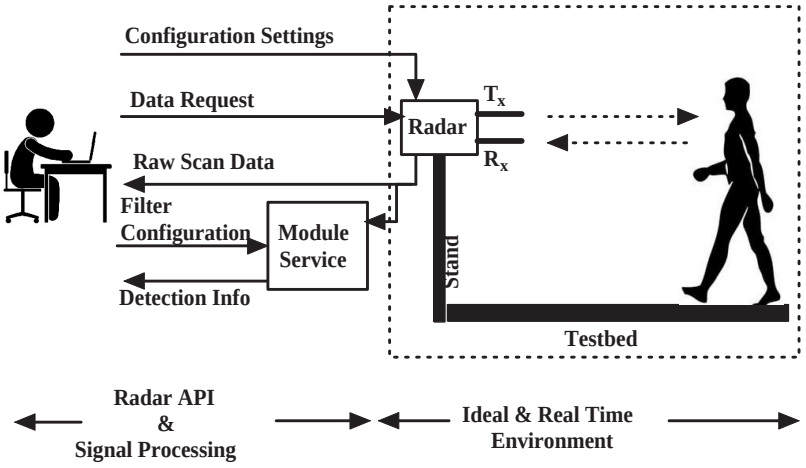

Figure 3.3: Schematic diagram of the proposed system setup.

The module box is connected to the PC/laptop with USB 2.0 through micro-B USB. Once, the radar module is configured then the participants are requested to walk in front of radar and raw data from the motion scans are accumulated through the RAPI. Also, the module service of the radar is configured to obtain detection information applying finite impulse response (FIR) filter of the moving participants. A four tap FIR filter has been configured for the experimental purpose where the taps are computed on the 3^{rd} order bandpass filtered data. A detection is reported when the output (=FIR filtered data $\times$ threshold) is greater than the average of previous 100 scans in each bin. The received raw scan data along with the detection information have been post-processed further to extract relevant gait parameters. The post-processing of UWB gait is discussed thoroughly in discussed in Chapter 4 and Chapter 5.

(a) UWB P410 radar module.

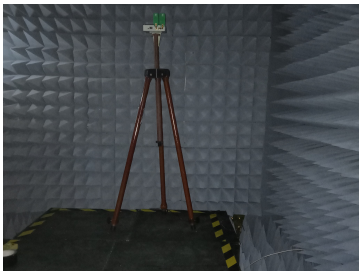

(b) Anechoic chamber.

(c) Normal environment.

Figure 3.4: The UWB module and both tested environments during data collection.

3.4 Device & Device Configuration: PulsON P410

The device is a UWB monostatic pulsed Doppler radio transceiver. The module utilizes TW-TOF omni-directional range measurement techniques have been employed here as hybrid ranging radio and a radar sensor device to non-intrusively measure the human gait. The device has been configured before data collection and the same configuration has been maintained for both the chosen (tested) environments. The device configuration has been detailed in Table 3.2. To avail of the large bandwidth of UWB it employs base band signal of nanosecond duration pulses and appropriate choice of UWB pulse shape has ability to adapt the multipath effect. Thus, the PulsON P410 module generates Gaussian pulses (shown in Figure 3.5) and transmits first order derivative of Gaussian pulse which provides high power efficiency by delivering extremely low power spectral density (PSD) to mitigate the influence of multipath environment. In addition, the nanosecond duration Gaussian pulses have low duty cycle that results high pulse repetition rate (PRR) of 10 MHz and enables vastly improved detection of human movements.

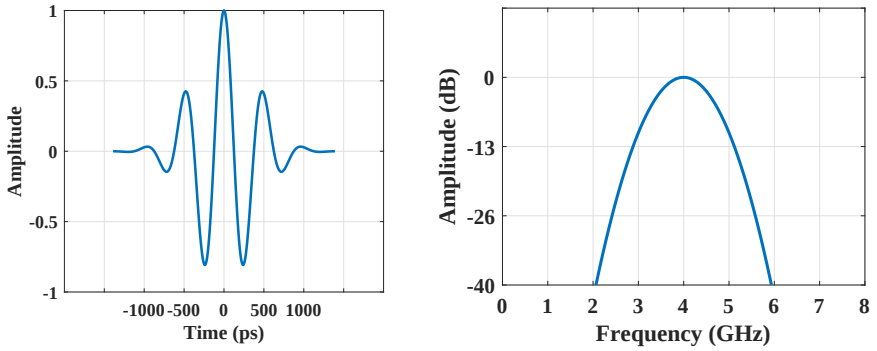

(a) Time domain. (b) Frequency domain.

Figure 3.5: Transmitted UWB pulse waveform.

It transmits radio frequency (RF) from a lower limit frequency f_L=3.1 GHz to the upper frequency limit f_U=5.3 GHz, with the centre frequency at f_C=4.3 GHz, and a bandwidth of $(f_U - f_L)$=2.2 GHz. According to the definition of UWB systems [104], the fractional bandwidth of a device should be more than 50%, in case of P410 device, $\frac{f_U - f_L}{f_C} = \frac{5.3-3.1}{4.3} = 51.16\%$, which follows FCC restrictions [98] for power. Transmission power to the antenna port is specified as -12.64 dBm for safe RF transmission, which abides with FCC regulations [98]. The scan time window for this experiment is 87.84 nanoseconds (ns) long, but the first 5 ns of the waveform contains noise because of the

direct path interference between transmitter and receiver antenna, thus the waveform during the first 5 ns is filtered from subsequent analysis.

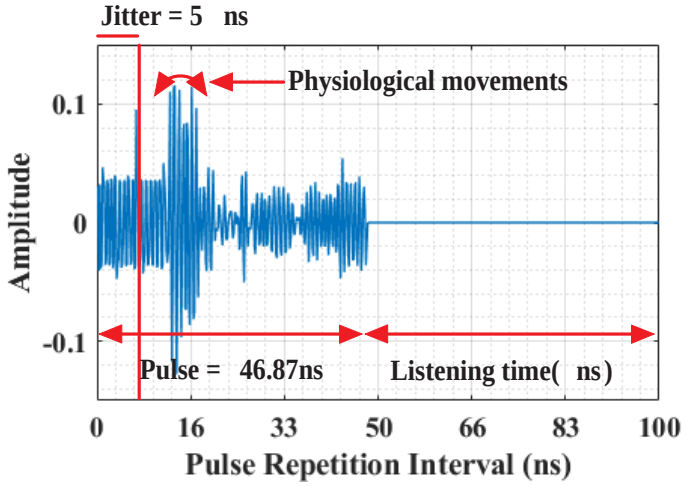

Figure 3.6: A received IR-UWB pulse and associated characteristics.

The pulse integration index (PII) has been set to 15 which allows the module to integrate $2^{15} = 32768$ pulses to cover 360° orientation, maximizing the usable signal to noise ratio (SNR). A typical received pulse is shown in Figure 3.6 to demonstrate the characteristics of received signal where, the x-axis indicates pulse propagation delay (or, pulse width) of 46.87 ns and a pulse repetition interval (PRI) of approximately 100 ns. The y-axis represents normalised amplitude of the received waves. The waveforms are sampled in 61 picoseconds (ps) frames, which results in a sampling frequency f_s=16.39 GHz and ensures PRR of 10 MHz. The pulse width in the current settings is 46.87 ns where, first 5 ns of the waveform contains noise because of the direct path interference between the transmitter and receiver antenna, and then physiological movements (potential targets) occur with higher amplitude or reflectivity. The scan interval is set to 25000 μs.

3.5 Corroboration of Results

The results obtained from the proposed model have been corroborated by measuring the same gait parameters with the existing device and algorithms. Each instrument contains it's own error by its varying nature besides the algorithms used. Thus, smartphone sensor applications have been used to support the outcomes of 2D gait identification (discussed in Chapter 4) and Microsoft Kinect Xbox sensor module has been used to support the results of 3D gait identification (discussed in Chapter 5). Differences has

Table 3.2: Parameter setting of the experiment.

Parameter	Values
Center frequency	4.3 GHz
Frequency range	3.1 GHz to 5.3 GHz
PII	15
SNR	75 dB
Scan interval	25 milliseconds
Sampling frequency	16.39 GHz
Pulse Repetition Interval (PRI)	100 nanoseconds (approx)
Transmit power	-12.64 dBm
Radar area coverage	upto 10 meter
Number of antennas	one T_x and one R_x
Ambient operating temperature	between 0°C to 70°C [105]

been determined between the outcomes of the proposed work and smartphone sensors in 2D gait identification, whereas Bland and Altman (B&A) statistics has been employed in the case of 3D gait detection. Theoretical backgrounds of the proposed work, error calculation, and B&A analysis have been demonstrated in the respective chapters. The overview and configuration settings of the existing methods for gait identification have been discussed in the following sections.

3.5.1 Smartphone Sensors

Three obtained parameters have been corroborated via popular smartphone applications. The parameters, walking speed, traversed distance during the observation period, and lower limb orientation have been compared with the outputs of accelerometer sensor, Samsung health application, and a gyroscope sensor. Each participant was asked to walk, carrying two smartphones and turning these applications on during their walking phase in both the ideal and normal environment, while the UWB system is also on. The accelerometer provided linear acceleration, with the Samsung health application delivering covered distance within a fixed time frame, and the gyroscope providing azimuth, pitch, and roll information. The average velocity of an individual has been determined from the average acceleration found the accelerometer and used for validation purpose against our UWB method. The distance covered within 30 seconds of the observation by an individual was compared with the distance determined by the Samsung health application. This work currently does not distinguish the left and right side information

thus, the absolute of azimuth (positive or negative) provided by gyroscope sensor has been employed for the validation purpose of azimuths measured by the proposed work.

3.5.2 Microsoft Kinect Xbox One

The outcomes of the proposed 3D model have been supported by employing the Microsoft Kinect Xbox One. It includes 3D imaging and employs time of flight (TOF) technology to deliver high resolution, low latency, light independent 3D image sensing [106, 107]. Kinect captures 3D human motion and track skeleton of human body using color and depth sensors. The proposed work aims to characterize human gait in a non-intrusive manner so, the device has been calibrated to obtain color and skeleton only from the video. Frames per second (FPS) has been fixed at 30 for color and depth sensor for video acquisition. The camera has the field view of 70° horizontal and 60° vertical operates at range from 0.8 to 4.2 meters from the device. It tracks the skeleton from the moving body posture (as shown in Figure 3.7) and provides 3D joint coordinates. Figure 3.7a shows the hardware device of Kinect module, Figure 3.7b displays the way it has been used during experiment, Figure 3.7c and Figure 3.7d demonstrates the tracked human skeleton and joints respectively. The Kinect sensor delivers 20 skeletal data (3D joint coordinates) at standing and 10 skeletal data at sitting condition from body posture. This skeletonization process is similar to the proposed prototype which supports the work through the Kinect sensor. Figure 3.7d shows the 20 joints (white markers) from a human body where the validation process has used only four joints from lower limb of a human body such as the hip left, knee left, hip right, and knee right. Then vector algebra has been employed on these joints to determine angles between the thighs to validate the proposed outcomes.

3.6 Conclusion

All the experiments have been conducted by considering the standard ethical guidelines in a controlled environment via non-intrusive, non-contact method. The chapter provides information on the participant profiles, configuration of instruments, and the data collection processes. Although some researchers have already used this technology but the measurements are limited to few gait parameters, which are unable to explore the

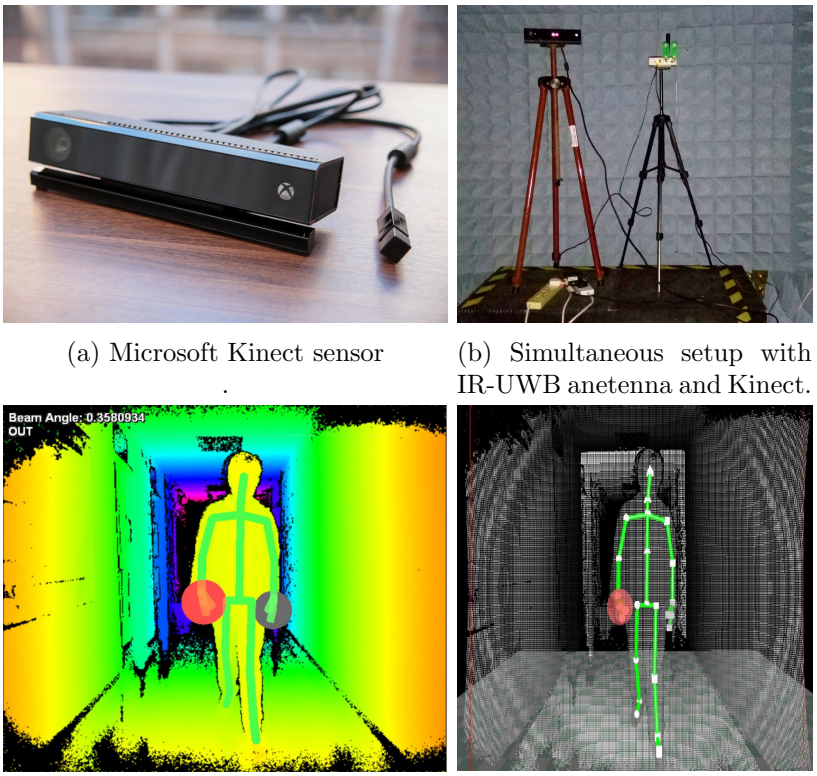

(a) Microsoft Kinect sensor .

(b) Simultaneous setup with IR-UWB anetenna and Kinect.

(c) Video frame from color sensor .

(d) Video frame from depth sensor (i.e., skeleton).

Figure 3.7: Microsoft Kinect and sample video frame of human gait tracked through Kinect color and depth sensor.

actual essence of human walk. Thus, the potentiality of UWB in gait identification is underexplored in literature, which is the main focus of this research. Processing of data with detailed theoretical background and algorithms have been demonstrated later in the respective chapters, where the biomechanical gait parameters have been explained. Though, the experiment performed in the anechoic chamber are not affected by multi-path reflection, the challenges such as those are faced in the normal environment. The transformation of data through developed model appears efficient and effective for both the environments. The results have been corroborated through existing measurement systems. Expensive gait and performance analysis laboratories and chambers are not always possible to setup. Thus the performance of the developed model in normal environment may be an efficient and robust gait identification for clinical/domestic use in future.

References

[98] Federal Communications Commission. "In the matter of revision of part 15 of the commission's rules regarding ultra-wideband transmission systems". In: *First Report And Order, ET Docket 98-153* (2002).

[99] General Assembly of the World Medical Association et al. "World Medical Association Declaration of Helsinki: ethical principles for medical research involving human subjects." In: *The Journal of the American College of Dentists* 81.3 (2014), p. 14.

[100] Soumya P Rana et al. "UWB localization employing supervised learning method". In: *IEEE 17th International Conference on Ubiquitous Wireless Broadband (ICUWB)*. Salamanca, Spain, 2017.

[101] Soumya P Rana et al. "Remote Vital Sign Recognition Through Machine Learning Augmented UWB". In: *IET 12th European Conference on Antennas and Propagation (EuCAP)*. London, United Kingdom, April, 2018.

[102] Soumya P Rana et al. "Signature Inspired Home Environments Monitoring System Using IR-UWB Technology". In: *Sensors* 19.2 (2019), p. 385.

[103] Soumya P Rana et al. "ITERATOR: A 3D Gait Identification from IR-UWB Technology". In: *IEEE 41st International Engineering in Medicine and Biology Conference (EMBC)*. Berlin, Germany, 2019.

[104] James D Taylor. *Introduction to ultra-wideband radar systems*. CRC press, 1994.

[105] *Monostatic Radar Module Reconfiguration and Evaluation Tool (MRM RET) User Guide*. https://www.timedomain.com. Online accessed: January, 2017.

[106] *Kinect for Xbox One*. https://www.xbox.com/en-GB/xbox-one/accessories/kinect. Online accessed: April, 2018.

[107] John Sell and Patrick O'Connor. "The xbox one system on a chip and kinect sensor". In: *IEEE Micro* 34.2 (2014), pp. 44–53.

Chapter 4

2D Gait Identification Employing IR-UWB

The chapter demonstrates human gait detection and parameter extraction from impulse radio ultra wideband (IR-UWB) technology using the device configuration presented in Chapter 3. Thus, the work aims to characterise gait biomechanics through the signal processing IR-UWB pulsed responses. Radar principles permit the determination of the range of a human while walking in front of the radar. Though, each pulse has its own range, azimuth, and elevation in a 3D plane, understanding and interpreting this coordinate system is a challenging task. Thus, a mathematical model has been prototyped and presented in this chapter which calculates the height where the pulse back-scatters from human motion. The height has been determined from the change of range over time and employing spherical trigonometry. The height information has further been augmented with subjective information recorded during data collection process to identify lower limb motion. This is a 2D gait identification approach since the work only involves range and height to realise gait where no other dimensions (e.g., a dimension that indicates width of motion) are involved. The approach filters gait patterns from other simultaneous biomechanical activities such as heartrate, breathing, and arm movements. The proposed work has been realized in both ideal (anechoic chamber) and normal environment to demonstrate its efficiency and robustness. The resulting gait parameters (walking speed, leg orientation, and traversed distance) have been corroborated via popular smartphone applications to enhance the outcomes. The relevant theories and results are detailed in the following sections.

4.1 Method

An approach to perform and analyse the non-stationary and multi-component radar signals back-scattered from human motions, specifically the lower limb are explained in this chapter. The received signals from physiological movements have been processed using spherical trigonometric model, radar principles and short term fourier transformation (STFT). A flow chart of the data processing procedure is provided in Figure 4.1. Here, the height of a physiological action has been determined and used to differentiate between lower and upper body sections. The orientation of the lower limb has also been calculated by azimuth or angle of arrival (AOA) measurement. Radar principles have been further employed to the pulsed waves back-scattered from human gait (includes both the thigh and shank motion) to calculate parameters such as, walking speed, step length, and total traversed distance. Subsequently, STFT has been performed to derive parameters such as, step frequency and step phase of human gait from radar time-frequency response. The theoretical background of the methods used has been established and presented in the following subsections.

4.1.1 Azimuth and Elevation Angles

To assist in the differentiation of body areas, azimuth and elevation angles are considered. Figure 4.2a and 4.2b show the elevation angle at a particular time, where ΔOAB, $\Delta OAB'$, ΔOCB, and $\Delta OCB'$ are drawn from the received pulsed radar waveform. Here, O is considered the radar receiver, which is fixed at a point of height OP' from the ground. Therefore, BC and CB' represent the height of a moving object from the radar line of sight (LOS) OA. The moving body section is elevated from the radar LOS at an angle θ and below the LOS at an angle θ'. The point O represents the radar transceiver so the area $OBAB$' of Figure 4.2a and area $OBCB'$ demonstrate an antenna section of the beamwidth of an omnidirectional radiation pattern where, the lines OA and OC divides the beam into two equal segments of radiation pattern. Hence, geometrically the OP and OP' are equal in length. Thus, $\Delta OAB \cong \Delta OAB'$ and $\Delta OCB \cong \Delta OCB'$, therefore the height BC and CB' can be determined from trigonometric relationships. Only the calculation of BC from ΔOAB is explained. Let, the angle between BC and OB be α. The travelled distances are OA, OB, and OB' in propagation delays t_1, t_2 and t_2' by the pulses, where $t_1 > t_2$, $t_1 > t_2'$ and $OA > OB$,

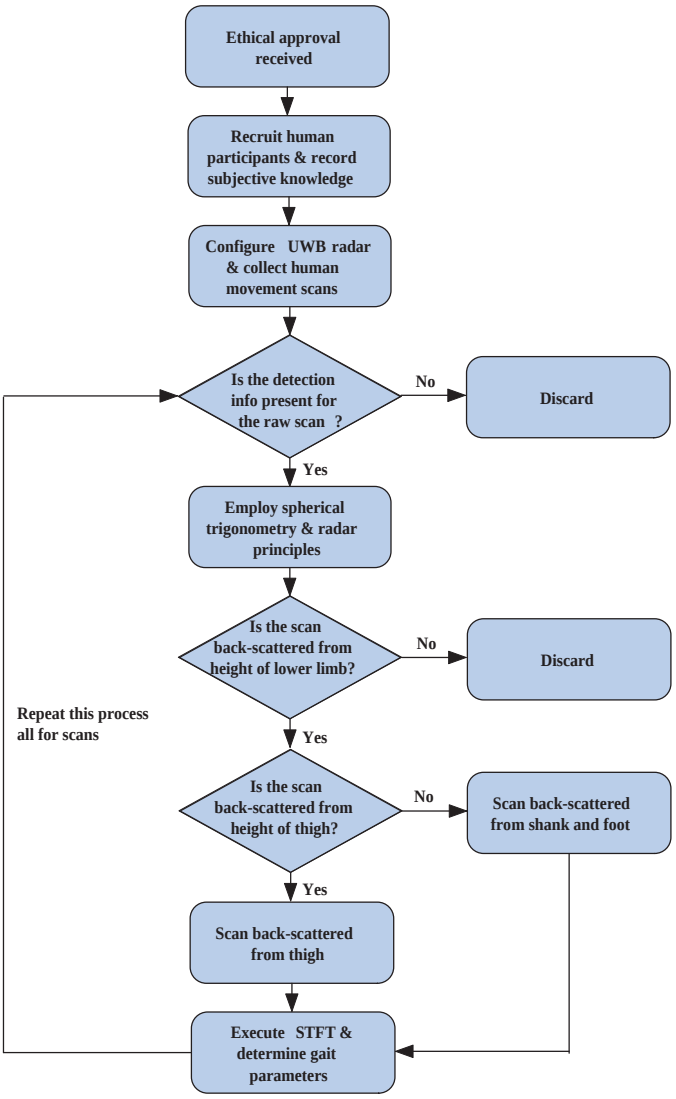

Figure 4.1: The flowchart of processing UWB data and extracting gait information.

$OA > OB'$. Thus, the change of distance is $(OA - OB) = \Delta d$, the change of time is $(t_1 - t_2) = \Delta t$, and speed of light or pulse is c. Therefore, a pulse can travel the distance in Δt is $BC = \Delta \times c$. From the trigonometric ratio in right triangle ΔOCB,

$$\begin{aligned} \cos\alpha = \frac{BC}{OB} &\Rightarrow BC = OB \times \cos\alpha \\ &\Rightarrow \alpha = \cos^{-1}\left[\frac{\Delta t \times c}{OB}\right] \end{aligned} \tag{4.1}$$

If the height of a moving object from the ground at a particular time is h then,

$$h = |OP - OB \times \cos\alpha| \tag{4.2}$$

This calculation has same outcome when $t_1 < t_2$, $t_1 < t_2'$ and $OA < OB$, $OA < OB'$.

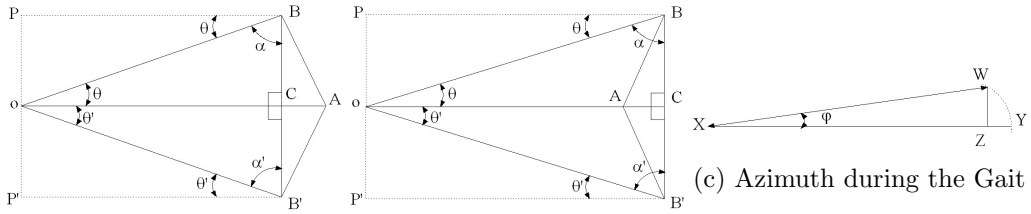

(a) Gait towards radar (b) Gait away from radar (c) Azimuth during the Gait

Figure 4.2: Elevation and azimuth angle during the gait.

Figure 4.2c displays the calculation of azimuth angle to determine the position, or orientation of moving limbs towards the radar. The spherical system measures the azimuth angle in a counter clockwise direction from the exact north of the receiver and is denoted by ϕ. Let the moving limb be deviated at an angle ϕ, where the travelled distances are XY and XW in propagation delay t_1, t_2. So, the change of distance is $(XY - XW) = YZ$ at the time interval $(t_1 - t_2) = \Delta t$. The object as deviated from the exact north of the receiver. Now, YZ is approximately equivalent to the arc YW created by the object at angle ϕ. Therefore, ϕ is calculated from the radian measure, and equivalent degree conversion being,

$$\phi = \frac{YZ \times 360^\circ}{XY \times 2 \times \pi} \tag{4.3}$$

4.1.2 Range and Velocity

The height of movement has been identified by the developed trigonometric calculations (Eq. 4.2) when the leg length of an individual is known. The trigonometric calculations evolve from the change of range, where the target range R is determined by the round-trip time of the received radar signal. Therefore, the range of the moving body section is evaluated via $R = \frac{c\triangle T}{2}$ where, $c = 3 \times 10^8$ meter/ seconds is the speed of light or radio pulse, and $\triangle T$ is the propagation delay(s). Walking velocity is obtained by measuring the Doppler frequency shift, with the help of track information found from the radar measurements of the subject's location over time period. Thus, the velocity

of an object is determined by $f_d = \frac{2v_p}{\lambda}$ where, f_d is the difference between the frequency of transmitted and received wave or Doppler shift, v_p is the radial component of the velocity, and λ is the wavelength of the transmitted wave. The range R decreases when the person comes closer to the radar and f_d increases and vice versa [108]. Therefore, if the range at t_1 and t_2 time are R_1 and R_2 respectively then, the change in distance or range is $(R_1 - R_2)$ which, describes the distance covered by the shank in $(t_1 - t_2)$ time, and maximum change of distance by the shanks is the step length of a stride. The change in range $(R_1 - R_2)$ has been summed up each time for shanks to get the total distance covered by an individual.

4.1.3 Short term fourier transformation (STFT)

As the spectral content of the UWB radar generated waveforms are non-stationary, applying the discrete Fourier transform (DFT) over a long window does not reveal transitions in the movement behaviour. To solve this issue, we can apply the DFT over short periods of time for which the radar signals can be considered stationary. This can be observed as a time-frequency trade-off. The DFT of the windowed radar waveform is defined as:

$$\begin{aligned} S(m,k) = S(m,\omega) \mid_{\omega=\frac{2\pi}{N}k} \\ = \textstyle\sum_{n=-\infty}^{\infty} s(n)w(n-m)e^{-j\omega n} \mid_{\omega=\frac{2\pi}{N}k} \\ = \textstyle\sum_{n=-\infty}^{\infty} s(n)w(n-m)e^{-j\frac{2\pi}{N}kn} \end{aligned} \quad (4.4)$$

Where the continuous spectrum of length N having k real cosine time sequence cycles, $s(n)$ is the received sequence obtained from the corresponding environment of the experiment sampled at f_s, $w(n-m)$ is the window function starting at discrete time $m, \omega = 2\pi f$ is the angular frequency with discrete values of $\omega = \frac{2\pi}{N}k$. Here, we are using the Hamming window [109] length of 40 (experimentally fixed) which is characterised by the following equation:

$$w(n) = 0.54 - 0.46\cos(\frac{2\pi n}{N-1}) \quad (4.5)$$

The discrete STFT [110] is used to create a collection of sequences, each corresponding to the frequency components of $s(n)$ falling within a particular frequency band which corresponds to a certain activity or physiological signal.

4.1.4 Signal to Noise Ratio

The radar takes a scan period or scan training period (STP) to determine the background noise before any detection occurs. The background noise strength P_{noi} is measured from the received waveforms during STP. The received signal strength P_{sig} is determined while radar detects the physiological movements. The signal to noise ratio (SNR) [108] is defined as the ratio of the power of a received signal and the power of background noise using $SNR = \frac{P_{sig}}{P_{noi}}$.

4.1.5 Algorithm Analysis

A high level description of the proposed study has been provided through the pseudo code presented in Algorithm 1. The relevant theoretical information has been outlined in Section 4.1.1 to 4.1.4. The configuration setting of the radar module and desired UWB gait parameters are listed in lines 1 to 9. Then, the pulses have been handled by employing radar detection information to obtain the raw signal amplitude and propagation delay and is described by line numbers 11 to 14. The propagation delay has been used further to determine the range of the physical action taking place around the radar module and this is executed via line numbers 15 to 22. Subsequently, the range of an action with respect to propagation delay has been further utilised to calculate the height and azimuth of that physical movement, outlined in line numbers 23 to 24. The obtained height of the back-scattered pulses have then been applied to distinguish the lower limb movement from other body sections and associated amplitudes have been transformed by STFT to determine the frequency of that movement, narrated in line number 26 to 28. Finally, the gait parameters have been identified and used for further analysis. Here, execution time of implementation is proportional to the square of scan number (or, number of received pulses). Thus, the study requires quadratic time which costs $O(n^2)$ running time.

Algorithm 1 Pseudo code of proposed method

Require: *Configure radar module (using Table 3.2)*
Require: *Scan data from RCM & MRM module*
Total number of scans $= NoS$
Number of datapoints per scan $= D_{PS}$
Array of raw amplitudes $= R_{amp}$
Detection flag $= D_{flag}$
Array of detection index $= D_{info}$
Speed of light $c = 3 \times 10^8$ *meters/second*
Length of leg of a person $= LoL$
Length of thigh of a person $= LoT$
Length of shank of a person $= LoS$
for all $Scan = 1$ **to** NoS **do**
  if $D_{flag} == TRUE$ **then**
    Take R_{amp} & D_{info}
    Two way time of flight for first detection $t_1 = 0$
    Two way time of flight for next detection $t_2 = 0$
    for all $D_{info} = 1$ **to** *Length of* D_{info} **do**
      if $D_{info} == 1$ **then**
        $t_1 = D_{info} \times 61$ *picoseconds*
      else
        $t_2 = D_{info} \times 61$ *picoseconds*
      end if
      Initial range $R_1 = \frac{c \times t_1}{2} \Leftarrow$ *Section 4.1.2*
      Range for t_2 *delay* $R_2 = \frac{c \times t_2}{2} \Leftarrow$ *Section 4.1.2*
      Determine height $h \Leftarrow$ *Equation 4.2*
      Determine Azimuth $\phi \Leftarrow$ *Equation 4.3*
    end for
    if $(h_{min} \geq 0)\&\&(h_{max} \leq LoS)$ **then**
      Scan backscattered from Shank
      do *STFT on* R_{amp} *to get frequency* $\Leftarrow$ *Section 4.1.3*
    end if
  end if
end for
Tabulate average of gait parameters
Plot gait route from Doppler effect

4.1.6 Result Corroboration

To establish and understand boundary conditions, the obtained results have been corroborated via popular smartphone applications. The gait parameters such as, walking speed, total traversed distance, and lower limb orientation have been determined using accelerometer sensor, Samsung health application, and gyroscope sensor respectively and to compare the outcomes with proposed work. Each participant has been requested to walk, carrying two smartphones and turning these applications on during the experiments (in ideal and normal environment) while the proposed UWB system was also

on. The accelerometer provides linear acceleration, Samsung health application delivers total covered distance within the observation time frame, and the gyroscope provides azimuth, pitch, and roll information. The average velocity of a subject has been calculated from the average acceleration obtained from the accelerometer and used for comparison purpose against the proposed UWB prototype. The distance covered within 30 seconds of observation time by an individual has been compared with the distance determined by the Samsung health application. The prototype does not distinguish between left and right side thus, the absolute of azimuth (positive or negative) provided by gyroscope sensor has been employed for the validation purpose of azimuths measured by the proposed work.

4.2 Result Analysis

Radar responses for physiological movements have been gathered and studied through the proposed spherical trigonometric system (described in Section 4.1.1) and radar principles (described in Section 4.1.2). Further, the height of the reflected pulses has been determined and subsequently, the recorded anatomical measurements (of Table 3.1) have been used to identify pulsed waveforms back-scattered from different areas of the body e.g., pulse reflections from the upper body includes breathing, heartbeat (chest movement), and arm swinging whereas, the pulse reflections from the lower body movement includes palm of hand, thigh, shank, and ankle movements. As the focus of this chapter is on gait parameter identification the pulses reflected within the height of shank and thigh have been considered for each participant. However, arm swinging and walking are two interrelated physiological events where, arms can cover some portion of the legs below the waist creating some redundancy in distinguishing the arm and thigh. Also, the shank reflects standard osteometrics better than the thigh, therefore shank movement has solely been considered to characterize an individual's gait pattern. The pulsed waveforms back-scattered from the shank has been transformed using STFT to determine the frequency of an event that occurs for the movement of shank. The waveforms reflected above the shank and thigh obviously include other physiological actions such as, arm movement, heart rate and breathing patterns which have been filtered out for this work. Thus, the height of body section has been considered to discriminate the gait from other bio-mechanical activities. The participants were asked to walk at different

paces (i.e., slow, medium, and fast) in both the ideal and normal environment to validate the proposed work. Corresponding results have been presented in the following sections.

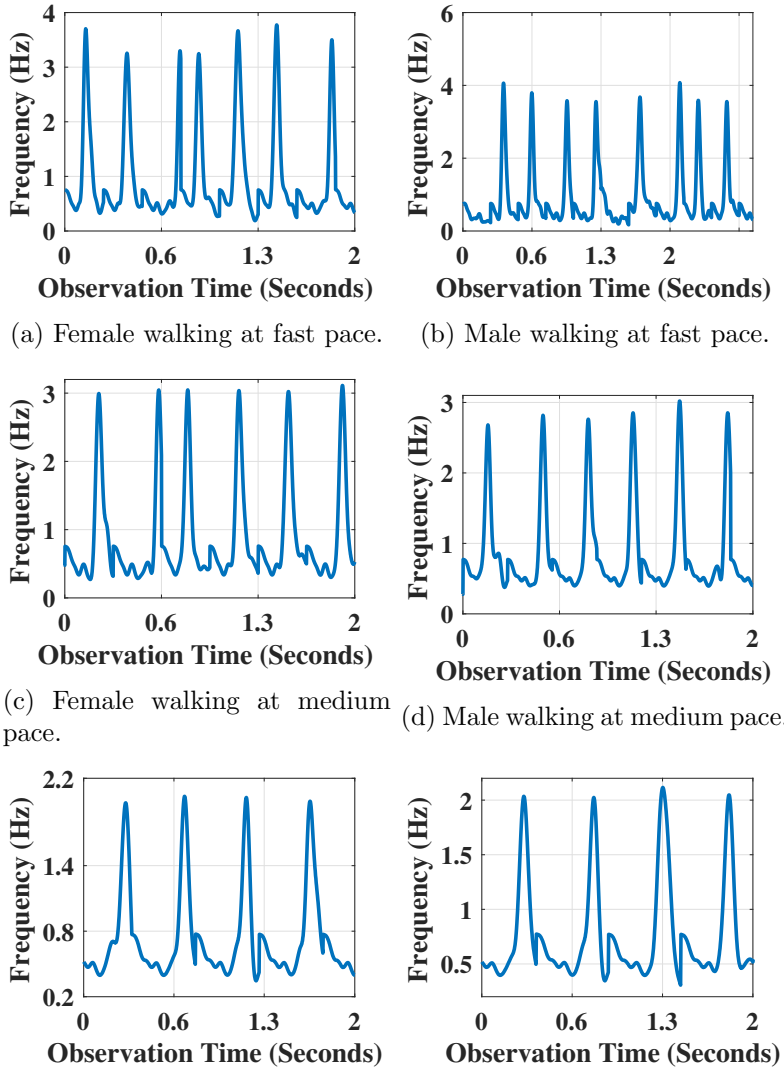

(a) Female walking at fast pace.

(b) Male walking at fast pace.

(c) Female walking at medium pace.

(d) Male walking at medium pace.

(e) Female walking at slow pace.

(f) Male walking at slow pace.

Figure 4.3: Shank movement frequency of participants walking at different pace obtained through UWB radar in ideal environment.

4.2.1 Results from Anechoic Chamber

Pulses backscatter from the human body when individuals walk back and forth in front of the radar. These pulsed waveforms have been processed in the following manner shown in Figure 4.1. If a pulsed wave or signal has been identified as reflecting from the shank then it is considered for further processing, otherwise it's discarded. The first pulse of each signal reflecting from the shank has been transformed by STFT,

characterizing the step movement of human gait. Figure 4.3 shows the frequency of lower leg movement obtained from the proposed STFT for an observation time of 2 seconds when the walking speed of participants are fast, medium and slow. The results for both female and male participants have been included here. The figure shows the repetitive shank movement demonstrating the step frequency (number of steps per second) of human gait. Figures 4.3a and 4.3b show the step frequency at a fast walking pace, which reaches 3.9 Hz for females and 4 Hz for male participants. Figure 4.3c and 4.3d displays the shank movement at a medium walking pace which results approximately 3 Hz for both female and male participants. Figure 4.3e and 4.3e demonstrates step frequency of approximately 2 Hz at slow walking pace for the participants. The variation of step frequency occurs when the participants reach one end of test bed and walk slowly to turnaround. For example, Figure 4.3a shows approximately 3.9 Hz initially but it decreases to 3.2 Hz when the person reached one end of the test bed and needed to slow down their walking speed. The step phase or the swing phase also has been determined (1/step frequency) from step frequency and detailed in Table 4.1 for all participants.

Table 4.1: Results of gait analysis from ideal environment.

No	S_f (Hz)	W_s (m/s)	C_a (c/min)	S_l (m)	T_d (m)	L_o (^{0})
1	3.033	1.527	181.892	0.501	45.603	±1.833
2	3.050	1.522	182.783	0.498	45.608	±1.714
3	3.003	1.500	180.030	0.499	45.000	±1.888
4	3.144	1.564	187.759	0.521	46.910	±1.876
5	2.954	1.469	176.398	0.489	44.072	±1.762
6	3.271	1.629	195.532	0.542	48.852	±1.954
7	2.815	1.400	168.026	0.466	41.980	±1.679
8	3.018	1.499	179.986	0.499	44.968	±1.798
9	2.990	1.489	178.790	0.496	44.669	±1.786
10	3.181	1.584	190.151	0.527	47.508	±1.900
11	3.193	1.589	190.749	0.529	47.657	±1.906
12	2.898	1.440	172.810	0.479	43.175	±1.727
13	3.040	1.514	181.779	0.504	45.416	±1.816
14	3.025	1.504	180.583	0.501	45.117	±1.804
15	3.122	1.554	186.563	0.517	46.611	±1.864

The relation between SNR and range is plotted in Figure 4.4 for two female and two male participants. The noise figure is evaluated from the STP and SNR is measured from the scans with the help of detection information and logarithmic relation is found between SNR and range. Here, the length of test bed in anechoic chamber is 3 meters. The module employs coherent pulse integration, as expected the system provides improved

SNR with number of pulses integrated to accommodate itself with background noise and achieve a certain range with logarithmically decreased SNR.

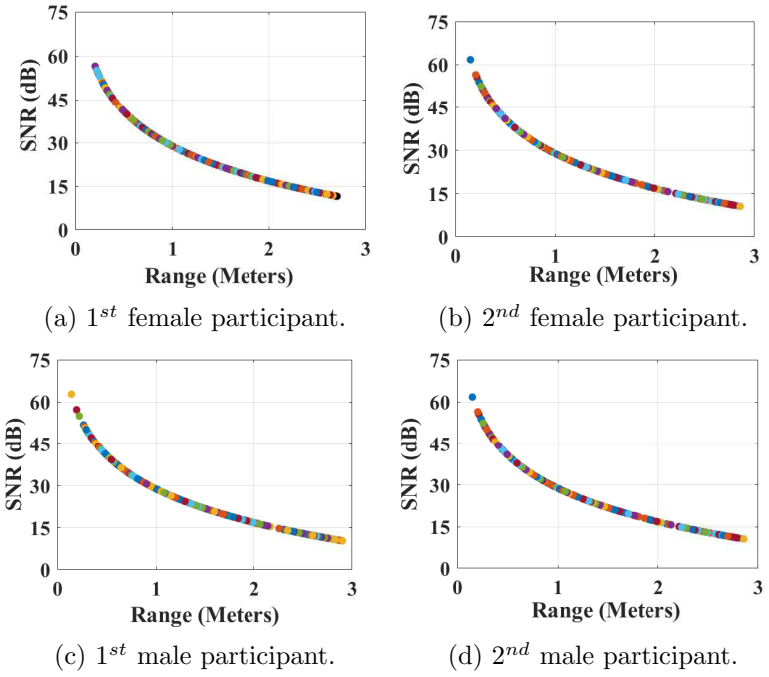

(a) 1^{st} female participant. (b) 2^{nd} female participant.

(c) 1^{st} male participant. (d) 2^{nd} male participant.

Figure 4.4: SNR and range relationship in the ideal environment during movement.

The route of participant's gait has been determined from the Doppler effect. The Doppler shift f_d (described in Section 4.1.2) has been calculated during the observation time and plotted to check the gait route of a person. The identified signals from shanks have been processed through STFT and plotted in Figure 4.5 as received over time, where the higher average movement in anechoic environment results prominent yellow color. The upside and downside of Figure 4.5a, 4.5b, 4.5c, and 4.5d specify the nearest and furthest point from radar during a walk two female and two male participants. Therefore, x-axis represents the increment of time with received signals. The total distance traversed by an individual has been obtained from summing up the changes in range during locomotion in front of the radar.

Table 4.1 includes the average gait parameters obtained from the experiment for human participants in an anechoic chamber/ideal environment. Seven parameters have been calculated from the proposed experimental data to define the human gait. The parameters such as, step length (S_l), cadence (C_a), stride length (ST_l), walking speed (W_s), and lower limb orientation (L_o) have been determined along with step frequency (S_f), and total traversed distance (T_d). The maximum change in distance by the shanks describe

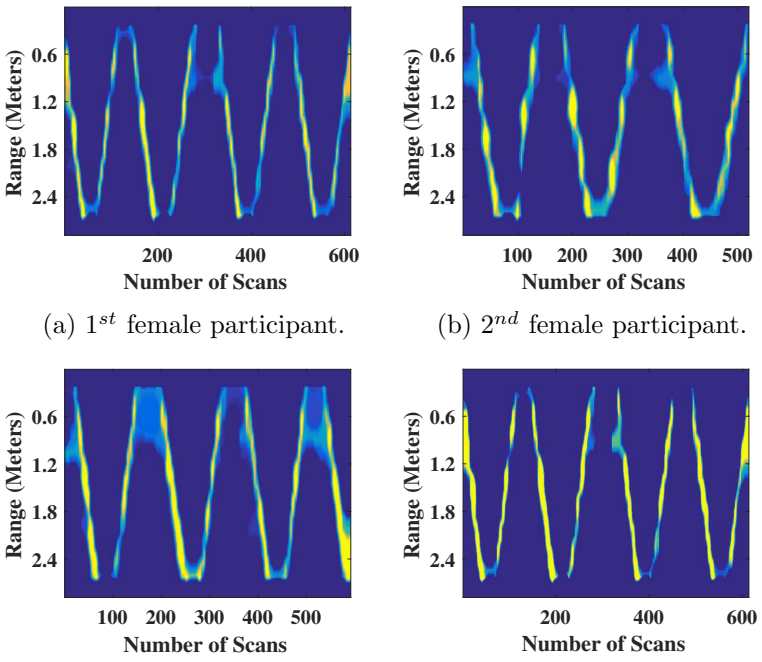

(a) 1^{st} female participant. (b) 2^{nd} female participant.

(c) 1^{st} male participant. (d) 2^{nd} male participant.

Figure 4.5: Radar movement patterns on test bed in anechoic chamber.

the step length. Cadence is the number of revolutions per minute (RPM) i.e., the number of steps per minute has been estimated from the gait frequency (i.e., cadence= step frequency×60). Walking speed has been obtained from the frequency shift (described in Section 4.1.2) for each human subject. The angle of arrival (AOA) or azimuths of pulses are calculated from the range and propagation delay (Eq.5.2) in spherical polar coordinates, providing a clear indication of the orientation of the moving lower limb (shank) with respect to the radar. The azimuth measurement provides the torso section orientation over 360° spherical plane where, 0° to 180° represent left hand side of antenna radiation pattern and 181° to 360° represents the right hand side of antenna radiation pattern. If the azimuth or AoA is more than 180° has been scaled to the supplementary angle for the interval 181° to 360° and denoted by negative angle sign (-ve) to signify the orientation of right side from the radar transmitter-receiver. Table 4.1 includes the average orientation of the shank.

4.2.1.1 Result Corroboration for Anechoic Chamber

Figure 4.6 displays the comparison of proposed research with outcomes from the smartphone sensors and applications used. Figure 4.6a illustrates the individual's velocity

comparisons obtained from the anechoic chamber. The result variation has been found to be approximately 3%. Lower limb orientation is also a important characteristic for human locomotion which has been compared in Figure 4.6b for the anechoic environment. The differences found here is negligible. The traversed distance by an individual in this environment has been shown in Figure 4.6c. The overall variation of results are approximately within 5%.

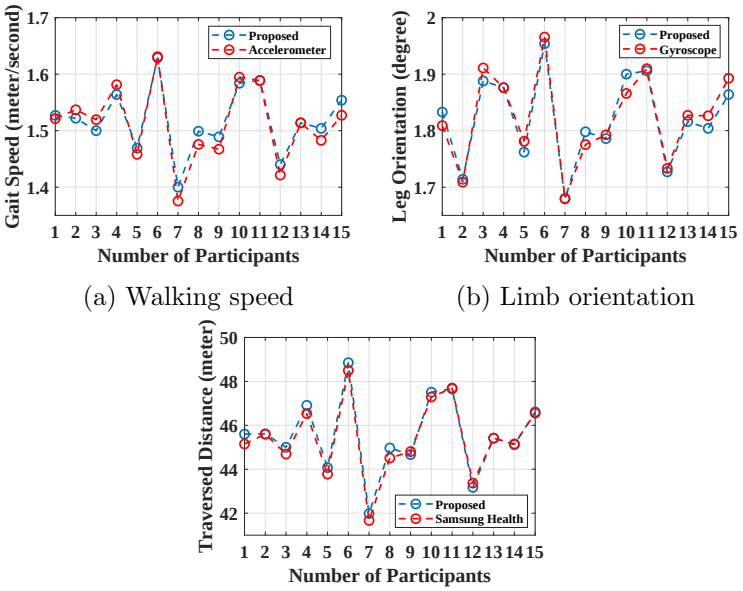

(a) Walking speed (b) Limb orientation

(c) Covered distance

Figure 4.6: Commercial and UWB method comparison of gait parameters identified by proposed method and obtained from smartphone applications in ideal environment.

4.2.2 Results from Multipath Environment

This section describes the results obtained from the real or normal environment, i.e. the laboratory room environment. To remain consistent, the same participants who participated in the anechoic chamber scenario have been involved again. The waveforms back-scattered from the shanks have been distinguished from other bio-mechanics activity in the same way as before. Figure 4.7 shows the frequency of lower leg movement attained from the proposed STFT for the observation time of 2 seconds when the walking speed of participants was in fast, medium and of a slow pace. The figure illustrates the repetition of shank movement when the persons walk along the test bed. Figure 4.7a, 4.7c, and 4.7e show the step frequency of female participants at different walking paces. Figures 4.7b, 4.7d, and 4.7f demonstrate the shank movement of males at

different walking paces. The step frequency and walking speed are interrelated processes thus, fast walking results in a greater number of steps and vice versa.

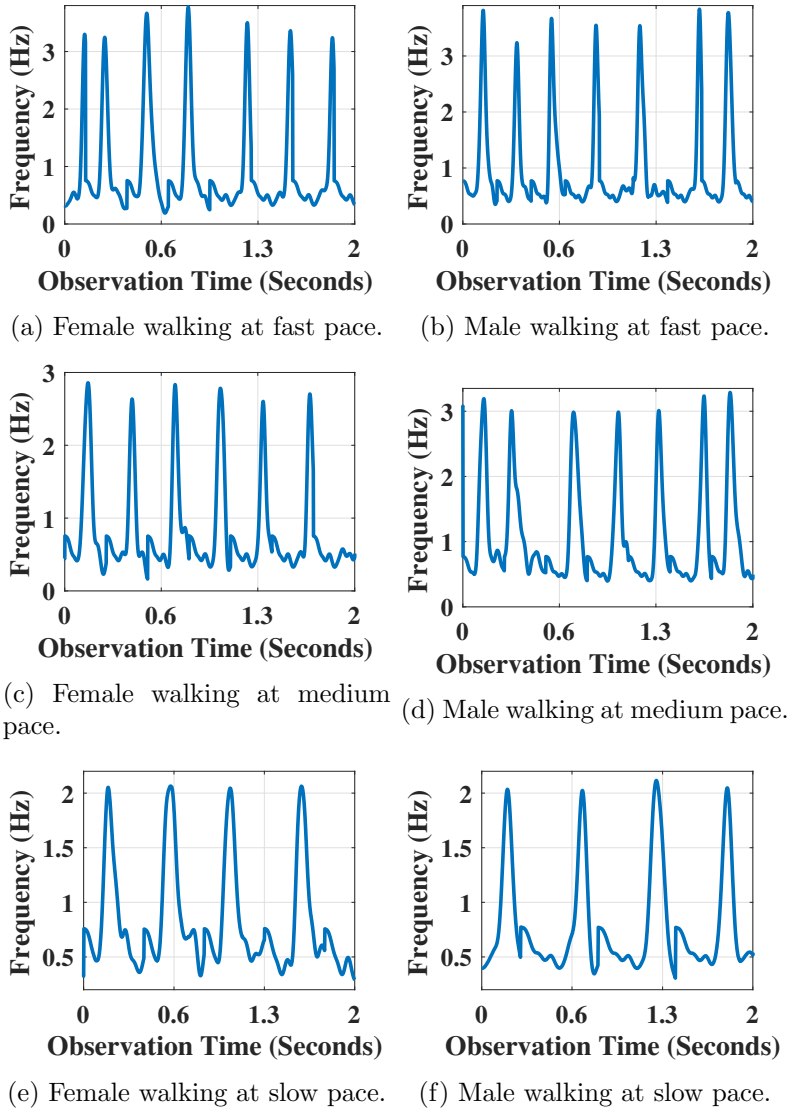

(a) Female walking at fast pace.

(b) Male walking at fast pace.

(c) Female walking at medium pace.

(d) Male walking at medium pace.

(e) Female walking at slow pace.

(f) Male walking at slow pace.

Figure 4.7: Shank movement frequency of participants walking at different pace obtained through UWB radar in multi-path environment.

The step frequency, or the number of steps in one minute reaches up to 4 Hz (240 steps/minute) during fast walking and approximately 2 Hz (120 steps/minute) during the slow walk for both female and male participants. The discrepancy of step frequency for a person has been found when the participant reaches one end of the test bed and walks slowly at that part to take a turn to continue their walk. The step phase has been calculated (1/step frequency) from step frequency and detailed in Table 4.2 for all participants.

Table 4.2: Results of gait analysis from multipath environment.

No	S_f (Hz)	W_s (m/s)	C_a (c/min)	S_l (m)	T_d (m)	L_o (^{0})
1	2.881	1.444	172.636	0.500	43.162	±1.926
2	3.033	1.520	181.898	0.497	45.447	±2.933
3	2.831	1.413	169.545	0.500	42.393	±2.771
4	3.176	1.582	190.268	0.561	47.572	±3.108
5	3.200	1.594	191.706	0.565	47.932	±3.132
6	2.946	1.467	176.507	0.521	44.132	±2.883
7	3.160	1.574	189.321	0.558	47.336	±3.093
8	3.147	1.568	188.542	0.556	47.141	±3.080
9	2.886	1.438	172.906	0.510	43.231	±2.825
10	2.863	1.426	171.523	0.506	42.885	±2.802
11	3.064	1.526	183.564	0.541	45.896	±2.999
12	3.308	1.648	198.218	0.585	49.560	±3.238
13	2.980	1.484	178.550	0.527	44.642	±2.917
14	3.110	1.54	186.326	0.550	46.587	±3.044
15	2.918	1.454	174.847	0.516	43.717	±2.856

The relationship between SNR and range in the real environment is plotted in Figure 4.8 for two female and two male participants. The noise figure evaluated from the STP and SNR is measured from the scans with the help of detection information. Here, the length of test bed in anechoic chamber is 6 meters. The module follows coherent pulse integration, the system provides improved SNR with number of pulses integrated to accommodate itself with background noise (collected during STP) and cover the said range with logarithmically decreased SNR.

The route of participant's gait has been determined from Doppler effect like that performed in the experiment carried out in the anechoic chamber. The Doppler shift f_d has been measured during the observation time and plotted to check the path of a human walk in the normal environment. Thus, the identified scans from the shank have been plotted as received in time in Figure 4.9, where the lower average movement in noisy environment results blurred yellow color. The top and bottom of Figure 4.9a, 4.9b, 4.9c, and 4.9d specify the nearest and furthest point from the radar respectively. These figures illustrate the repetitive route of a participants walk. Table 4.2 includes the average of parameters obtained from the experiment in normal or laboratory environment. The parameters of gait have been determined by following the same way in case of ideal environment.

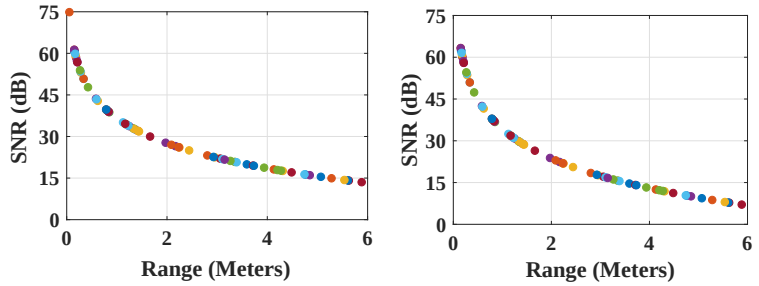

(a) 1^{st} female participant. (b) 2^{nd} female participant.

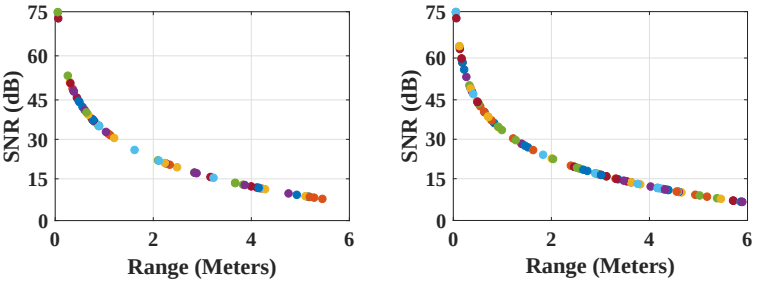

(c) 1^{st} male participant. (d) 2^{nd} male participant.

Figure 4.8: Relationship between SNR and range in multi-path environment during gait.

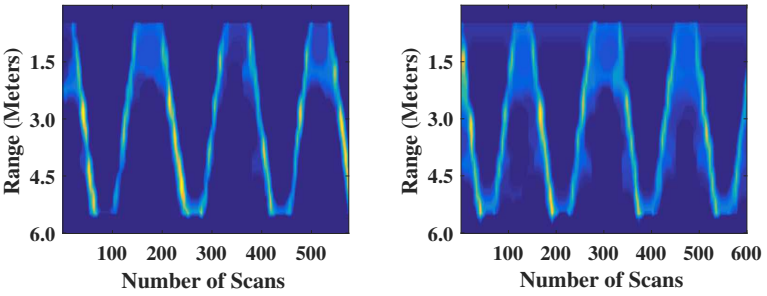

(a) 1^{st} female participant. (b) 2^{nd} female participant.

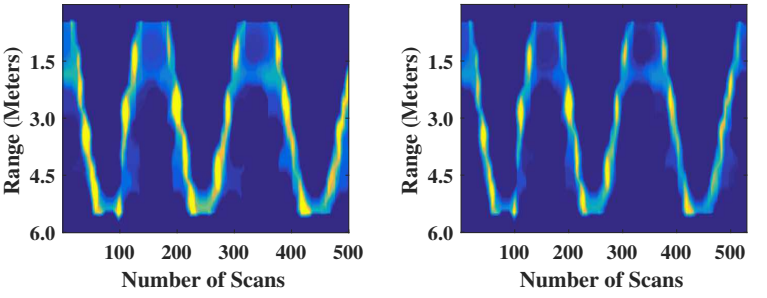

(c) 1^{st} male participant. (d) 2^{nd} male participant.

Figure 4.9: Movement patterns on test bed in normal environment.

4.2.2.1 Result Corroboration for multipath environment

Figure 4.10 shows the comparison of proposed outcomes with the outcomes of smartphone sensors and applications. Figure 4.10a demonstrate comparison of individual's

velocity obtained from and normal environment respectively where the result variation has been found less than 3%. Orientation of lower limb has been compared in Figure 4.10b. The traversed distance by an individual in normal environment has been presented in Figure 4.10c where the result variation is again within 5%.

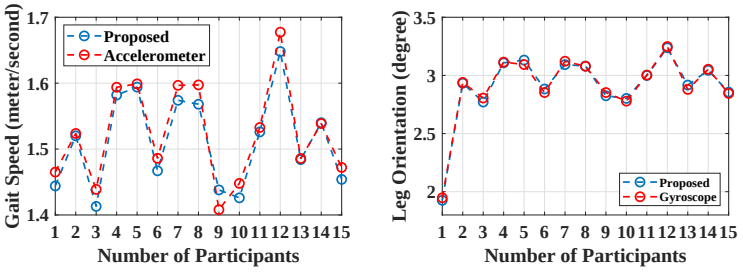

(a) Walking speed (b) Limb orientation

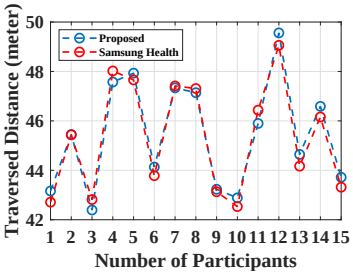

(c) Covered distance

Figure 4.10: Commercial and UWB method comparison of gait parameters identified by proposed method and obtained from smartphone applications in multi-path environment for the same experiments.

4.2.3 Result Comparison & Discussion

As expected, minor variations have been observed in gait parameter measurements between the outcomes of Table 4.1 and 4.2 in the cases of S_f, W_s, S_l, and T_d as defined in Section 4.2.1. The proposed model has been experimented in two different environments. The anechoic environment was dark with a narrow testbed (3 m), the participants were more cautious when asked to walk and turn during the requested sessions. However, the length of laboratory testbed was 6 m in bright conditions and participants walked with more confidence. This had an effect on walking pattern in with same participants. Gait is an interrelated and coordinated outcome of all lower limb sections, thus a change of behaviour provides reasons for dissimilar gait as well as different step length (S_l), step frequency (S_f), walking speed (W_s), etc. for the same person. Also, the reflecting elements of the real environment cause small-scale multipath effects which are a more realistic to test the model and account for the usual obstructions present in real life

scenarios. In the real environment, the receiver antenna sustains back-scattered pulses from the human body and reflected pulses from walls, book selves, tables, metals, etc. This creates off beam azimuth and range measurement for a leg movement which reflects in the average gait parameters presented in Table 4.2. Thus, gait parameters measured for each person in the anechoic chamber are more accurate than the laboratory environment. They are not realistic, importantly the model and subsequent tests have shown that gait could be measured in both settings accurately and can be realised from the validation procedure.

The work aims to propose an efficient, locally based radar system that can be used in home environment without any complex setup for gait monitoring, totally non-contact and non-intrusive based UWB gait identification technique comprising the heuristic understanding of spherical trigonometry and radar principles. In this study a comprehensive framework has been developed to identify different walking pattern types without hampering a person's privacy and comfort (no wearables). A number of healthy human walking patterns were involved for data accumulation in the two types of environments chosen (ideal and real). Due to the complexity of human gait processing radar signals, a new theory to calculate the height of a movement and employ them heuristically to differentiate upper and lower body movement has been developed. Further, all the different walking style (male and female) towards and away from the radar has been evaluated. The rigorous analysis made this gait identification system robust and precise. Additionally, the obtained outcomes of this investigation have been tested and validated to prove this method can create a powerful and productive human gait detection method that could be employed in work at home in harsh environments, opening up door to clinical studies, security, health monitoring and many more perspectives.

4.3 Conclusion

This chapter presents the first ever description and experimental demonstration of a non-contact pulsed UWB sensor system to identify and estimate human gait from other simultaneous bio-mechanic actions such as, arm swing, breathing and heart rates. A UWB radar sensor with in-house developed algorithms is used for data collection and processing. These signals are processed by STFT with fundamental radar principles employed to extract gait parameters including walking speed, step length, step phase,

that define the quality and type of locomotion of a person. Also, important parameter such as distance travelled is evaluated which is effective for long term gait and mobility quality monitoring. The results show the unique effectiveness and advantages of pulsed UWB radar to analyse the quality of movement in an autonomous way. The proposed prototype has some limitations. The radar threshold value for physiological movement detection (a numeric multiple to the transmitted power) plays a pivotal role in the experiment and has been decided experimentally by a trial-error approach. An inappropriate threshold results in unwanted movement detection, a too high threshold may miss slow joint and torso motion, whereas too low threshold detects more limb motion due to multipath reflection especially in normal environment. Thus, the threshold needs to be decided carefully to employ in normal environment for the experiment. The work shows potential to measure human gait even in normal environments when multipath reflections are accommodated. Further research is underway to - (*i*) incorporate multipath reflections and mirror the normal environments so that behaviour changes can be eliminated, (*ii*) calculate stance (posture), joint angles, and duration of stops, (*iii*) recruit more participants with normal and abnormal walking patterns and improve the model towards handling the greater multipath situations, (*iv*) determine leg/arm swing and stance times to understand/recognise abnormal gait patterns e.g., scissors, steppage, waddling, and propulsive gait, (*v*) the creation of a database of human gait patterns from IR-UWB.

References

[108] Mark A Richards. *Fundamentals of radar signal processing*. Tata McGraw-Hill Education, 2005.

[109] Ronald W Schafer and Alan V Oppenheim. *Discrete-time signal processing*. Prentice Hall Englewood Cliffs, NJ, 1989.

[110] Jingang Zhong and Yu Huang. "Time-frequency representation based on an adaptive short-time Fourier transform". In: *IEEE Transactions on Signal Processing* 58.10 (2010), pp. 5118–5128.

Chapter 5

3D Gait Identification Employing IR-UWB: ITERATOR

Gait or human locomotion is bipedal and a forward propulsive movement of the human body. The locomotion has been charaterised through a 2D approach presented in Chapter 4, where range and height are both involved. That work is limited to only a few gait parameters such as, step frequency, step count, distance covered, etc. and are not sufficient to provide the potential of gait pattern diagnosis. Other gait parameters such as angles of hip and knees during flexion and extension respectively are commonly used to measure the quality of gait. Thus, this work has been extended to a 3D impulse radio ultra wideband (IR-UWB) gait identification method presented in this chapter. The prototype is 3D human motion model for gait disorder identification from impulse radio ultra wideband (ITERATOR) with the understanding of spherical trigonometry and vector algebra. Here, range, height, and width (gait motion width) have been determined from radio responses enabling the model to detect gait in 3D. Subsequently, normal and abnormal walking subjects were involved in this study. Abnormal gait subjects belong to the spastic gait category only in the initial study. The prototype has been tested in both the anechoic and multipath environments. The outcomes have been corroborated with simultaneous Kinect Xbox sensor and supported by statistical graphical approach Bland and Altman (B&A) analysis.

5.1 Method

The prototype has been described in this chapter only focuses on thigh or hip angles of human gait during flexion and extension of leg muscles. The work is divided into five parts; participants and their subjective data, IR-UWB radar module and device settings, proposed mathematical model from UWB and Kinect sensor data, corroboration of results, result analysis, and a case study with spastic gait patterns. Here, four new participants were involved with spastic gait along with the twenty participants have introduced in Chapter 3. The device settings have remained the same for UWB radar module and Kinect described in Chapter 3. All other relevant parts have been detailed here in the following sections.

5.1.1 Azimuth and Elevation Angles

To differentiate the lower limb, upper limb, and body sections, height has been calculated and used here. Azimuth and elevation angles are significant to define 3D space and calculate the height, range, and arc from radar beam angle. Thus, a 3D scenario has been considered in Figure 5.1 to obtain elevation and azimuth angle at different time and all the ranges have been denoted here by vector notation as they have a particular direction at a time.

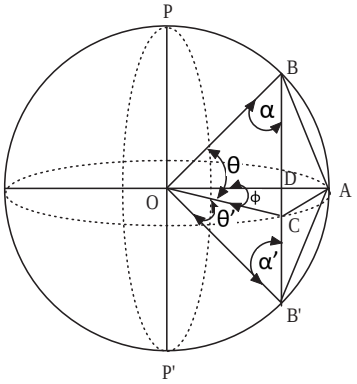

Figure 5.1: Elevation and azimuth angle during the gait.

Here, O is considered as the radar receiver fixed at a point of height $\overrightarrow{OP'}$ from the ground. Triangles ΔOAB, $\Delta OAB'$, ΔOCB, and $\Delta OCB'$ have been drawn from the received radar pulses. Therefore, $\overrightarrow{BC}$ and $\overrightarrow{CB'}$ represent the height of a moving object from the radar line of sight (LOS) $\overrightarrow{OA}$. The moving body section is elevated from the

radar LOS at an angle θ and below the LOS at an angle θ'. The point O represents the radar transceiver so the area $OBAB$' of Figure 5.1 and area $OBCB'$ demonstrate an antenna section of the beamwidth of an omnidirectional radiation pattern where, the lines OA and OC divides the beam into two equal segments of radiation pattern. Hence, geometrically the OP and OP' are equal in length. Here, $\Delta OAB \cong \Delta OAB'$ and $\Delta OCB \cong \Delta OCB'$, therefore the height $\overrightarrow{BC}$ and $\overrightarrow{CB'}$ can be determined from the trigonometric understanding. Let, the angle between $\overrightarrow{BC}$ and $\overrightarrow{OB}$ be α from ΔOAB. The ranges are $\overrightarrow{OA}$, $\overrightarrow{OB}$, and $\overrightarrow{OB'}$ for the propagation delays of t_1, t_2 and t_2' by the pulses, where $t_1 > t_2$, $t_1 > t_2'$ and $\overrightarrow{OA} > \overrightarrow{OB}$, $\overrightarrow{OA} > \overrightarrow{OB'}$. Therefore, the change in range is $(\overrightarrow{OA} - \overrightarrow{OB}) = \Delta d$, the change in propagation delay is $(t_1 - t_2) = \Delta t$, and speed of light or pulse is c. Therefore, pulse can travel the distance in Δt is $\overrightarrow{BC} = \Delta t \times c$. From the right triangle ΔOCB, $\overrightarrow{BC} = \overrightarrow{OB} \times \cos\alpha$. Thus, the height of the moving body section from the radar receiver is $\overrightarrow{OB} \times \cos\alpha$. The UWB radar has been fixed to a certain height of $\overrightarrow{OP'}$, thus the actual height of that moving object from the ground h would be defined by,

$$h = |\overrightarrow{OB} \times \cos\alpha - \overrightarrow{OP'}| \tag{5.1}$$

Now, the azimuth angle has been determined to measure orientation of a moving body section from the radar beam angle (shown in Figure 5.1). The spherical system measures the azimuth angle in a counter clockwise direction from the north beam angle of the radar receiver. Let, the moving limb is deviated at an angle ϕ, where the ranges are $\overrightarrow{OA}$ and $\overrightarrow{OC}$ in propagation delay t_1, t_2. So, the change in range is $(\overrightarrow{OA} - \overrightarrow{OC}) = \overrightarrow{DA}$ at the time interval $(t_1 - t_2) = \Delta t$. The object is deviated from the exact north of the receiver. Now, $\overrightarrow{DA}$ is approximately equivalent to the arc AC created by the object at angle ϕ. Therefore, ϕ is calculated from the radian measure, and equivalent degree conversion is,

$$\phi = \frac{\overrightarrow{DA} \times 360^\circ}{\overrightarrow{OA} \times 2 \times \pi} \tag{5.2}$$

Therefore, the coordinate of a pulse reflecting from a human body has been determined with the help of range, elevation, and azimuth calculation. Let, a pulse back-scattered from human body have its motion width, distance, height be a, r, h respectively. Thus, each pulse has it's coordinate and direction when back-scattered from any physiological

movement permitting the points to be considered as vectors such as, $a\hat{i}+r\hat{j}+h\hat{k}$ where, $\hat{i}$, $\hat{j}$, and $\hat{k}$ are unit vectors of three planes in a 3D space. The subscripts of a, r, and h have been used through out the thesis to denote motion width, distance, and height of a back-scattered pulse. The height of a back-scattered pulse has been considered here with the a priori knowledge of body sections to differentiate the lower limb from upper limb. The back-scattered pulses within the height of lower limb has been considered here to determine angles between alternative thighs and detailed in the following sections.

5.1.2 Hip Angle Measurement from IR-UWB

The angles between two alternative thighs or hip angles are pivotal parameters for gait characterization [111]. Thighs are connected through the pelvis via the ball-socket and femoral head, bearing human body weight and the force of the strong muscles of the hips and legs. Therefore, the angle between thighs changes during extension and flexion movements. Here, two random points on the thigh $\overrightarrow{L_T} = a_1\hat{i} + r_1\hat{j} + h_1\hat{k}$, $\overrightarrow{R_T} = a_2\hat{i} + r_2\hat{j} + h_2\hat{k} \in \mathbb{R}^3$ Euclidean space at time t has been assumed on the left and right thighs respectively (shown in Figure 5.2) where, the extension of these two vectors towards infinity intersect at human pelvis joint.

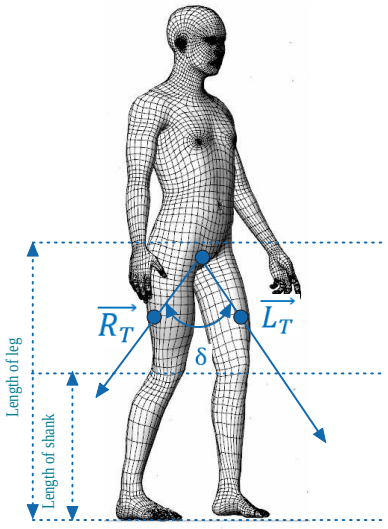

Figure 5.2: Consideration of vector while a person is walking.

Consequently, the extension of any two vectors (that represent the reflection position of a pulse on both thighs) from the left and right leg respectively, create and indicate the hip angle of human walk. The acute angle between any two vectors (for left and right thigh) denotes the hip angles which is determined by employing the dot or scalar

product operation. The acute angle is denoted by δ here and the measurement of δ shown in Eq. 5.3.

$$\begin{aligned}
\overrightarrow{L_T}.\overrightarrow{R_T} &= |\overrightarrow{L_T}||\overrightarrow{R_T}|\cos\delta \\
\Rightarrow \cos\delta &= \frac{\overrightarrow{L_T}.\overrightarrow{R_T}}{|\overrightarrow{L_T}||\overrightarrow{R_T}|} \\
\Rightarrow \cos\delta &= \frac{(a_1\hat{i}+r_1\hat{j}+h_1\hat{k}).(a_2\hat{i}+r_2\hat{j}+h_2\hat{k})}{|a_1\hat{i}+r_1\hat{j}+h_1\hat{k}||a_2\hat{i}+r_2\hat{j}+h_2\hat{k}|} \\
\Rightarrow \cos\delta &= \frac{(a_1a_2+r_1r_2+h_1h_2)}{\sqrt{a_1^2+r_1^2+h_1^2}\sqrt{a_2^2+r_2^2+h_2^2}} \\
\Rightarrow \quad \delta &= \cos^{-1}\left(\frac{(a_1a_2+r_1r_2+h_1h_2)}{\sqrt{a_1^2+r_1^2+h_1^2}\sqrt{a_2^2+r_2^2+h_2^2}}\right)
\end{aligned} \tag{5.3}$$

5.2 Result Corroboration via Kinect Xbox One

The outcomes of the proposed work have been validated with the Microsoft Kinect Xbox One. It includes 3D imaging and employs time of flight (TOF) technology to deliver high resolution, low latency, light independent 3D image sensing [112]. Kinect captures 3D human motion and tracks skeleton of human body using color and depth sensor. The proposed work aims to characterize human gait in a non-intrusive manner so the device has been calibrated to obtain color and skeleton only from the video. Frames per second (FPS) has been fixed at 30 for color and depth sensor for video acquisition. The camera has the field view of 70° horizontal and 60° vertical operates at range from 0.8 to 4.2 meters from the device. It tracks the skeleton from moving body posture (as shown in Figure 5.3) and provides 3D joint coordinates.

The Kinect sensor delivers 20 skeletal data (3D joint coordinates) at standing and 10 skeletal data at sitting condition from body posture. This skeletonization process is similar to the proposed prototype permitting the validation of the work through Kinect sensor. Figure 5.3b shows the 20 joints (white markers) from a human body where, the validation process has used only four joints from lower limb of a human body such as, hip left ($\overrightarrow{HL}$), knee left ($\overrightarrow{KL}$), hip right ($\overrightarrow{HR}$), knee right ($\overrightarrow{KR}$). Then the vector algebra has been employed on these joints to determine angles between thighs and validate the proposed outcomes.

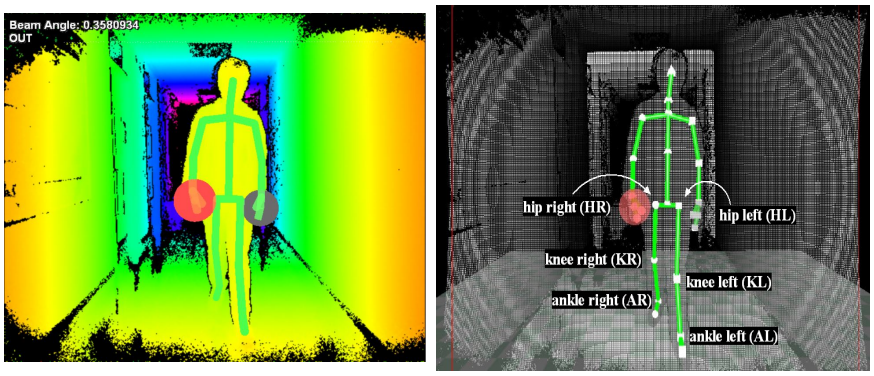

(a) Video frame from color sensor .

(b) Video frame from depth sensor (i.e., skeleton).

Figure 5.3: Sample video frame of human gait tracked through Kinect color and depth sensor.

Let, the vectors $\overrightarrow{HL}$, $\overrightarrow{KL}$, $\overrightarrow{HR}$, $\overrightarrow{KR} \in \mathbb{R}^3$. The component form of these vectors have been denoted as, $\overrightarrow{HL} = a_3\hat{i} + r_3\hat{j} + h_3\hat{k}$, $\overrightarrow{KL} = a_4\hat{i} + r_4\hat{j} + h_4\hat{k}$, $\overrightarrow{HR} = a_5\hat{i} + r_5\hat{j} + h_5\hat{k}$, $\overrightarrow{KR} = a_6\hat{i} + r_6\hat{j} + h_6\hat{k}$ where, subscripts with a, r, h represents the distance from $\hat{i}$, $\hat{j}$, $\hat{k}$ planes respectively. These vectors have been further used to determine angle between alternative thighs for gait characterization in the following sections.

5.2.1 Hip Angle Measurement from Kinect

The angle between thighs or hip angle has been defined and calculated by the proposed prototype earlier. Now, the angle between thighs has been measured using the hip joints $\overrightarrow{HL}$, $\overrightarrow{HR}$, $\overrightarrow{KL}$, and $\overrightarrow{KR}$ obtained from Kinect skeletal data. Therefore, the two lines are required to calculate the acute angle or the angle of thighs between left and right thigh. Thus, the connecting line between two vectors $\overrightarrow{HL}$ and $\overrightarrow{KL}$ would be spanned by a vector $\overrightarrow{L_{Tk}} = (a_3-a_4)\hat{i}+(r_3-r_4)\hat{j}+(h_3-h_4)\hat{k}$ which represents the space of left thigh. Similarly, the position vector of right thigh $\overrightarrow{R_{Tk}} = (a_5 - a_6)\hat{i} + (r_5 - r_6)\hat{j} + (h_5 - h_6)\hat{k}$. The acute angle between $\overrightarrow{L_{Tk}}$ and $\overrightarrow{R_{Tk}}$ has been determined by their dot product and denoted by δ' (detailed in Eq. 5.4) where, $(a_3-a_4) = a_{34}$, $(r_3-r_4) = r_{34}$, $(h_3-h_4) = h_{34}$, $(a_5-a_6) = a_{56}$, $(r_5 - r_6) = r_{56}$, $(h_5 - h_6) = h_{56}$ have been considered for simplification of the calculations.

$$\begin{aligned}
&\overrightarrow{L_{Tk}}.\overrightarrow{R_{Tk}} = |\overrightarrow{L_{Tk}}||\overrightarrow{R_{Tk}}| \cos\delta\,' \\
&\Rightarrow \cos\delta\,' = \frac{\overrightarrow{L_{Tk}}.\overrightarrow{R_{Tk}}}{|\overrightarrow{L_{Tk}}||\overrightarrow{R_{Tk}}|} \\
&\Rightarrow \cos\delta\,' = \frac{(a_{34}\hat{i} + r_{34}\hat{j} + h_{34}\hat{k}).(a_{56}\hat{i} + r_{56}\hat{j} + h_{56}\hat{k})}{|a_{34}\hat{i} + r_{34}\hat{j} + h_{34}\hat{k}||a_{56}\hat{i} + r_{56}\hat{j} + h_{56}\hat{k}|} \\
&\Rightarrow \cos\delta\,' = \frac{a_{34}a_{56} + r_{34}r_{56} + h_{34}h_{56}}{\sqrt{a_{34}^2 + r_{34}^2 + h_{34}^2}\sqrt{a_{56}^2 + r_{56}^2 + h_{56}^2}}
\end{aligned} \tag{5.4}$$

5.3 Bland and Altman (B&A) Plot Analysis

There two different models: the proposed ITERATOR prototype and the Kinect module have been used here to measure same gait parameter where, some amount of variation in outcomes have been found. Thus, the outcomes have been compared using B&A analysis [113, 114] based on the quantification of the agreement between two quantitative measurements proposed ITERATOR and Kinect system by studying mean difference and constructing limits assessing comparability between these two methods. The statistical limits are calculated by using the mean, standard deviation of the differences between the two measurements, and a hypothetical graphical approach to indicate the agreement. Hip or thigh angle has been measured through proposed ITERATOR and Kinect system for gait analysis. Let, the measured hip or thigh angles from the proposed and the Kinect systems be h_p and h_k respectively, the mean of the hip or thigh angles is m_h, differences between paired hip angles be d_h, standard deviation of the differences obtained for hip angles is s_h. The graphical approach is used to check the assumptions of normality of differences and other characteristics, where the x-axis represents the measurements average and y-axis shows the difference between the two measurements. The two systems would agree when most of the consequences lie within $d_h \pm 1.96 s_h$ for the measurement of hip angles. More precisely, 95% of differences must be within $d_h \pm 1.96 s_h$ for measuring hip angles according to B&A analysis. Thus, null hypothesis states here there is no significant difference between populations (measurements) taken ITERATOR and Kinect for determining hip angles of participants where probability value $p < 0.05$ indicates acceptance of null hypothesis and correctness of assumption.

5.4 Result Analysis

As explained the experiment has been conducted in two different environments: anechoic and multipath environment to investigate robustness, cost effectiveness, and suitability. In addition to this, the preciseness and acceptance of the work for gait characterisation has been supported through B&A plot analysis in each environment. The results and B&A plot analysis have been analysed in the following sections.

5.4.1 Result Analysis from Anechoic Chamber

The comparative analysis of the obtained results from the proposed prototype and Kinect sensor are demonstrated in this section. The processing of IR-UWB data and interpretation has been discussed in Section 5.1.1, which explains the positions of back-scattered pulses from a human body and defines motion through the IR-UWB. Figure 5.4 shows one of the twenty normal walking patterns through the IR-UWB response in 3D over an observation period, where Figure 5.4a and 5.4b lay out front and side views of walking motion captured through proposed model.

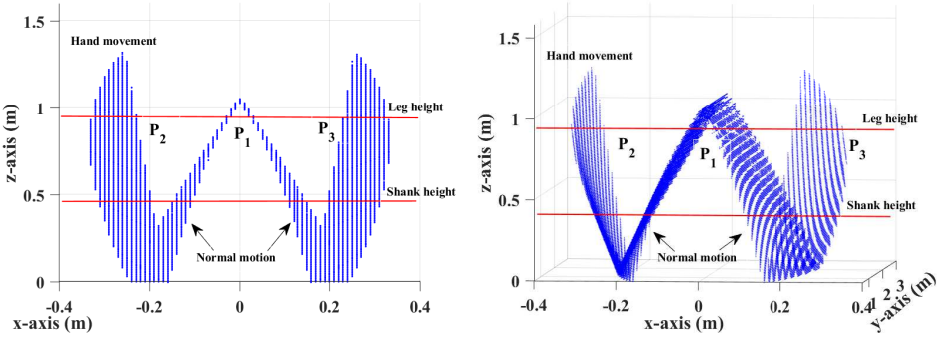

(a) The front view of IR-UWB 3D response from a normal walk.

(b) The side view of IR-UWB 3D response from a normal walk.

Figure 5.4: The front and side views of IR-UWB 3D response from a normal walk.

The x, y, and z axis signify gait motion width, distance from radar, and height of movement respectively. The motion appears like the letter 'W', showing the symmetry of the human body and there are three areas labeled with P_1, P_2, and P_3. Here, the area P_1 reflects hip joint of that person, P_1 to P_2 and P_1 to P_3 denotes the change of position of human body due to gait motion when one leg is lifted off of the ground and another leg is contacted the ground to push forward the body during walking. The

person walked back and forth in front of the radar (within the 3 m testbed) during the observation times that creates separate areas (P_1, P_2, and P_3) in 3D for change of position. Also, the distance between the bottom of P_2 and P_3 areas represent the step base width i.e., the perpendicular distance between two steps during gait. In addition, two areas detected above leg height are the hand movements (both right and left legs). Figure 5.5a displays the front view of walking pattern captured through the IR-UWB response and 5.5b demonstrates the skeletonization of that gait pattern acquired from the Kinect in the anechoic chamber.

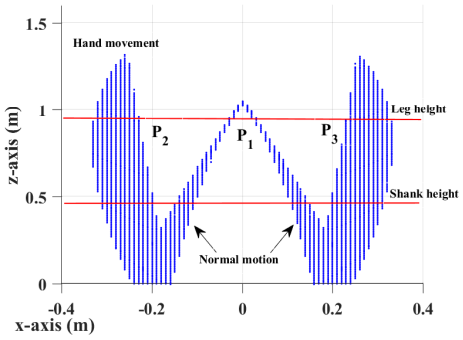

(a) 3D human motion from IR-UWB.

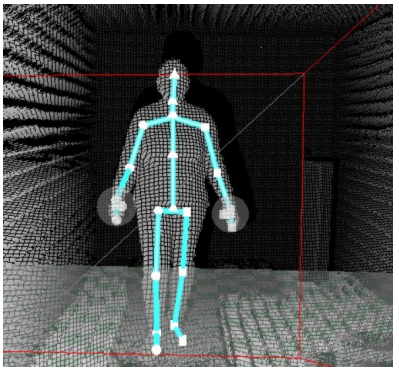

(b) 3D human skeleton from Kinect.

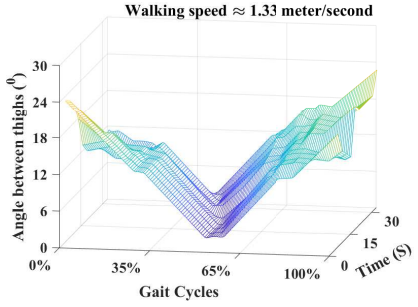

(c) Changes of thigh angles determined from proposed model.

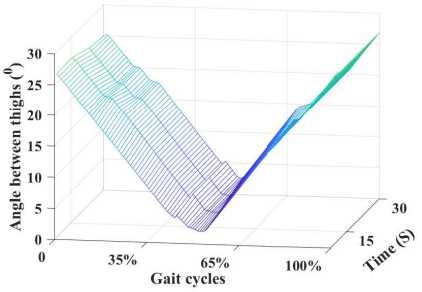

(d) Changes of thigh angles determined from Kinect skeleton.

Figure 5.5: The human motion and thigh angles obtained from proposed model and Kinect respectively for a person having normal walking pattern.

Figure 5.5a shows a 3D structure resembles the letter 'W' which, includes the flexion and extension of skeletal muscle's (i.e., arm and legs) motion over time. The skeletal muscles move faster than the other body sections which implies the transmission of higher energy by the bio-mechanical process that allows UWB radar to capture motion. The extension of lower limbs (left and right) creates a separate motion area, whereas the flexion (right and leg) of the lower limb and upper limbs creates a linear region from the shoulders that explains the human motion. The person depicted in 5.5a and 5.5b has an actual height of 1.55 m whereas the estimated height of the shape is 1.35 m. This is because the

model has captured all movements by UWB upto the shoulder height from the ground level. The leg length of that participant is 0.95 m and knee height is 0.45 m from the ground level that have been used to separate each lower limb sections to determine the angles between alternative thighs. Figure 5.5c and 5.5d demonstrates the estimation of thigh angles from the proposed study and Kinect respectively using the method of Eq. 5.3 and Eq. 5.4. The x-axis denotes the single gait cycle (in percentage) of a person by considering two consecutive steps and the process has been repeated for 30 seconds then plotted in y-axis and z-axis which represents the angles between the thighs during the observation time. The outcomes have been detailed here for 30 s for each participant. This participant has walked at a speed of 1.33 m/s (obtained from Doppler effect) and the thigh angles obtained the from proposed prototype is approximately 24° whereas, the angles obtained from Kinect results approximately 26°. The troughs here represent the angles during flexion and crest signifies the angles at the time of leg extension.

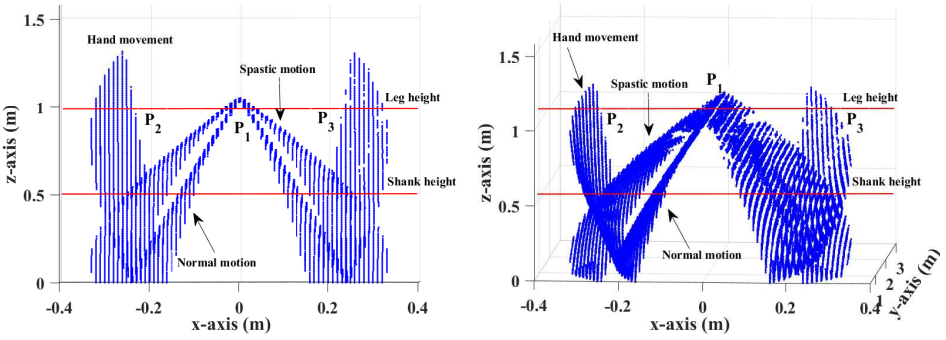

(a) The front view of IR-UWB 3D response from a abnormal walk.

(b) The side view of IR-UWB 3D response from a abnormal walk.

Figure 5.6: The front and side views of IR-UWB 3D response from an abnormal walk.

Figure 5.6 shows one of the abnormal walking patterns through the IR-UWB response in 3D over an observation period as before, where Figure 5.6a and 5.6b lay out the front and side views of the walking motion captured through the proposed model. The x, y, and z axis signify gait motion width, distance from the radar, and height of movement respectively. The motion again appears like the letter 'W', shows symmetry of the human body and again there are three areas are labeled with P_1, P_2, and P_3. But, Figure 5.6 has differences from Figure 5.4. There the abnormality creates two extra regions for the abnormal leg movement (spasticity). Similarly, the area P_1 reflects the hip joint of that person, P_1 to P_2 and P_1 to P_3 denotes the change of position of human body due to gait motion when one leg is lifted off of the ground and another leg is contacted to the ground

to push the body forward during walking. As before the person walked back and forth in front of radar (within 3 m of testbed) during observation time that creates separate areas (P_1, P_2, and P_3) in 3D for change of position. Overall the person's movement is effected by their condition in particular one leg is affected by their spasticity, hence the 'normal' and 'abnormal' leg creates two separate areas in P_2 and P_3. This shows the person needs to stretch and drag one leg more than a regular walker and is reflected in the proposed IR-UWB model outcomes. Also, the distance between the bottom of P_2 and P_3 areas represents step base width which is also different from normal walk. In addition, two areas detected above leg height are the hand movements (both right and left legs).

Figure 5.7 displays the gait analysis of that person through IR-UWB and Kinect. Figure 5.7b displays the motion of that said participant and stiffness of the left leg muscle forces the person to stretch the leg more during walking, increasing the angles between the two thighs. Figure 5.7a shows that the leg deviates more from the center of the body during walking, which resulting the unusual thigh angle of approximately 40°, determined from the proposed prototype. The angle between alternative thighs obtained from Kinect is approximately 38°.

5.4.2 B&A Plot: Results Obtained in Anechoic Chamber

This section includes statistical analysis of hip or thigh angle measurements taken in the anechoic chamber environment using the proposed ITERATOR and Kinect systems. The analysis has been performed to check the relation between these two techniques and discover agreement between their measurements. Figure 5.8 shows B&A plots have been constructed on the hip or thigh angle measurements from the ITERATOR and Kinect sensor data, where Figure 5.8a demonstrates B&A plots of hip angle measurements taken for twenty normal gait persons using ITERATOR and Kinect and Figure 5.8b demonstrates B&A plots of hip angle measurements taken for four abnormal gait persons again from ITERATOR and Kinect. The x and y axis represents the mean of the two hip angle measurements and the difference between their paired measurements respectively. Figure 5.8a shows bias or mean of difference is -0.215 which signifies that Kinect always produces 0.215 degree units more than the proposed ITERATOR where p value is 1.902×10^{-4} (i.e., $p < 0.05$). In addition, Figure 5.8b displays the bias at +0.165 when measuring

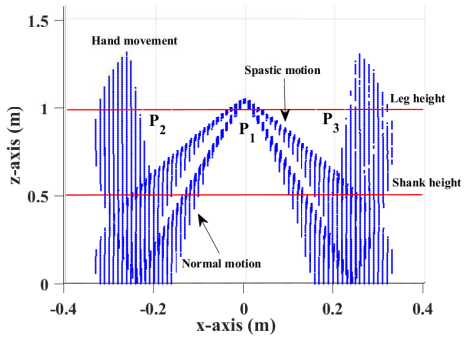

(a) 3D human motion captured by IR-UWB from spastic gait.

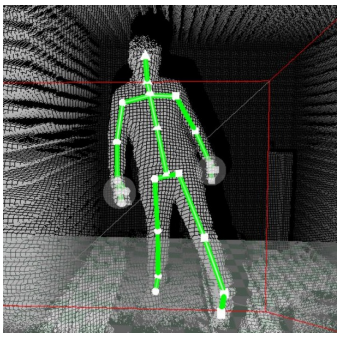

(b) 3D human skeleton captured by Kinect from spastic gait.

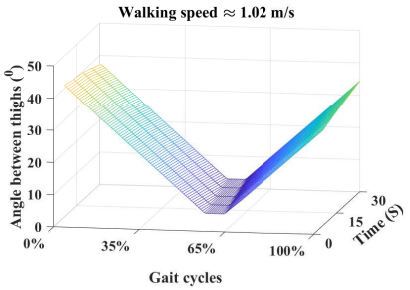

(c) Changes of thigh angles determined from proposed model for spastic gait.

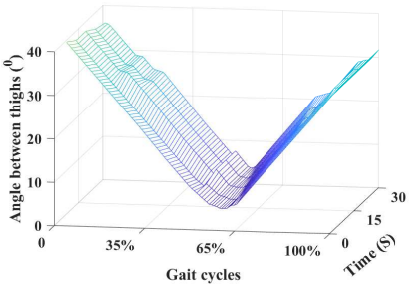

(d) Changes of thigh angles determined from Kinect skeleton for spastic gait.

Figure 5.7: Human motion and thigh angles obtained from proposed model and Kinect respectively for a person with spasticity.

hip angles of abnormal gait persons, this indicates Kinect always delivers 0.165 degree units less than proposed ITERATOR for measurement of hip or thigh angles where p is 0.0058 (i.e., $p < 0.05$). Thus, the null hypothesis has been found to be true in both cases (normal and abnormal gaits), so 95% differences are within $d_h \pm 1.96 s_h$ and there is no significant difference between ITERATOR and Kinect system's magnitude while measuring hip or thigh angles in the anechoic chamber.

5.4.3 Result Analysis from Multipath Environment

Figure 5.9a and 5.9b illustrate the 3D motion captured from a person's gait by proposed prototype and Kinect respectively in the multipath environment (laboratory and corridor environment). Figure 5.9c and 5.9d demonstrate obtained hip or thigh angles from proposed and Kinect system respectively. The x-axis of the Figures 5.9c and 5.9d indicate the fractions of gait cycles covered by hip angles during the observation time where, each gait cycle contains two consecutive steps (stance $\approx$ 60% and swing $\approx$ 40% phase)

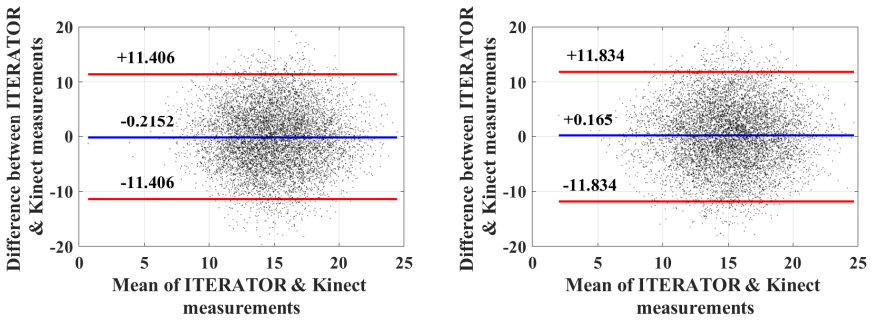

(a) B&A plot of measured hip angles from ITERATOR and Kinect for normal gait persons.

(b) B&A plot of measured hip angles from ITERATOR and Kinect for abnormal gait persons.

Figure 5.8: B&A plot of hip angle measurements in anechoic environment.

with respect to the reference leg (left leg in this case) involved in the walking. The hip angle decreases and knee angle increases nearly at the same time till the reference leg leaves the ground, shown in Figure 5.9c and 5.9d. Then, the reference leg leaves the ground and stays in the air during the swing phase when the hip angle start increasing and knee angle start decreasing. The variation of hip angles have been captured in the same way from proposed IR-UWB and Kinect system (in Figure 5.9c and 5.9d). The hip angle varies between 0° to 24° and 0° to 22° while using proposed prototype and Kinect system respectively.

5.4.4 B&A Plot: Results Obtained in Multipath Environment

Here, the measurements taken in the multipath environment (laboratory environment) has been supported through B&A plot analysis as for anechoic chamber experiment. Figure 5.10 shows the B&A plots constructed on hip or thigh angle measurements from ITERATOR and Kinect sensor, where Figure 5.10a demonstrates B&A plots of hip angle measurements taken for twenty normal gait persons from the ITERATOR and Kinect with Figure 5.10b demonstrating the B&A plots of the hip angle measurements taken for four abnormal gait persons via the ITERATOR and Kinect in the normal or multipath environment. The x and y axis represent the mean of two hip angle measurements and the differences between their paired measurements respectively. Figure 5.10a shows the bias or mean of difference is -0.266 which signifies that Kinect always produces 0.266 degree units more than the proposed ITERATOR to determine hip angles of normal gait persons where p value is 2.2744×10^{-6} (i.e., $p < 0.05$). In addition, Figure 5.10b displays the bias at -0.187 when measuring hip angles of abnormal gait persons, this

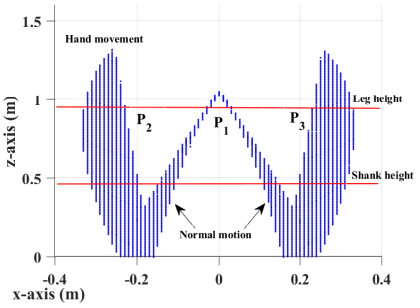

(a) 3D human motion obtained from IR-UWB in multipath environment.

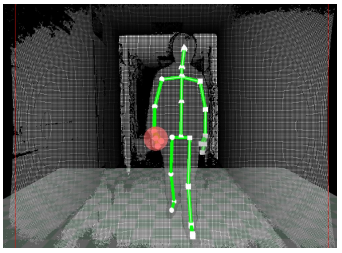

(b) 3D human skeleton obtained from Kinect in multipath environment.

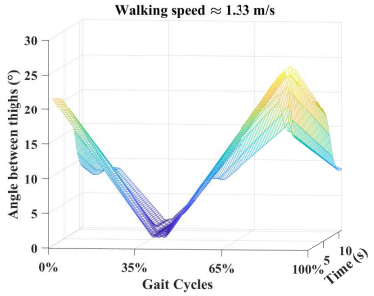

(c) Changes of thigh angles determined from proposed model in multipath environment.

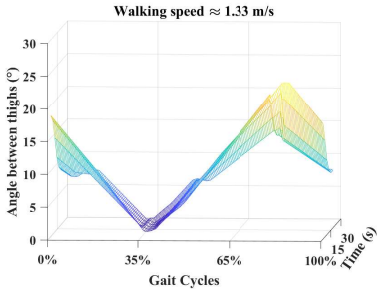

(d) Changes of thigh angles determined from Kinect skeleton in multipath environment.

Figure 5.9: The human motion and thigh angles obtained from proposed model and Kinect respectively for a person having normal walking pattern in multipath environment.

indicates Kinect always delivers 0.187 degree units more than proposed ITERATOR for measurement of the hip or thigh angles where p is 0.0015 (i.e., $p < 0.05$). Thus, the null hypothesis have been found to be true in both cases (normal and abnormal gaits) in normal environment, so 95% differences are within $d_h \pm 1.96 s_h$ and there is no significant difference between ITERATOR and Kinect system's magnitude while measuring hip or thigh angles in normal environment.

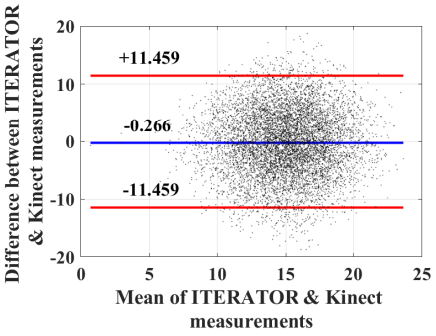

(a) BAA-Multipath-Normal-Thigh.

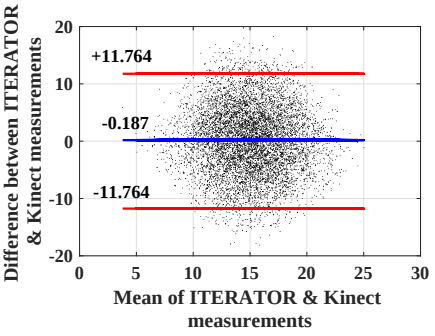

(b) BAA-Multipath-Abnormal-Thigh.

Figure 5.10: B&A plot of hip angle measurements in normal environment.

5.5 Conclusion

The proposed ITERATOR model intends to demonstrate a non-intrusive, non-contact, wireless system for gait analysis and an identification system capable and recognizing disorders related to human walking patterns. In this work, for the first time a proposed 3D model of human motion has been generated from IR-UWB sensing by employing trigonometry and vector algebra where, subjective knowledge enabled the study to further characterize human gait. This work is currently limited to identifying the angles between thighs, the extended research has been performed to determine knee angles and is presented in Chapter 6. Additionally, a greater number of participants, including those with conditions such as, propulsive, waddling, steppage, etc. would be considered for future experiments. The Kinect sensor has been considered as a reference system and employed to evaluate the performance of proposed model. The experiment has been conducted in anechoic chamber and normal environments where the proposed prototype and Kinect sensor have an accuracy of approximately 9 mm and 18 mm [115] respectively, whereas the performance of both systems are influenced by multipath effect in a non-anechoic environment. The Kinect system principle depends upon the viewing angle to identify joint angles. Thus, when a person turns 360° in front of the camera half of the body is occluded by the other half which is known as the self-occlusion problem [116]. The proposed model doesn't rely solely on joint angles but also the reflected pulses from other body parts mitigating the chances of self occlusion. The maximum range of the Kinect is 4 meters in one room whereas, the IR-UWB radar module can be calibrated for longer range if required. In addition to this, the proposed radar module is able to track small changes than Kinect system because of higher resolution and across walls. Overall, the proposed model would be cutting edge solution for addressing health issues by non-contact IR-UWB technology. Further, this study would be extended by employing supervised machine learning (SML) techniques to automatically recognise changes and identify the human walking disorders in the next chapter. This would provide a cutting-edge solution in health and medical perspective to assist in clinical and pathological gait diagnosis.

References

[111] Martin Hora et al. “Body size and lower limb posture during walking in humans”. In: *PloS one* 12.2 (2017), e0172112.

[112] Erik E Stone and Marjorie Skubic. “Unobtrusive, continuous, in-home gait measurement using the Microsoft Kinect”. In: *IEEE Transactions on Biomedical Engineering* 60.10 (2013), pp. 2925–2932.

[113] John M Bland and Douglas G Altman. “Statistical methods for assessing agreement between two methods of clinical measurement”. In: *The lancet* 327.8476 (1986), pp. 307–310.

[114] Davide Giavarina. “Understanding bland altman analysis”. In: *Biochemia medica: Biochemia medica* 25.2 (2015), pp. 141–151.

[115] Oliver Wasenmüller and Didier Stricker. “Comparison of kinect v1 and v2 depth images in terms of accuracy and precision”. In: *Asian Conference on Computer Vision*. Springer. 2016, pp. 34–45.

[116] Björn Müller et al. “Validation of enhanced kinect sensor based motion capturing for gait assessment”. In: *PloS one* 12.4 (2017), e0175813.

Chapter 6

3D Gait Recognition Employing IR-UWB: Intelligent ITERATOR

Biomedical engineering can integrate innovations from areas such as health informatics and computing to develop cutting-edge solutions for abnormal gait or lower limb disorder recognition and effect how patients are diagnosis, monitored, and treated, lowering the cost of care and improving individual outcomes. Thus, further research has been conducted to improve the gait disorder identification from impulse radio ultra wideband (ITERATOR) model to an automated impulse radio ultra wideband (IR-UWB) based 3D human gait analysis prototype with the help of supervised machine learning and is presented in this chapter. The work is divided into two main phases; knee angle extraction employing the proposed trigonometric and vector algebra, and applying the knee angle variation of a person's gait to the machine learning (ML) system. Hence, the enhanced ITERATOR can recognise 'normal' and 'abnormal' gait automatically based on person's knee angle variation. It can to identify gait pattern objectively (quantitatively) and automatically rather than subjectively (observation only), which could enable a greater level of flexibility creating easier adaption of such a sensor system in many locally based environments. The work intends to provide a rewarding assistive biomedical application assisting doctors and clinicians to monitor human gait trait and abnormalities with less human intervention in the fields of physiological examinations, physiotherapy, home assistance, rehabilitation success determination and health diagnostics, etc. The work comprises IR-UWB gait data gathered from a number of male

and female participants involved and introduced in previous chapters. The 3D postural model discussed in Chapter 5 has been improved here to measure the knee angles (both right and left) of the individuals. Simultaneously, Kinect sensor and Blant Altman (B&A) plot have been employed to support the fidelity of the work. The work for this comprises data from the anechoic chamber only. Further, the knee angles have been employed to train popular supervised machine learning (SML) techniques and perform an initial test towards automation of the prototype. The outcomes have been validated through statistical metrics. Results are promising and indicate the capability to predict/ recognise gait abnormalities in an intelligent way.

6.1 Method

The knee angles have been considered and determined here from leg extension and flexion of the twenty four individuals in the study. Relevant settings of the IR-UWB and Kinect sensor have been outlined in Chapter 3. The 3D model stated in Chapter 4 has been improved to measure knee angle and make an autonomous IR-UWB prototype for gait recognition in this chapter. The workflow to automatically recognise normal and abnormal gaits from the proposed ITERATOR employing SML is presented in Figure 6.1.

The same steps discussed hitherto in Section 3.2 of Chapter 3 to collect UWB gait data have been followed under ethical approval. Chapter 5 includes measurement of hip or thigh angles of gait from proposed prototype that needs back-scattered pulses from thigh of lower limb. This chapter proposes a method to calculate another significant gait parameter i.e., knee angles. Since the ITERATOR relies on 3D interpretation of human motion from UWB pulses, the calculation of knee angle through vectorisation require pulses reflected from both the thigh and knee. The intersection of lines obtained from those 3D coordinates form knee angles which has been determined through the proposed work. Further, the trend of knee angles of normal and abnormal gait has been classified employing SML. Hence, the prototype is able to understand the difference between normal and abnormal gait, and would support health professionals to take decisions for gait problem diagnosis. The related theories and results are presented in the following sections.

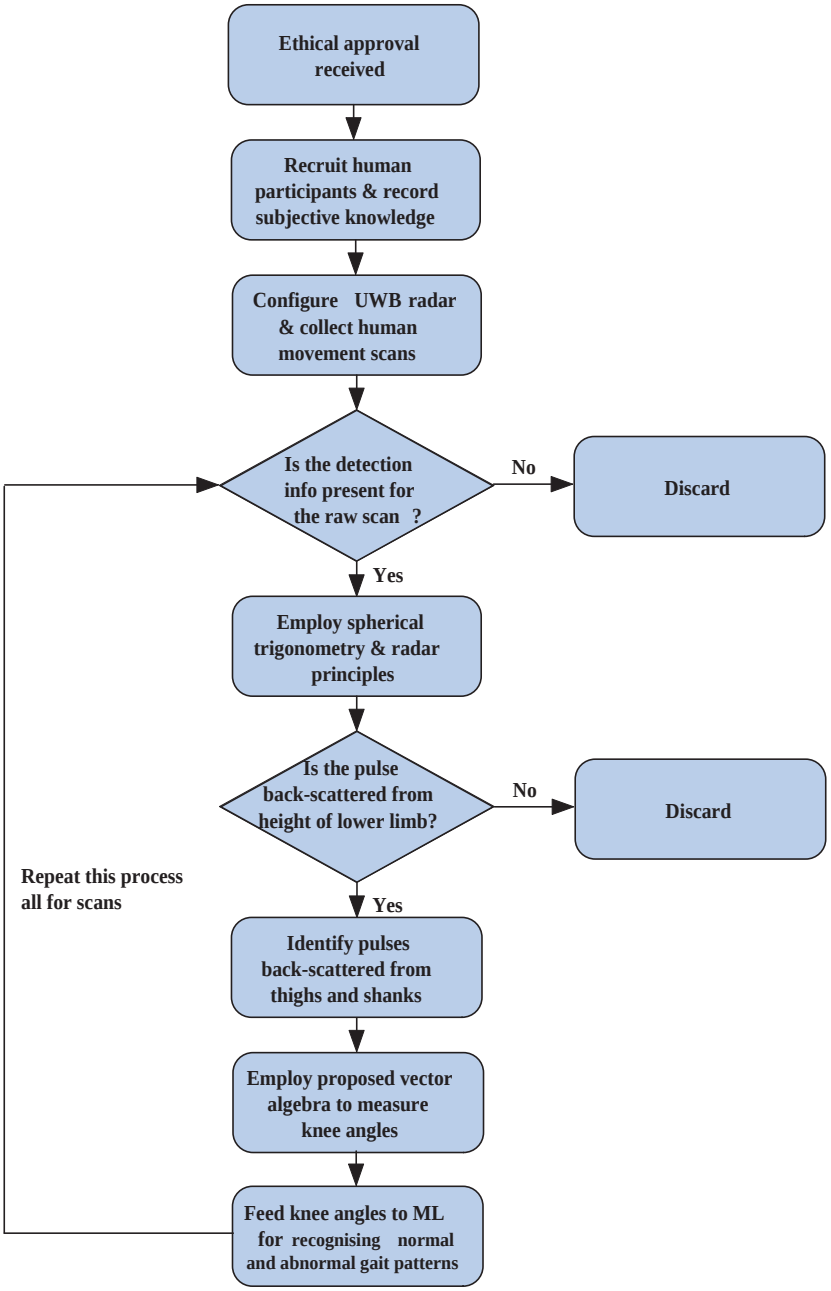

Figure 6.1: Flowchart of proposed intelligent ITERATOR prototype.

6.1.1 Knee Angles Calculations from IR-UWB Sensing

The knee joint has two sections, the thigh and shank. Thus, human gait creates angles between these two muscles during the walking phases. The angle increases during muscles extension (i.e., straightening of legs) and decreases during the flexion of muscles (i.e., articulation of legs). The change of knee joint angle is significant to characterize human gait [117]. Figure 5.2 shows a human walking posture where, two points $\overrightarrow{L_T}$, $\overrightarrow{L_S} \in \mathbb{R}^3$ Euclidean space at time t have been assumed on thigh and shank of left leg respectively.

The dot product of these two points provides the acute angle γ_L between them whereas, the measurement of obtuse angle (β_L) is anatomically more significant. The detailed calculations of γ and β have been included in Eq. 6.1 and Eq. 6.2.

$$\begin{aligned}
\overrightarrow{L_T}.\overrightarrow{L_S} &= |\overrightarrow{L_T}||\overrightarrow{L_S}|\cos\gamma \\
\Rightarrow \cos\gamma_L &= \frac{\overrightarrow{L_T}.\overrightarrow{L_S}}{|\overrightarrow{L_T}||\overrightarrow{L_S}|} \\
\Rightarrow \cos\gamma_L &= \frac{(a_1\hat{i}+r_1\hat{j}+h_1\hat{k}).(a_2\hat{i}+r_2\hat{j}+h_2\hat{k})}{|a_1\hat{i}+r_1\hat{j}+h_1\hat{k}||a_2\hat{i}+r_2\hat{j}+h_2\hat{k}|} \\
\Rightarrow \cos\gamma_L &= \frac{(a_1a_2+r_1r_2+h_1h_2)}{\sqrt{a_1^2+r_1^2+h_1^2}\sqrt{a_2^2+r_2^2+h_2^2}} \\
\Rightarrow \quad \gamma_L \quad &= \cos^{-1}\left(\frac{(a_1a_2+r_1r_2+h_1h_2)}{\sqrt{a_1^2+r_1^2+h_1^2}\sqrt{a_2^2+r_2^2+h_2^2}}\right)
\end{aligned} \tag{6.1}$$

Therefore, the obtuse knee angle (β_L) for the left leg,

$$\beta_L = 180^\circ - \gamma_L \tag{6.2}$$

Similarly, the acute knee angle γ_R between $\overrightarrow{R_T}$ and $\overrightarrow{R_S}$ for right leg has been determined in Eq. 6.3.

$$\Rightarrow \quad \gamma_R \quad = \cos^{-1}\left(\frac{(a_3a_4+r_3r_4+h_3h_4)}{\sqrt{a_3^2+r_3^2+h_3^2}\sqrt{a_4^2+r_4^2+h_4^2}}\right) \tag{6.3}$$

Therefore, the obtuse knee angle for right leg has been included in Eq. 6.4,

$$\beta_R = 180^\circ - \gamma_R \tag{6.4}$$

6.1.2 Knee Angles from Kinect Xbox Sensing

The knee angles (left and right) have been measured in a similar way to hip joint calculation by using dot products of vectors. The knee and ankle joints (shown in Figure 3.7d) from skeletal data of both legs have been used two calculate knee angles

of human gait. In case of left leg, the connecting line between vectors $\overrightarrow{HL}$ and $\overrightarrow{KL}$ would be spanned through the vector $\overrightarrow{L_{Tk}} = (a_5 - a_6)\hat{i} + (r_5 - r_6)\hat{j} + (h_5 - h_6)\hat{k}$ and the straight line between points $\overrightarrow{KL}$ and $\overrightarrow{AL}$ would spanned through the vector $\overrightarrow{L_{Sk}} = (a_6 - a_7)\hat{i} + (r_6 - r_7)\hat{j} + (h_6 - h_7)\hat{k}$. The dot product of $\overrightarrow{L_{Tk}}$ and $\overrightarrow{L_{Sk}}$ provides the acute angle between these two whereas, inner knee angle would be the obtuse angle between them. The acute angle has been denoted by $\gamma\,'_L$ and detailed in Eq. 6.5.

$$
\begin{aligned}
&\overrightarrow{L_{Tk}}.\overrightarrow{L_{Sk}} = |\overrightarrow{L_{Tk}}||\overrightarrow{L_{Sk}}|\cos\gamma\,' \\
\Rightarrow \cos\gamma\,'_L &= \frac{\overrightarrow{L_{Tk}}.\overrightarrow{L_{Sk}}}{|\overrightarrow{L_{Tk}}||\overrightarrow{L_{Sk}}|} \\
\Rightarrow \cos\gamma\,'_L &= \frac{((a_5 - a_6)\hat{i} + (r_5 - r_6)\hat{j} + (h_5 - h_6)\hat{k}).((a_6 - a_7)\hat{i} + (r_6 - r_7)\hat{j} + (h_6 - h_7)\hat{k})}{|(a_5 - a_6)\hat{i} + (r_5 - r_6)\hat{j} + (h_5 - h_6)\hat{k}||(a_6 - a_7)\hat{i} + (r_6 - r_7)\hat{j} + (h_6 - h_7)\hat{k}|} \\
\Rightarrow \cos\gamma\,'_L &= \frac{(a_5 - a_6)(a_6 - a_7) + (r_5 - r_6)(r_6 - r_7) + (h_5 - h_6)(h_6 - h_7)}{\sqrt{(a_5 - a_6)^2 + (r_5 - r_6)^2 + (h_5 - h_6)^2}\sqrt{(a_6 - a_7)^2 + (r_6 - r_7)^2 + (h_6 - h_7)^2}} \\
\Rightarrow \quad \gamma\,'_L &= \cos^{-1}\left(\frac{(a_5 - a_6)(a_6 - a_7) + (r_5 - r_6)(r_6 - r_7) + (h_5 - h_6)(h_6 - h_7)}{\sqrt{(a_5 - a_6)^2 + (r_5 - r_6)^2 + (h_5 - h_6)^2}\sqrt{(a_6 - a_7)^2 + (r_6 - r_7)^2 + (h_6 - h_7)^2}}\right)
\end{aligned}
\tag{6.5}
$$

Therefore, the inner knee angle or obtuse knee angle for the left leg,

$$\beta'_L = 180^\circ - \gamma\,'_L \tag{6.6}$$

Similarly, the acute knee angle $\gamma_R{}'$ between $\overrightarrow{R_{Tk}}$ and $\overrightarrow{R_{Sk}}$ for right leg has been determined in Eq. 6.7.

$$
\Rightarrow \quad \gamma_R{}' = \cos^{-1}\left(\frac{(a_8 - a_9)(a_9 - a_{10}) + (r_8 - r_9)(r_9 - r_{10}) + (h_8 - h_9)(h_9 - h_{10})}{\sqrt{(a_8 - a_9)^2 + (r_8 - r_9)^2 + (h_8 - h_9)^2}\sqrt{(a_9 - a_{10})^2 + (r_9 - r_{10})^2 + (h_9 - h_{10})^2}}\right) \tag{6.7}
$$

Therefore, the obtuse angle or inner knee angle for right leg would be,

$$\beta'_R = 180^\circ - \gamma_R{}' \tag{6.8}$$

6.2 Bland Altman (B&A) Plot Analysis

Two different models are presented: the proposed IR-UWB prototype and Kinect have been used here to measure the same gait parameter i.e., knee angle. Differences were found, so the outcomes have been compared using B&A plot analysis [118, 119] based on the quantification of the agreement between two quantitative measurements by studying the mean difference and constructing limits of agreement for assessing the comparability between methods. The statistical limits are calculated by using the mean, standard deviation of the differences between two the measurements, and a hypothetical graphical approach to indicate the agreement. Knee angle of participants has been measured through proposed and kinect system for gait analysis. Let, the measured knee angles from the proposed and Kinect system be k_p and k_k respectively, mean of knee angle is m_k, differences between paired knee angle is d_k, standard deviation of the differences obtained for knee angle is s_k. The graphical approach is employed to observe the assumptions of normality of differences and other characteristics where, the x-axis represents the average of measurements and y-axis shows the difference between the two measurements. The two systems would agree when most of the consequences lie within $d_k \pm 1.96 s_k$ for the measurement of knee angle. More precisely, 95% of differences must lie within $d_k \pm 1.96 s_k$ for measuring the knee angle according to Bland Altman analysis. Thus, the null hypothesis states here there is no significant difference between populations (measurements) taken the ITERATOR and Kinect for determining knee angles of participants where probability value $p < 0.05$ indicates acceptance of null hypothesis and correctness of assumption.

6.3 Knee Angles as Features

The settings of UWB radar module used for the experiment have been detailed in Section 3.4 of Chapter 3. Subsequently, the length of testbeds used were 3 meters and 6 meters for the anechoic chamber and multipath environment respectively. The experimental work presented in this chapter comprises data from the anechoic chamber only, where the radar module requires a scan window or propagation delay of 23.436 nanoseconds to cover 3 meters range of anechoic chamber testbed. The amplitude of each pulse is represented by a sequence of 288 samples. UWB pulses back-scatter from left and right legs during

gait motion where left and right legs have been considered separately to calculate knee angles. Hence, the proposed work employs 288 data points to represent left knee angles and 288 data points to represent right knee angles. Thus, the prototype generates (288 $\times$ 2) = 576 knee angles from each pulse response. Further these 576 data points (i.e., knee angles) have been considered as feature to represent human gaits from IR-UWB technology and solve two class (normal and abnormal gait) classification problem. The knee angle's feature vector has been visualised as $\{\beta_{L_1}, \beta_{L_2}, ...\beta_{L_{288}}, \beta_{R_1}, \beta_{R_1}, ...\beta_{R_{288}}\}$, where β_L and β_R indicate the left and right knee angles respectively.

6.4 IR-UWB Gait Recognition Employing Supervise Machine Learning (SML)

Selection of appropriate SML technique for classification of UWB gait is intuitive and depends upon feature distribution in Euclidean hyperspace. The feature distribution has been observed and it was found that the data are non-linearly separable in hyperspace. Hence, the leading non-linear classifiers such as, k-nearest neighbour (kNN) and support vector machine (SVM) have been implemented to recognise UWB gait patterns and investigate feasibility for applying SML in this context. The kNN [120] classifier has been incorporated by fine, medium, and coarse neighbourhoods that signifies 1, 3, and 5 numbers of neighbourhood respectively. kNNs with fine, medium, and coarse nearest neighbourhoods have been signified with $k\text{NN}_F$, $k\text{NN}_M$, and $k\text{NN}_C$ respectively in the rest of the chapter. Two effective distance metrics, Euclidean and Mahalanobis perform well with kNN, but Mahalanobis distance requires the inversion of covariance matrix which could increase the computational overhead. Therefore, the Euclidean distance is considered here to measure the distance of a feature vector from its nearest neighbor. The k is chosen as odd for this two-class problem that one pattern could not predict under the same class label by the classifier. Further, SVM has been also enforced with both linear and non-linear (quadratic) kernels [121, 122] because, linear kernel of SVM has reputation for separating non-linear data in high dimension by linear decision boundary. The linear and quadratic kernel based SVMs have been denoted by SVM_L and SVM_Q respectively in rest of the chapter. The ground truth information of UWB gait data has been created during data collection phase by observing simultaneous skeletons of participants visualised from Kinect interface.

6.5 Cross Validation & Performance Evaluation

A cross validation technique has been employed to better use the data prepared for classification and know the amount of training data required for the model to make good predictions. In addition, it prevents the prototype from the overfitting or underfitting problems and selects the data model for developing efficient SML prototype here. Model selection by cross-validation has been implemented by repeated random sub-sampling of the data, which is also known as Monte Carlo cross-validation [123]. The dataset has been randomly partitioned to select the training and validation dataset, where training and validation sets have been used to train and evaluate performance of a selected SML model. The ratio of training and testing data has been specified during each round e.g., training has been started with 10% randomly selected data when rest of the 90% data have been considered as validation/testing data. The amount of training data has been increased by 10% while amount of validation dataset decreased by 10% in each round and this process has been repeated till the model has not overfitted. Each model has been run 10 rounds to select the appropriate ratio of training and testing and found 40% of training and 60% of testing data is necessary to prevent the SML algorithms from overfitting. The results (statistical metrics) have been aggregated and averaged over all the rounds. A number of statistical metrics [124] such as, accuracy, sensitivity, and specificity have been used to investigate performance of implemented classifiers. Subsequently, Matthews correlation coefficient (MCC) [125] and Youden's index [126] have been implemented to investigate the classification outcomes, where, MCC and Youden's index estimate quality of classification and probability of the informed decision respectively. The outcomes and it's analysis have been described in following section and metrics have been defined as follows:

$$A_c = \frac{TP + TN}{TP + TN + FP + FN} \tag{6.9}$$

$$S_e = \frac{TP}{TP + FN} \tag{6.10}$$

$$S_p = \frac{TN}{TN + FP} \tag{6.11}$$

$$MCC = \frac{TP \times TN - FP \times FN}{\sqrt{(TP + FP)(TP + FN)(TN + FP)(TN + FN)}} \tag{6.12}$$

$$Y_i = S_e + S_p - 1 \tag{6.13}$$

Here, A_c, S_e, S_p, MCC, and Y_i denotes accuracy, sensitivity, specificity, Matthews correlation coefficient, and Youden's index respectively. In addition, true positive, true negative, false positive, and false negative have been denoted by TP, TN, FP, and FN respectively. Accuracy measures the fraction of normal and abnormal gait predictions that the proposed model correctly observed, sensitivity determines proportion of actual positives (i.e., abnormal gaits) that are correctly identified, specificity measures the proportion of actual negatives (i.e., normal gaits) that are correctly identified, MCC provides essence through correlation coefficient between actual and predicted outcomes of gait conditions. Youden's index is a statistic, which expresses the overall quality of the performance of the proposed experiment.

6.6 Result Analysis

The obtained knee angles from proposed 3D prototype has been compared with the outcomes obtained from Kinect sensor. The experiments has been conducted only in anechoic chamber at this stage. Further, the gait behaviour of a person has been characterised and recognised in this section. The results are discussed in following sections.

6.6.1 Results from Proposed Work & Kinect Sensor

The processing and transformation of IR-UWB response from human motion have been demonstrated in Chapter 5. The motion has been captured and interpreted into a 3D shape similar to the letter 'W', shown in Figure 6.2a. It has three dimensions, x-axis as motion width, y-axis as distance from radar, and z-axis as height. This includes flexion and extension of body muscles, where the lower limb has been divided into thigh and shank sections, using a priori subjective data collected previously. Simultaneously, Kinect sensor shows the skeleton data of the human subject in Figure 6.2b. Figure 6.2c

and 6.2d present only the left knee angle of that person obtained from IR-UWB and Kinect sensor respectively. The x and y axis of Figure 6.2c and 6.2d represent the proportion of gait cycle associated with measured knee angle variation from proposed prototype and Kincet sensor respectively, where each gait cycle consists of 60% of stance time and 40% of swing time. It has been found that knee angle changes from 120^o to 180^o and 122^o to 175^o while using proposed prototype and Kinect respectively.

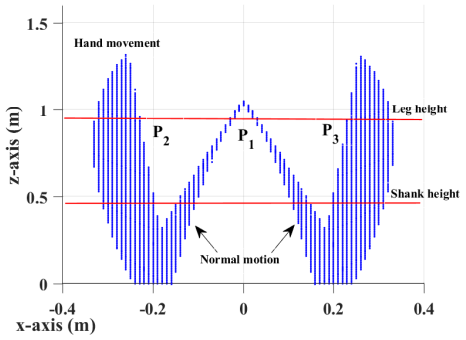

(a) 3D human motion obtained from IR-UWB in anechoic chamber.

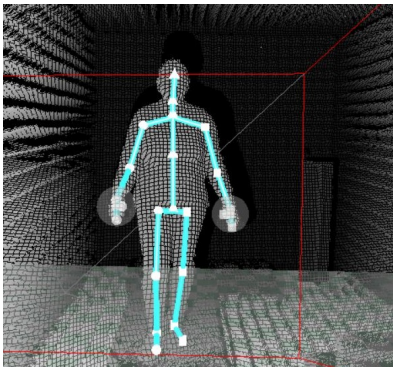

(b) 3D human skeleton obtained from Kinect in anechoic chamber.

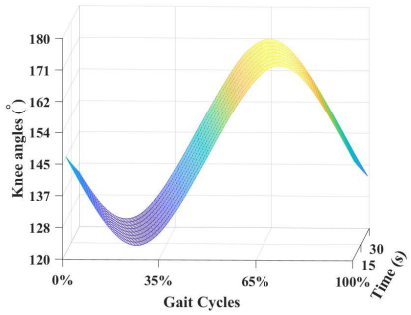

(c) Variation of knee angles determined from proposed model in anechoic chamber.

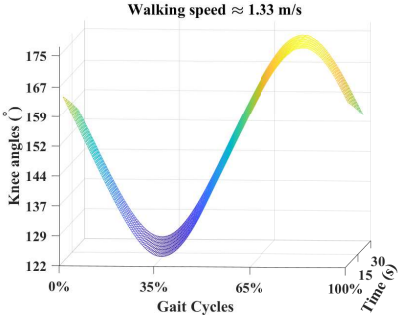

(d) Variation of knee angles determined from Kinect skeleton in anechoic chamber.

Figure 6.2: The human motion and knee angles obtained from proposed model and Kinect for a person having normal walking pattern.

6.6.2 Bland Altman (B&A) Plot Outcomes

The results obtained from the proposed ITERATOR and Kinect system have been corroborated through a B&A plot analysis. Theoretical details of B&A plot has been demonstrated in 6.2 to support the measurement of knee angle done utilising proposed ITERATOR model. Figure 6.3 shows B&A plots have been constructed on knee angle measurements from ITERATOR and Kinect sensor, where Figure 6.3a demonstrates

B&A plots of knee angle measurements taken for twenty normal gait persons from ITERATOR and Kinect respectively and Figure 6.3b demonstrates B&A plots of knee angle measurements taken for four abnormal gait persons from ITERATOR and Kinect. The x and y axis represents mean of two measurements and difference between two paired measurements respectively. Both the ITERATOR and Kinect methods imply some degree of error but B&A plot indicates relationship and agreement between these two methods for gait analysis. Figure 6.3a shows the bias or mean of difference is -0.653 which signifies the second method here Kinect always produces 0.653 degree units more than proposed ITERATOR and 95% differences are within $d_k \pm 1.96 s_k$ while measuring knee angles. In addition, Figure 6.3b displays the bias at -2.277 when measuring abnormal gait persons, this indicates Kinect always delivers 2.277 degree units more than proposed ITERATOR for measurement knee angles and 95% differences are within $d_k \pm 1.96 s_k$. Thus, both the cases suggest null hypothesis (there is no significant difference between ITERATOR and Kinect system's magnitude while measuring knee angles) is true and ITERATOR would be an alternative gait analysis method in future.

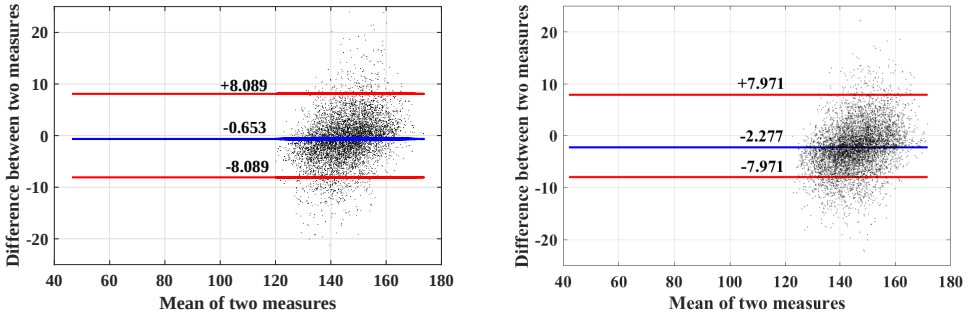

(a) B&A plot of knee angles from normal gaits.

(b) B&A plot of knee angles from abnormal gaits.

Figure 6.3: B&A plot of obtained knee angles experimented in anechoic chamber.

6.6.3 Machine Learning Outcomes

Initially, the investigation began by employing the kNN classifier [120]. This classifier is particularly simple, measuring the proximity of features in the hyperspace without any assumption of the underlying data distribution to predict a category making it flexible for decision making. Table 6.1 displays the classification outcomes and results. Classification outcomes would improve with increasing amount of training data, though the proposed experiment intends to achieve optimal performance with fewer training data.

Thus, models have been trained maximum 40% of total labeled data. In case of kNN, where k is varied from 1 to 5 and 10%, 20%, 30%, and 40% data are randomly selected for the training phase. Here, $k = 1$, produces highest accuracy A_c among other NNs with 40% of training data volume. It attained the testing accuracy A_c =0.944 (≡94.4%). The $k\text{NN}_M$ has produced highest sensitivity S_e among all implemented classifiers with 40% training data. Sensitivity S_e measures ability of the prototype to identify abnormal walks which is 0.978 (≡97.8%) in case of $k = 3$. It produces fewer false predictions FPs close to the decision boundary bringing improved sensitivity S_e over $k\text{NN}_F$ and $k\text{NN}_C$; also, truly positive prediction TPs for having abnormality and vice versa. But, MCC measurements over prediction results are not cogent for $k\text{NN}_F$, $k\text{NN}_M$, and $k\text{NN}_C$ and decreases towards 0 with the increment of k. This trend states that the addition of random predictions with greater number of NN. The average proportions obtained from Youden's index Y_i are also not very significant, 0.856, 0.810, and 0.589 for $k\text{NN}_F$, $k\text{NN}_M$, and $k\text{NN}_C$ respectively and decreases with higher k. This trend further indicating the probability to classify is random and unreliable. Therefore, the overall performance of $k\text{NN}_M$ is better than the other NNs because of data compactness, where three nearest neighbor results good prediction if a greater number of neighbors have been chosen, the misclassification increases.

Table 6.1: Results obtained from nearest neighbor algorithm.

KNN's	Training Data	Accuracy	Sensitivity	Specificity	MCC	Youden
$k\text{NN}_F$	10	0.934	0.954	0.887	0.841	0.84
	20	0.939	0.957	0.899	0.855	0.856
	30	0.941	0.955	0.905	0.858	0.861
	40	0.944	0.959	0.910	0.867	0.869
$k\text{NN}_M$	10	0.922	0.970	0.809	0.810	0.779
	20	0.935	0.975	0.838	0.840	0.813
	30	0.935	0.973	0.846	0.842	0.819
	40	0.941	0.978	0.851	0.855	0.829
$k\text{NN}_C$	10	0.827	0.960	0.507	0.558	0.467
	20	0.844	0.952	0.588	0.608	0.540
	30	0.866	0.937	0.698	0.669	0.635
	40	0.897	0.953	0.762	0.746	0.715

Subsequently, the SVM is investigated with two different kernel functions to acquire the hyperplane that can separate participants with normal and abnormal gait pattern from proposed UWB gait prototype. Table 6.2 shows the results for classification of the 2 subject types where, SVM_L and SVM_Q represents the SVMs using the linear and quadratic kernel functions [121, 122] for prediction. SVM_L uses the optimization method, $c = \sum_i w_i k(s_i, x) + b$ where, UWB gait pattern vector x has been targeted to

classify, s_i is the support vector, w_i is weight, and b is the bias. Here, the linear kernel function is k. The vector x is considered as a member of normal gait group when, $c \geq 0$ or abnormal gait group otherwise. This creates a hyperplane that achieved lowest accuracy A_c than the other classifiers used here but produced highest sensitivity S_e among all. SVM_L has been trained using 10% to 40% data and associated testing results are shown in the Table 6.2. It produces the highest testing accuracy A_c among implemented SVMs with 30% training data which is 0.810 ($\equiv$81.00%). It achieved sensitivity S_e of 0.990 ($\equiv$99.00%) in that case, which indicates a best performance to identify persons with abnormal gaits among both KNNs and SVMs. But, specificity S_p ($0.346 \equiv 34.6\%$) shows a weak performance in identifying persons with normal gait. Though the probability in identifying abnormal gaits is better than the subjects who have normal gait patterns. This creates a number of FPs which result low average MCC and Youden's index Y_i of 0.498 and 0.339 respectively. It can be understood from Eq. 6.12 for calculating MCC that denominator increases with increment of FP which results no better than random prediction outcomes. Youden's index Y_i gets higher when sensitivity S_e and specificity S_p both achieve high score signifies requirement of lower FNs and FPs and this can also be understood from Eq. 6.13. Since, SVM_L produces more FPs that results low specificity S_p as well as low Youden's index Y_i.

Table 6.2: Results obtained from SVM using different kernel.

SVM's	Training Data	Accuracy	Sensitivity	Specificity	MCC	Youden
SVM_L	10	0.795	0.992	0.325	0.479	0.317
	20	0.797	0.992	0.337	0.489	0.329
	30	0.810	0.990	0.382	0.523	0.372
	40	0.802	0.994	0.346	0.502	0.340
SVM_Q	10	0.894	0.948	0.765	0.740	0.714
	20	0.899	0.960	0.752	0.750	0.712
	30	0.906	0.955	0.789	0.769	0.744
	40	0.907	0.963	0.773	0.770	0.736

Subsequently, SVM_Q have been employed to obtain an improved testing accuracy to differentiate normal and abnormal gaits by minimising the gap between two groups. The considered quadratic function is $\min_x \frac{1}{2}x^T Hx + c^T x$, where $Ax \leq b$, c is a real valued vector, H is real symmetric matrix, A is real matrix, b is a real vector, and the notation $Ax \leq b$ means that every entry of the vector A_x is less than or equal to the corresponding entry of the vector b. The quadratic programming aims to find the vector x which could minimize that function. The cross validation has also been implemented for experiment with SVM_Q. The model creates a hyperplane to classify gait subjects and achieved

maximum testing accuracy A_c of 0.907 (≡90.7%) with 40% training data to identify normal and abnormal subjects where sensitivity S_e is 0.963 ≡ 96.3% and specificity S_p is 0.773 ≡ 77.3%. The fraction of sensitivity S_e represents few number of abnormal gaits misclassified but fraction of specificity S_p represents many normal gait patterns predicted as abnormal gaits by the SVM_Q i.e., presence of TN. Thus, low fraction of specificity S_p diminishes the performance of SVM_Q that directly affects MCC and Y_i.

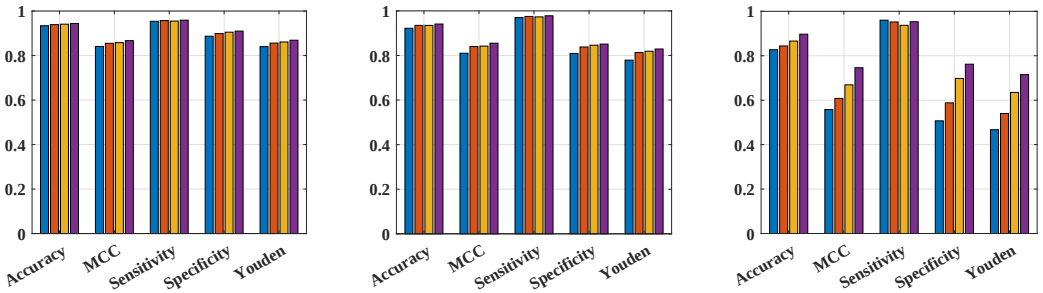

(a) $k\text{NN}_F$ classifier. (b) $k\text{NN}_M$ classifier. (c) $k\text{NN}_C$ classifier.

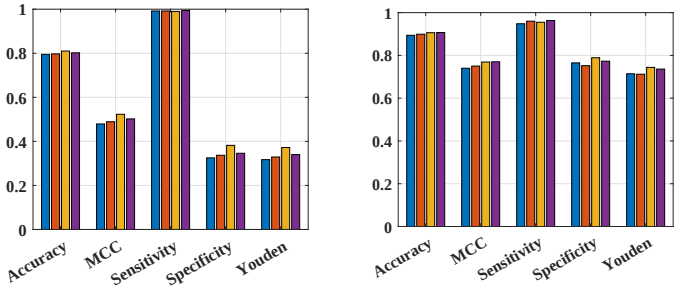

(d) SVM_L classifier. (e) SVM_Q classifier.

Figure 6.4: Comparison of performance metrics obtained from kNN and SVM classifiers.

Finally, the classification results have been compared to conclude the investigation. Figure 6.4 shows the visual comparison of average accuracy A_c, sensitivity S_e, specificity S_p, Mathews correlation coefficient MCC, and Youden's index Y_i to make the contrast over performance, where x and y-axis represent different classifiers and A_c, S_e, S_p, MCC, and Y_i respectively. It can be understood, the performance of $k\text{NN}_F$ is better than other classifiers attempted here in terms of average A_c=93.95%, S_e=95.62%, S_p=90.02%, MCC=85.52%, and Y_i=85.65% which illustrates robust and efficient ability to detect gait abnormality based on their thigh and shank movement from new UWB based intelligent ITERATOR prototype.

6.7 Conclusion

The chapter comprises study on normal and abnormal gait classification from the proposed non-contact, non-invasive intelligent ITERATOR model. Chapter 5 and Chapter 6 demonstrate the measurement of thigh and knee angle from IR-UWB gait data. However, obtained knee angles from IR-UWB (left and right) have been employed as features to train and test constructed model. This is an initial study to check feasibility of employing SMLs to classify gait patterns which does not include type of gait abnormality. Persons participated in experiment only belongs to spastic gait group. Thus, experiment intends to classify normal and spastic gait patterns (abnormal gait group) based on knee angles where empirically KNN_F delivers optimal performance with respect to statistical performance metrics. Once more participants are involved to make generalised decisions about gait abnormality, this work will be extended further to identify type of abnormality such as, spastic, scissors, propulsive, waddling, steppage gait automatically using SML. The performance may differ from present outcomes when types of abnormal gaits will be classified. The performance analysis directs focus on hyperplane created by nearest neighbour classifier function, thus the fine tuning of mechanisms such as, correlation of features within feature vector, distance metrics, and number of nearest neighbours would be observed subsequently.

References

[117] Jos Meuleman et al. “LOPES II—Design and Evaluation of an Admittance Controlled Gait Training Robot With Shadow-Leg Approach”. In: *IEEE Transactions on Neural Systems and Rehabilitation Engineering* 24.3 (2016), pp. 352–363.

[118] John M Bland and Douglas G Altman. “Statistical methods for assessing agreement between two methods of clinical measurement”. In: *The lancet* 327.8476 (1986), pp. 307–310.

[119] Davide Giavarina. “Understanding bland altman analysis”. In: *Biochemia medica: Biochemia medica* 25.2 (2015), pp. 141–151.

[120] Thomas M Cover, Peter Hart, et al. “Nearest neighbor pattern classification”. In: *IEEE transactions on information theory* 13.1 (1967), pp. 21–27.

[121] Shigeo Abe. *Support vector machines for pattern classification*. Vol. 2. Springer, 2005.

[122] Bernhard Scholkopf and Alexander J Smola. *Learning with kernels: support vector machines, regularization, optimization, and beyond*. MIT press, 2001.

[123] Richard R Picard and Ralph D Cook. "Cross-validation of regression models". In: *Journal of the American Statistical Association* 79.387 (1984), pp. 575–583.

[124] David M Powers. "Evaluation: from precision, recall and F-measure to ROC, informedness, markedness and correlation". In: (2011).

[125] Brian W Matthews. "Comparison of the predicted and observed secondary structure of T4 phage lysozyme". In: *Biochimica et Biophysica Acta (BBA)-Protein Structure* 405.2 (1975), pp. 442–451.

[126] William J Youden. "Index for rating diagnostic tests". In: *Cancer* 3.1 (1950), pp. 32–35.

Chapter 7

Discussion & Conclusion

Biomedical research and innovation is the fastest growing field in modern era. The objective of that research is to discover engineering solutions to efficiently diagnose and help patients from recover critical health problems through precise and intelligent engineering tools, making health care improvements across healthcare sector. Gait disorder is one area where human perception and observation are more involved for diagnosis. Gait dysfunction or walking abnormality is when a person is unable to walk in 'a normal' way. It can be caused through injury, underlying conditions, or other problems with the legs and feet. Subjective and objective approaches are used to diagnose gait related problems. Predominantly, subjective gait evaluation includes only observation and question-answer rounds related to health conditions. Objective gait evaluation includes technological devices to measure bio-mechanical gait parameters. Popular technologies for gait diagnosis are dedicated camera and wearable sensor based solutions, however they are limited by security and skin irritation issues. Thus, the thesis work has concentrated on with intention of creating a non-contact and non-intrusive gait recognition method from impulse radio utlra-wide band (IR-UWB) sensing phenomenon, where a standalone IR-UWB system would be able to detect and recognise gait problems with less human intervention. The work has been supported through theoretical and experimental analysis. The background knowledge, literature of gait analysis (subjective or objective) to construct problem statement and find scope to contribute gait understanding using IR-UWB, and experimental set-up have been discussed in Chapter 1, Chapter 2, and Chapter 3 respectively. The proposed work has been divided in three main parts such as, 2D gait identification (i.e., gait detection through range and height of physiological

action estimation from IR-UWB), 3D gait identification or gait disorder identification from impulse radio ultra-wide band (ITERATOR) (i.e., gait detection through gait motion width, range and height of physiological action estimation from IR-UWB), and 3D gait recognition or intelligent ITERATOR (i.e., gait recognition through learning IR-UWB gait parameter) have been discussed in Chapter 4, Chapter 5, and Chapter 6 respectively. The explanation of work done to relate findings, limitations, and future works of proposed work has been discussed in following sections.

7.1 Discussion

A IR-UWB radar module with single transmitter and receiver has been employed to acquire human gait. A new spherical trigonometric model has been developed to interpret IR-UWB gait response and calculate gait motion, distance, and height to represent x, y, and z axis of coordinate system. Subsequently, experiments have been performed in both; anechoic and multipath environments. There are a number of gait parameters used for evaluation discussed in Chapter 2. Here, only few of them have been considered such as, step frequency, walking speed, cadence, step length, distance covered, hip or thigh angle, and knee angle. In total, twenty four participants including normal and abnormal gait persons were involved in the study. Initially, gait parameters such as, step frequency, walking speed, cadence, step length, and distance covered have been calculated employing developed distance and height theory, and short term Fourier transform (STFT) to measure gait in 2D. However, these parameters alone are insufficient to define human gait and unable to provide structural information about gait. The parameters such as, step frequency, walking speed, cadence, step length, and distance covered may vary for a person's walk even in normal condition. Also, the experiment performed in multipath or normal environment is effected by mutlipath problem which causes time dispersion, angular dispersion, and frequency dispersion that lead to errors in calculation of gait parameters. Thus, the spherical model has been improved to calculate gait motion width along with distance and height from change of range to incorporate realistic settings. The proposed 3D model is then capable to measure hip and knee angles which represent structural gait information more than previous model. In addition, detection threshold of radar has been tuned to mitigate multipath problem. A simultaneous Kinect sensor system and statistical Bland-Altman (B&A) plot analysis also have been employed to

justify gait measurements from the proposed model. The B&A plot analysis indicates potentiality of the proposed work to measure human gait in 3D where multipath problem is still there. Subsequently, popular supervised machine learning (SML) algorithms have been applied to inspect the feasibility of automation of the work. Statistical metrics have been calculated to understand performance of automatic gait recognition where promising results obtained. The result analysis shows the strong potential of the work for creating an IR-UWB sensing based intelligent gait diagnosis tool in future. The work hitherto is limited to calculate the hip and knee angles where the obtained knee angles have been used to be learned by SML algorithms. The future research aspects have been discussed in the following section.

7.2 Future Research Directions

The study indicates potentiality of a non-contact, non-invasive gait identification and recognition through IR-UWB. There are some limitations and scope to improve the work would be addressed in future:

1. **Mathematical Model for Wireless Channel:** Wireless channel implications have not been studied deeply in proposed work. But, a mathematical model will be developed in future to handle multi-path reflections and mirror the results of normal environment in better way. It would lower signal attenuation and mitigate delay, angular, and frequency dispersion occur due to mutlipath problem.

2. **Employ Directional UWB Antenna:** Single omni-directional UWB transmitter and receiver have been used to collect data and construct 3D model. Directional UWB antenna will be investigated in future to gather UWB gait data for better gait identification experiment through improved SNR and directionality employment.

3. **More Bio-mechanical Gait Parameter Extraction:** The current is only able to measure gait parameters such as, step frequency, walking speed, cadence, step length, distance covered, hip angle, and knee angle. The model will be improved further to measure angles of ankles (both left and right), stance (posture), and duration of stops for representing human gait better.

4. **Enhance IR-UWB Gait Database:** Twenty four participants involved till date in proposed experiment where twenty persons having normal walking pattern and four persons having spastic gait abnormality. More participants will be recruited for experimenting gait and making a bigger IR-UWB gait database.

5. **Involve Medical Professional & Sports Laboratory:** Smart phone applications and Microsoft Kinect sensor have been employed to corroborate results. In addition, statistically agreement of gait measurement using proposed work has been proved. However, none of them reference and comply minimum error. Thus, medical professionals and LSBU sports laboratory will be involved in this study to perform gold standard test comparison.

6. **Analysis of Different Gait Disorder:** The normal and abnormal specifically spastic patterns have been experimented and classified through SML. More participants with spastic, scissors, propulsive, steppage, and waddling gait (as shown in Figure 1.3) including normal gait persons will be experimented. So, SML can be used to classify gait disorders and take decisions for identify specific gait abnormality.

7. **Improve Machine Learning Application:** The performance may differ when more participants with different gait are involved. So, fine tuning of SML algorithm's parameters will be explored and modified to achieve better performance in IR-UWB gait classification.

7.3 Concluding Remarks

This is first work which is able to address bio-mechanical gait parameters from IR-UWB in 3D and employ them for classifying gait disorders. The model would be a strong alternative for objective gait analysis such as, supporting doctor to help in gait diagnosis, making smart and intelligent gait care, supporting in physiotherapy, improving performance of athlete, and even in detecting intruders through IR-UWB gait pattern.

Publications

□ **Conference & Symposium Publications**

1. **S. P. Rana**, M. Dey, M. Ghavami, S. Dudley. "ITERATOR: A 3D Gait Identification from IR-UWB Technology", The 41st IEEE International Engineering in Medicine and Biology Conference, Berlin, Germany, 2019.
2. **S. P. Rana**, M. Dey, M. Ghavami, S. Dudley. "Intelligent three-dimensional gait analysis using IR-UWB sensing", The 41st PhotonIcs & Electromagnetics Research Symposium (PIERS), Rome, Italy, 2019.
3. M. Dey, **S. P. Rana**, and S. Dudley. "Semi-Supervised Learning Techniques for Automated Fault Detection and Diagnosis of HVAC Systems", The 30th IEEE International Conference on Tools with Artificial Intelligence (ICTAI), Volos, Greece, 2018.
4. **S. P. Rana**, M. Dey, R. Brown, H. Siddiqui, S. Dudley. "Remote Vital Sign Recognition Through Machine Learning Augmented UWB", The 12th IEEE International Conference on European Conference on Antennas and Propagation (EuCAP), London, UK, 2018.
5. M. Dey, M. Gupta, **S. P. Rana**, M. Turkey, S. Dudley. "A PID Inspired Feature Extraction for HVAC Terminal Units" , The IEEE International Conference on Sustainability and Technology (SusTech), Phoenix, AZ, USA, 2017.
6. **S. P. Rana**, M. Dey, H. Siddiqui, G. Tiberi, M. Ghavami, S Dudley. "UWB Localization Employing Supervised Learning Method", The 17th IEEE International Conference on Ubiquitous Wireless Broadband (ICUWB), Salamanca, Spain, 2017.

7. D. Misra, **S. P. Rana**. "Accordance of KM & ANN in Data Mining forwarded to DSS", International Conference on Business Applications and Management Issues (ICBAMI), Durgapur, India, 2012.

□ **Journal Publications**

1. **S. P. Rana**, M. Dey, G. Tiberi, L. Sani, A. Vispa, G. Raspa, M. Duranti, M. Ghavami, and S. Dudley. "Machine Learning Approaches for Automated Lesion Detection in Microwave Breast Imaging Clinical Data", Scientific Reports, Springer Nature Publishing, 2019. DOI: 10.1038/s41598-019-46974-3. ***(Impact factor-4.525)***
2. **S. P. Rana**, M. Dey, M. Ghavami and S. Dudley. "Non-Contact Human Gait Identification through IR-UWB Edge Based Monitoring Sensor", IEEE Sensors Journal, IEEE, 2019. DOI: 10.1109/JSEN.2019.2926238. ***(Impact factor-3.076)***
3. **S. P. Rana**, M. Dey, and S. Dudley. "Signature Inspired Home Environments Monitoring System Using IR-UWB Technology", Sensors, MDPI, 19(2): 385, 2019. ***(Impact factor-3.031)***
4. M. Dey, **S. P. Rana**, and P. Siarry, "A robust FLIR target detection employing an auto-convergent pulse coupled neural network", Remote Sensing Letters, Taylor & Francis, 10(7): 639-648, 2019. ***(Impact factor-2.024)***
5. **S. P. Rana**, M. Dey, M. Ghavami, and S. Dudley. "A Self Regulating and Crowdsourced Indoor Positioning System through Wi-Fi Fingerprinting for Multi Storey Building", Sensors, MDPI, 18(11): 3766, 2019. ***(Impact factor-3.031)***
6. **S. P. Rana**, M. Dey, and P. Siarry. "Boosting content based image retrieval performance through integration of parametric & nonparametric approaches", Journal of Visual Communication and Image Representation, Elsevier, 58: 205-219, 2019. ***(Impact factor-2.259)***
7. M. Dey, **S. P. Rana**, and S. Dudley. "Smart building creation in large scale HVAC environments through automated fault detection and diagnosis", Future Generation Computer Systems, Elsevier, 2018. DOI: 10.1016/j.future.2018.02.019. ***(Impact factor-5.768)***

8. R. Amin, T. Maitra, **S. P. Rana**. "An improvement of wang. et. al.'s remote user authentication scheme against smart card security breach", International Journal of Computer Applications, 75(13): 37-42, 2013.

□ **Book Chapters**

1. M. S. Obaidat, **S. P. Rana**, T. Maitra, D. Giri, S. Dutta. "Biometric Security and Internet of Things (IoT), Biometric-Based Physical and Cybersecurity Systems, pp. 477-509, Springer, Cham, 2019.

Appendix

Matlab Code 1

```
function stft_ = STFT(signal)

[row_signal,col_signal]=size(signal);
fs=16390000000; %fs=16.39 GHz
L=30; % window length
w = hamming(L,'periodic'); % type of window
window_index=0;
% R=2;
R=1;

if(mod(col_signal,R)~=0)
    rem=mod(col_signal,R);
    signal=signal(row_signal,1:(col_signal-rem));
end

[row_signal,col_signal]=size(signal);

stft_=zeros(row_signal,(col_signal)/R);
signal = padarray(signal,[0 L],0,'post');
summation=0;

for j=1:R:col_signal
    for k=j:j+L-1
        window_index=window_index+1;
        summation=summation+(signal(row_signal,k)*w(window_index,1)*(complex(cos
    (2*pi*fs*k),sin(2*pi*fs*k))));
    end
    window_index=0;
    stft_(row_signal,j)=summation;
    summation=0;
end

end
```

Matlab Code 2

```
1
2  clc;
3  clear all;
4  close all;
5
6  tic
7  c = 300000000; % speed of light
8  LegLength = input('Please enter the length of leg in meters : ');
9  ShankLength = input('Please enter the shank length in meters : ');
10 ThighLength = LegLength-ShankLength;
11 StandHeight=1.02;
12 ObservationTime = input('Please enter the observation time in seconds : ');
13
14 Files=dir('*.csv');
15 %%
16 for k=1:length(Files)
17
18     fileID = fopen('exp.txt','w');
19     FileNames=Files(k).name;
20     [num, txt, raw]=xlsread(Files(k).name);
21     [row_raw, col_raw]=size(raw);
22     RawData=zeros(row_raw, col_raw);
23     DetectionData=zeros(row_raw, col_raw);
24     config_counter=0;
25     mrm_counter=0;
26     Azimuth = 0;
27     mrm_string=" MrmFullScanInfo";
28     configuration_string=" Config";
29     detection_string=" MrmDetectionListInfo";
30     InitialRange=0;
31     FinalRange=0;
32
33     for i=1:row_raw-4
34         X = sprintf('Scan No = %d',i); disp(X)
35         X = sprintf('
       ------------------------------------------------------------------------');
       disp(X)
36         if(string(raw{i,2})==configuration_string)
37             config_counter=config_counter+1;
38             if(config_counter==2)
39                 ScanStart=num(i-1,4); % in Nanoseconds
40                 ScanStop=num(i-1,5); % in Nanoseconds
41                 ScanResolutionBins=num(i-1,6);
42                 PII=num(i-1,7);
43                 ACP=360/(2^PII);
44                 TransmitGain=num(i-1,17);
```

```
45              end
46          end
47          if(string(raw{i,2})==mrm_string)&&(string(raw{i,13})==string(1))
48              mrm_counter=mrm_counter+1;
49              msgid=string(raw{i,3});
50              if(rem(mrm_counter,2^PII)==0)
51                  Azimuth = 0;
52              else
53                  Azimuth = Azimuth + ACP;
54              end
55              if(string(raw{i+1,2})==detection_string)&&(string(raw{i,3})==msgid)
56                  RawData(i,:)=num(i-1,:);
57                  RawData(i,6)=num(i-1+1,4);
58                  RawData(i,7)=num(i-1+1,5);
59                  DetectionData(i,:)=num(i-1+1,:);
60              end
61
62              if(string(raw{i+2,2})==detection_string)&&(string(raw{i,3})==msgid)
63                  NoOfSamples=num(i-1,16);
64                  RawData(i,:)=num(i-1,:);
65                  RawData(i,6)=num(i-1+2,4);
66                  RawData(i,7)=num(i-1+2,5);
67                  DetectionData(i,:)=num(i-1+2,:);
68              end
69
70              if(string(raw{i+3,2})==detection_string)&&(string(raw{i,3})==msgid)
71                  NoOfSamples=num(i-1,16);
72                  RawData(i,:)=num(i-1,:);
73                  RawData(i,6)=num(i-1+3,4);
74                  RawData(i,7)=num(i-1+3,5);
75                  DetectionData(i,:)=num(i-1+3,:);
76              end
77
78           if(mrm_counter==2)||(mrm_counter==3)
79               NoOfSamples=num(i-1,16); % number of samples in each radar signal
80               PropagationDelay=round((NoOfSamples*61)/1000);
81               NoOfInsigCol=round((NoOfSamples*5)/PropagationDelay);
82           end
83           counter=1;
84           for inRowCounter=1:2:length(DetectionData(i,:))
85               if(isnumeric(DetectionData(i,inRowCounter))==1)&&(counter==1)&&(
    DetectionData(i,inRowCounter)-DetectionData(i,inRowCounter-2)==1)
86                   InitialRange=abs(DetectionData(i,inRowCounter)
    *61*0.000000000001)*(c/2);
87                   counter=counter+1;
88               elseif(isnumeric(DetectionData(i,inRowCounter))==1)&&(counter>1)&&(
    DetectionData(i,inRowCounter)-DetectionData(i,inRowCounter-2)==1)
```

```
89                  FinalRange=abs(DetectionData(i,inRowCounter)*61*0.000000000001)
    *(c/2);
90                  counter=counter+1;
91              end
92              Height=sqrt(abs((InitialRange*InitialRange)-(FinalRange*FinalRange))
    );
93              if(Height>StandHeight)
94                  Height=(Height-StandHeight);
95              elseif(Height<StandHeight)
96                  Height=StandHeight-Height;
97              end
98
99              if(Azimuth<180)
100                 Arc=(InitialRange*(atand(abs(InitialRange-FinalRange)/
    InitialRange)));
101             elseif(Azimuth>180)
102                 Arc=-(InitialRange*(atand(abs(InitialRange-FinalRange)/
    InitialRange)));
103             end
104             if(isnan(Height)==1)
105                 Height=0;
106             end
107             if(isnan(FinalRange)==1)
108                 FinalRange=0;
109             end
110             if(isnan(InitialRange)==1)
111                 InitialRange=0;
112             end
113             fprintf(fileID,'%.2f %.2f %.2f\n', Arc, FinalRange, Height);
114         end
115        end
116    end
117 end
```